

# The Star Formation in Radio Survey: 3 – 33 GHz Imaging of Nearby Galaxy Nuclei and Extranuclear Star-forming Regions

S.T. LINDEN,<sup>1</sup> E.J. MURPHY,<sup>2</sup> D. DONG,<sup>3</sup> E. MOMJIAN,<sup>4</sup> R. C. KENNICUTT JR.,<sup>5</sup> D.S. MEIER,<sup>6</sup> E. SCHINNERER,<sup>7</sup> AND J.L. TURNER<sup>8</sup>

<sup>1</sup>*Department of Astronomy, University of Virginia, 530 McCormick Road, Charlottesville, VA 22904, USA*

<sup>2</sup>*National Radio Astronomy Observatory, 520 Edgemont Road, Charlottesville, VA 22903, USA*

<sup>3</sup>*California Institute of Technology, MC 100-22, Pasadena, CA 91125, USA*

<sup>4</sup>*National Radio Astronomy Observatory, P.O. Box O, 1003 Lopezville Road, Socorro, NM 87801, USA*

<sup>5</sup>*Institute of Astronomy, University of Cambridge, Madingley Road, Cambridge CB3 0HA, UK*

<sup>6</sup>*New Mexico Institute of Mining and Technology, 801 Leroy Place, Socorro, NM 87801, USA*

<sup>7</sup>*Max Planck Institut für Astronomie, Knigstuhl 17, Heidelberg D-69117, Germany*

<sup>8</sup>*Department of Physics and Astronomy, UCLA, Los Angeles, CA 90095, USA*

(Dated: April 23, 2020)

## ABSTRACT

We present 3, 15, and 33 GHz imaging towards galaxy nuclei and extranuclear star-forming regions using the Karl G. Jansky Very Large Array as part of the Star Formation in Radio Survey. With 3 – 33 GHz radio spectra, we measured the spectral indices and corresponding thermal (free-free) emission fractions for a sample of 335 discrete regions having significant detections in at least two radio bands. After removing 14 likely background galaxies, we find that the median thermal fraction at 33 GHz is  $92 \pm 0.8\%$  with a median absolute deviation of 11%, when a two-component power-law model is adopted to fit the radio spectrum. Limiting the sample to 238 sources that are confidently identified as star-forming regions, and not affected by potential AGN contamination (i.e., having galactocentric radii  $r_G \geq 250$  pc), results in a median thermal fraction of  $93 \pm 0.8\%$  with a median absolute deviation of 10%. We further measure the thermal fraction at 33 GHz for 163 regions identified at  $7''$  resolution to be  $94 \pm 0.8\%$  with a median absolute deviation of 8%. Together, these results confirm that free-free emission dominates the radio spectra of star-forming regions on scales up to  $\sim 500$  pc in normal star-forming galaxies. We additionally find a factor of  $\sim 1.6$  increase in the scatter of the measured spectral index and thermal fraction distributions as a function of decreasing galactocentric radius. This trend is likely reflective of the continuous star-formation activity occurring in the galaxy centers, resulting a larger contribution of diffuse nonthermal emission relative to star-forming regions in the disk.

*Keywords:* galaxies: nuclei - HII regions - radio continuum: general - stars: formation

## 1. INTRODUCTION

The radio spectra of star-forming galaxies, typically characterized as a power law ( $S_\nu \propto \nu^\alpha$ ), encode information about the thermal and non-thermal energetic processes which power them. Both thermal (Bremsstrahlung) and non-thermal (synchrotron) emission are associated with massive ( $\geq 8M_\odot$ ) star formation, underlying the basis for the well-known far-infrared (FIR: 42-122 $\mu$ m)-radio correlation (de Jong et al. 1985; Helou et al. 1985; Condon 1992; Bell 2003). FIR emission arises from the absorption and re-radiation of UV and optical photons that heat dust grains surrounding massive star-forming regions. The O and B stars in such

regions, with lifetimes of  $\leq 10$  Myr, produce ionizing (Lyman continuum) radiation whose strength is directly proportional to the amount of free-free emission. These same massive stars end their lives as core-collapse supernovae, whose remnants accelerate cosmic ray (CR) electrons/positrons that produce the diffuse non-thermal synchrotron emission observed in star-forming galaxies (Condon 1992; Koyama et al. 1995; Murphy et al. 2006; Lacki & Thompson 2010; Lacki et al. 2010).

However, the connection between the non-thermal synchrotron emission and the current star-formation rate (SFR) of a galaxy is far less direct relative to thermal free-free emission. Variations in the generation and propagation of CRs through the interstellar medium

(ISM) can affect the observed low-frequency emission surrounding star-forming regions. Despite the complexity in interpreting this non-thermal emission from galaxies, several empirical (Bell 2003; Koyama et al. 1995; Murphy et al. 2006; Heesen et al. 2014; Tabatabaei et al. 2017) and theoretical (Condon 1992; Murphy et al. 2011) calibrations for the star-formation rate (SFR) exist in the literature. These studies demonstrate that at frequencies low enough (typically  $\sim 1$  GHz) the emission is dominated by the non-thermal, steep spectrum component ( $\alpha^{\text{NT}} \sim -0.8$ ), and at frequencies high enough ( $\sim 30$  GHz) the emission becomes dominated by thermal emission ( $\alpha^{\text{T}} \sim -0.1$ ). Hence, radio observations can serve as an excellent, extinction-free, diagnostic for the current SFR within nearby galaxies.

This was the motivation for initiating the Star Formation in Radio Survey (SFRS), which began as a 33 GHz imaging campaign with the Green Bank Telescope (GBT) to study 103 galaxy nuclei and extranuclear star-forming complexes at a matched resolution of  $25''$ . In the initial investigation, Murphy et al. (2012) used the Westerbork Synthesis Radio Telescope (WSRT) in combination with the GBT to construct 1.7-to-33 GHz radio spectra for 53 galaxy nuclei and extranuclear star-forming regions on  $\sim$ kpc scales. They found evidence that the measured thermal fraction at 33 GHz varied significantly for star-forming regions observed at different physical resolution due to the range in galaxy distance. Photometric apertures larger than  $\sim 1$ kpc were observed to have thermal fractions as low as 40 – 50%, whereas regions measured with apertures  $\leq 1$ kpc appeared to be heavily dominated by free-free emission, with thermal fractions as high as  $\sim 90\%$ . However, without high-resolution maps of both free-free and non-thermal emission from individual HII regions within these larger complexes, it is difficult to determine the physical nature of these trends within nearby galaxies.

This study served as the foundation for extending the SFRS into a multi-frequency Karl G. Jansky Very Large Array (VLA) campaign to image hundreds of star-forming regions in 50 galaxies taken from the *Spitzer* Infrared Nearby Galaxies Survey (SINGS; Kennicutt et al. 2003) and the Key Insights on Nearby Galaxies: a Far-Infrared Survey (KINGFISH; Kennicutt et al. 2011). The results from our 33 GHz observations, along with corresponding H $\alpha$  and *Spitzer*/MIPS  $24\mu\text{m}$  photometry were recently presented in Murphy et al. (2018a), hereafter M18a, and explored the H $\alpha$ -to-33 GHz and  $24\mu\text{m}$ -to-33 GHz flux density ratios of star-forming regions as a function of galactocentric radius and physical resolution. An outlier of these distributions, NGC 4725 B, was later followed up with higher-

frequency observations (Q-band:  $\sim 44$  GHz) in order to confirm this region as the second known source of extragalactic anomalous microwave emission (AME; Murphy et al. 2018b). Building on this analysis, we have also obtained 3 and 15 GHz imaging for the SFRS, allowing us to map the full radio spectrum of each star-forming region at a matched-resolution of  $\sim 2''$ . In this paper, we focus our presentation on the results associated with the radio spectral indices and corresponding free-free emission fractions for the entire sample.

The paper is organized as follows: In §2 we describe our sample selection, data reduction, and imaging procedure for the 3 - 33 GHz VLA data. In §3 we describe the ancillary data products included in this study as well as the analysis procedures used. Our results are presented in §4, and discussed in §5. Our main conclusions are summarized in §6. In the Appendix we additionally provide ancillary photometry from the Galaxy Evolution Explorer (GALEX), *Spitzer*, and ground-based H $\alpha$  observations at a matched resolution of  $7''$  that are not used in the present analysis. Throughout the paper we report the median absolute deviations rather than standard deviations, as this statistic is more resilient against outliers in a data set.

## 2. SAMPLE AND DATA ANALYSIS

In this section we describe the sample selection, and present the VLA observations along with the data reduction and imaging procedures.

### 2.1. Sample Selection

The SFRS sample includes targeted observations from 56 nearby galaxies ( $d_L < 30$  Mpc) in the SINGS and KINGFISH legacy programs (Table 1). All nuclear and extranuclear star-forming regions were chosen to have mid-infrared spectral mappings carried out by the IRS instrument on board *Spitzer*, and *Herschel*/PACS far-infrared spectral mappings, for a combination of the principal atomic ISM cooling lines ([OI]  $63\mu\text{m}$ , [OIII]  $88\mu\text{m}$ , [NII]  $122, 205\mu\text{m}$ , and [CII]  $158\mu\text{m}$ ). NGC 5194 and NGC 2403 are exceptions; these galaxies were part of the SINGS sample, but are not formally included in KINGFISH. They were observed with *Herschel* as part of the Very Nearby Galaxy Survey (VNGS; PI: C. Wilson). Similarly, there are additional KINGFISH galaxies that were not part of SINGS, but have existing *Spitzer* data: NGC 5457 (M101), IC 342, NGC 3077, and NGC 2146.

The SINGS and KINGFISH galaxies are fully representative of the integrated properties and ISM conditions found in the local Universe, spanning the full range in morphological types, as well as a factor of 100 in IR

**Table 1.** Galaxy Properties

Galaxy	Type <sup>a</sup>	Dist. <sup>b</sup> (Mpc)	Nuc. Type <sup>c</sup>	$D_{25}$ <sup>a</sup> (arcmin)	$i$ ( $^{\circ}$ )	P.A. <sup>a</sup> ( $^{\circ}$ )
NGC 0337	SBd	19.3	SF	$2.9 \times 1.8$	52	130
NGC 0628	SAC	7.2	...	$10.5 \times 9.5$	25	25
NGC 0855	E	9.73	SF	$2.6 \times 1.0$	70	67 <sup>d</sup>
NGC 0925	SABd	9.12	SF	$10.5 \times 5.9$	57	102
NGC 1097	SBb	14.2	AGN	$9.3 \times 6.3$	48	130
NGC 1266	SB0	30.6	AGN	$1.5 \times 1.0$	49	108 <sup>d</sup>
NGC 1377	S0	24.6	...	$1.8 \times 0.9$	61	92
IC 0342	SABcd	3.28	SF(*)	$21.4 \times 20.$	21	153 <sup>d</sup>
NGC 1482	SA0	22.6	SF	$2.5 \times 1.4$	57	103
NGC 2146	Sbab	17.2	SF(*)	$6.0 \times 3.4$	56	57
NGC 2403	SABcd	3.22	SF(*)	$21.9 \times 12.3$	57	128
Holmberg II	Im	3.05	...	$7.9 \times 6.3$	37	16
NGC 2798	SBa	25.8	SF/AGN	$2.6 \times 1.0$	70	160
NGC 2841	SAB	14.1	AGN	$8.1 \times 3.5$	66	147
NGC 2976	SAC	3.55	SF	$5.9 \times 2.7$	64	143
NGC 3049	SBab	19.2	SF	$2.2 \times 1.4$	51	25
NGC 3077	I0pec	3.83	SF(*)	$5.4 \times 4.5$	34	45
NGC 3190	SAap	19.3	AGN(*)	$4.4 \times 1.5$	73	125
NGC 3184	SABcd	11.7	SF	$7.4 \times 6.9$	21	135
NGC 3198	SBc	14.1	SF	$8.5 \times 3.3$	68	35
IC 2574	SABm	3.79	SF(*)	$13.2 \times 5.4$	67	50
NGC 3265	E	19.6	SF	$1.3 \times 1.0$	39	73
NGC 3351	SBb	9.33	SF	$7.4 \times 5.0$	48	13
NGC 3521	SABbc	11.2	SF/AGN(*)	$11.0 \times 5.1$	63	163
NGC 3621	SAd	6.55	AGN	$12.3 \times 7.1$	55	159
NGC 3627	SABb	9.38	AGN	$9.1 \times 4.2$	64	173
NGC 3773	SA0	12.4	SF	$1.2 \times 1.0$	33	165
NGC 3938	SAC	17.9	SF(*)	$5.4 \times 4.9$	25	29 <sup>d</sup>
NGC 4254	SAC	14.4	SF/AGN	$5.4 \times 4.7$	30	24 <sup>d</sup>
NGC 4321	SABbc	14.3	AGN	$7.4 \times 6.3$	32	30
NGC 4536	SABbc	14.5	SF/AGN	$7.6 \times 3.2$	66	130
NGC 4559	SABcd	6.98	SF	$10.7 \times 4.4$	67	150
NGC 4569	SABab	9.86	AGN	$9.5 \times 4.4$	64	23
NGC 4579	SABb	16.4	AGN	$5.9 \times 4.7$	37	95
NGC 4594	SAa	9.08	AGN	$8.7 \times 3.5$	69	90
NGC 4625	SABmp	9.3	SF	$2.2 \times 1.9$	31	28 <sup>d</sup>
NGC 4631	SBd	7.62	SF(*)	$15.5 \times 2.7$	83	86
NGC 4725	SABab	11.9	AGN	$10.7 \times 7.6$	45	35
NGC 4736	SAab	4.66	AGN(*)	$11.2 \times 9.1$	35	105
NGC 4826	SAab	5.27	AGN	$10.0 \times 5.4$	59	115
NGC 5055	SAbc	7.94	AGN	$12.6 \times 7.2$	56	105
NGC 5194	SABbcp	7.62	AGN	$11.2 \times 6.9$	53	163
NGC 5398	SBdm	7.66	...	$2.8 \times 1.7$	53	172
NGC 5457	SABcd	6.7	SF(*)	$28.8 \times 26.$	26	29 <sup>d</sup>
NGC 5474	SACd	6.8	SF(*)	$4.8 \times 4.3$	27	98 <sup>d</sup>
NGC 5713	SABbcp	21.4	SF	$2.8 \times 2.5$	27	10
NGC 5866	S0	15.3	AGN	$4.7 \times 1.9$	69	128
NGC 6946	SABcd	6.8	SF	$11.5 \times 9.8$	32	53 <sup>d</sup>
NGC 7331	SAb	14.5	AGN	$10.5 \times 3.7$	72	171
NGC 7793	SAd	3.91	SF	$9.3 \times 6.3$	48	98

<sup>a</sup> Morphological types, diameters, and position angles were taken from the Third Reference Catalog of Bright Galaxies (RC3; de Vaucouleurs et al. 1991).

<sup>b</sup> Redshift-independent distance taken from the list compiled by Kennicutt et al. (2011), except for the two non-KINGFISH galaxies NGC 5194 (Ciardullo et al. 2002) and NGC 2403 (Freedman et al. 2001).

<sup>c</sup> Nuclear type based on optical spectroscopy: SF = Star-Forming; AGN = Non-thermal emission as given in Table 5 of Moustakas et al. (2010) or (\*) Table 4 of Lonsdale Persson & Helou (1987).

<sup>d</sup> Position angle taken from Jarrett et al. (2003).

luminosity ( $L_{\text{IR}}$ : 8-1000 $\mu\text{m}$ ), global IR/optical flux ratio, and the star formation rate. Similarly, the spectroscopically targeted star-forming regions included in the SFRS cover the full range of physical conditions found in nearby galaxies, including the extinction-corrected production rate of ionizing photons  $Q(H_0)$ , metallicity, visual extinction, radiation field intensity, and ionizing stellar temperature.

The full sample over the entire sky consists of 118 star-forming complexes (56 nuclei and 62 extranuclear regions), 112 of which (50 nuclei and 62 extranuclear regions; see Tables 2 and 3, respectively) are observable with the VLA (i.e., having  $\delta > -35^\circ$ ). The coordinates given in both tables list the pointing center for the VLA observations (see Section 2.2), which correspond to the centers of the *Spitzer* mid-infrared and *Herschel* far-infrared spectral line maps. Morphologies, adopted distances, optically-defined nuclear types, diameters ( $D_{25}$ ), inclinations ( $i$ ), and position angles (P.A.) for each source are given in Table 1 and described in detail in M18a.

## 2.2. VLA Observations and Data Reduction

The observational set-up and reduction procedure for the Ka-band (29 – 37 GHz) data (11B-032,13A-129) is described in detail in M18a. Observations in the S-band (2 – 4 GHz) were taken during the 2013 VLA B-configuration cycle (13B-215), and utilized the 8-bit sampler. Observations in the Ku-band (12 – 18 GHz) were taken November 2014 in the C-configuration (13B-215) using the 3-bit samplers. Both sets of observations utilized the full available bandwidth of the respective receivers. Given the large range in brightness among our targeted regions, we varied the time spent on-source by estimating the expected 3 – 15 GHz flux density using the *Spitzer*/MIPS 24  $\mu\text{m}$  maps. The median integration time for regions in our sample was  $\sim 10$  minutes at both frequencies. The choice of array configurations were made to match the angular resolution (i.e., FWHM of the synthesized beam  $\sim 2''$ ) of the observations at each band. This allows us to probe the same spatial scales across the full 3 – 33 GHz frequency range, and ensures that any differences in the measured spectral index of individual star-forming regions is due to physical variation in the region being measured, and not due to resolving out more emission at higher frequencies.

The standard VLA flux density calibrators 3C48, 3C286, and 3C147 were used, and the data reduction procedures presented in M18a are repeated for our present analysis, and briefly described here. To reduce the VLA data, we used the Common Astronomy Software Applications (CASA; McMullin et al. 2007) ver-

sions 4.6.0 and 4.7.0, and followed standard calibration and flagging procedures, including the utilization of the VLA calibration pipeline. We further inspected the visibilities and calibration tables for evidence of bad antennas, frequency ranges, and time ranges, flagging correspondingly. We also flagged any instances of radio frequency interference (RFI). Importantly, the fractional bandwidth of our observations lost to RFI flagging is negligible relative to the full bandwidth of the receivers. After flagging, we re-ran the pipeline, and repeated this process until all poorly-calibrated data were removed. For all delay and bandpass tables applied on-the-fly, we used the default nearest-neighbor interpolation. For complex gain and flux density scale tables, we used a linear interpolation.

## 2.3. Interferometric Imaging

Calibrated VLA measurement sets for each source were imaged using the task TCLEAN in CASA version 4.6.0. For some cases, the Ka-band images contain data from observations taken during both the 11B and 13A semesters, but are heavily weighted by the 13A semester observations, as those include significantly more data. The mode of TCLEAN was set to multi-frequency synthesis (MFS; Conway et al. 1990; Sault & Wieringa 1994). We chose a pixel scale of  $0''.2$  for all three bands, and adopted Briggs weighting with ROBUST = 0.5 and NTERMS = 2. This allows the cleaning procedure to also model the spectral index variations on the sky. Although this procedure utilizes the large fractional bandwidths of each observation to generate in-band spectral index maps, we do not use them in our analysis given that the signal-to-noise ratio ( $S/N$ ) of our sources is typically too low for them to be reliable. To help deconvolve extended low-intensity emission, we took advantage of the multiscale CLEAN option (Cornwell 2008; Rau & Cornwell 2011) in CASA, searching for structures with scales  $\sim 1$  and 3 times the FWHM of the synthesized beam. The choice of our final imaging parameters was the result of extensive experimentation to identify values that yielded the best combination of brightness-temperature sensitivity and reduction of artifacts resulting from strong sidelobes in the naturally weighted beam for these snapshot-like observations.

A primary beam correction was applied using the CASA task IMPBCOR before analyzing the images. The primary-beam-corrected continuum images at 3–33GHz are shown in Figure 1. The FWHM of the synthesized beam along with the corresponding point-source and brightness temperature sensitivities for each image are given in Tables 2 and 3. Finally, in order to accurately compare the flux density measured for each star-forming region across the full 3–33 GHz frequency range, we use



**Table 2.** Nuclear Source Positions and Imaging Characteristics

Galaxy	R.A.	Decl.	3 GHz			15 GHz		
			Synthesized	$\sigma$	$\sigma_{T_b}$	Synthesized	$\sigma$	$\sigma_{T_b}$
			Beam (J2000)	( $\mu\text{Jy bm}^{-1}$ )	(mK)	Beam (J2000)	( $\mu\text{Jy bm}^{-1}$ )	(mK)
NGC 0337	00 59 50.3	-07 34 44	2''43 × 1''74	18.7	597.32	2''00 × 1''13	9.1	21.71
NGC 0628	01 36 41.7	+15 46 59	1''96 × 1''78	14.0	543.15	1''55 × 1''19	9.6	28.14
NGC 0855	02 14 03.7	+27 52 38	1''80 × 1''62	13.2	613.61	1''50 × 1''25	8.6	24.93
NGC 0925	02 27 17.0	+33 34 43	1''80 × 1''59	13.0	611.30	1''47 × 1''23	9.1	27.04
NGC 1097	02 46 19.1	-30 16 28	5''76 × 1''80	44.9	586.45	3''81 × 0''99	16.9	24.11
NGC 1266	03 16 00.8	-02 25 38	2''20 × 1''78	14.0	485.33	1''80 × 1''17	11.3	28.86
NGC 1377	03 36 38.9	-20 54 06	3''56 × 1''71	17.4	385.40	2''61 × 1''09	11.6	21.93
IC 0342	03 46 48.5	+68 05 46	2''23 × 1''76	41.6	1430.61	1''72 × 1''13	11.4	31.44
NGC 1482	03 54 39.5	-20 30 07	3''25 × 1''67	16.8	419.18	2''42 × 1''33	14.1	23.56
NGC 2146	06 18 37.7	+78 21 25	2''55 × 1''55	35.5	1214.57	1''93 × 0''94	14.9	44.68
NGC 2403	07 36 50.0	+65 36 04	2''21 × 1''53	13.8	551.32	1''88 × 1''15	9.8	24.41
Holmberg II	08 19 13.3	+70 43 08	2''59 × 1''67	14.9	465.55	1''97 × 1''15	9.4	22.41
NGC 2798	09 17 22.8	+41 59 58	2''13 × 1''78	14.6	520.66	1''58 × 1''38	11.3	27.83
NGC 2841	09 22 02.7	+50 58 36	2''11 × 1''62	13.3	526.88	1''59 × 1''23	18.1	50.13
NGC 2976	09 47 15.3	+67 55 00	2''83 × 1''66	14.4	413.49	2''02 × 1''13	9.7	23.08
NGC 3049	09 54 49.6	+09 16 17	2''14 × 1''84	14.9	510.77	2''07 × 1''13	12.2	27.98
NGC 3077	10 03 19.1	+68 44 02	2''90 × 1''67	14.4	402.59	1''98 × 1''12	10.2	24.82
NGC 3190	10 18 05.6	+21 49 55	2''12 × 1''81	13.5	475.29	1''61 × 1''26	8.5	22.63
NGC 3184	10 18 16.7	+41 25 27	2''42 × 1''76	14.0	444.09	1''29 × 1''18	8.5	30.49
NGC 3198	10 19 54.9	+45 32 59	2''25 × 1''66	14.4	521.10	1''34 × 1''17	8.5	29.06
IC 2574	10 28 48.4	+68 28 02	2''96 × 1''64	14.2	393.53	2''03 × 1''14	8.8	20.73
NGC 3265	10 31 06.7	+28 47 48	2''23 × 1''78	14.9	505.30	1''44 × 1''25	7.8	23.42
NGC 3351	10 43 57.8	+11 42 14	2''00 × 1''75	18.4	708.89	1''95 × 1''67	15.3	25.34
NGC 3521	11 05 48.9	-00 02 06	3''07 × 1''95	19.9	448.93	1''88 × 1''19	16.4	39.79
NGC 3621	11 18 16.0	-32 48 42	4''76 × 1''53	15.7	291.11	4''17 × 1''08	8.5	10.16
NGC 3627	11 20 15.0	+12 59 30	1''95 × 1''77	15.7	616.48	2''36 × 1''97	14.0	16.23
NGC 3773	11 38 13.0	+12 06 45	1''95 × 1''76	13.1	518.26	1''53 × 1''14	9.8	30.21
NGC 3938	11 52 49.5	+44 07 14	3''13 × 1''73	15.1	376.61	1''25 × 1''10	7.9	31.23
NGC 4254	12 18 49.4	+14 24 59	1''99 × 1''81	15.3	577.12	1''53 × 1''11	9.0	28.58
NGC 4321	12 22 54.9	+15 49 21	1''89 × 1''72	15.0	622.65	1''53 × 1''17	9.8	29.55
NGC 4536	12 34 27.1	+02 11 17	2''16 × 1''86	15.5	524.37	2''44 × 1''45	10.2	15.58
NGC 4559	12 35 57.7	+27 57 36	1''75 × 1''63	13.6	646.04	1''32 × 1''27	9.0	29.13
NGC 4569	12 36 49.8	+13 09 46	2''01 × 1''80	15.4	572.68	1''68 × 1''18	10.7	29.15
NGC 4579	12 37 43.6	+11 49 02	2''12 × 1''85	23.4	807.73	1''72 × 1''21	50.9	132.87
NGC 4594	12 39 59.4	-11 37 23	2''76 × 1''74	19.7	554.75	2''01 × 1''09	13.4	32.88
NGC 4625	12 41 52.4	+41 16 24	1''73 × 1''56	13.5	677.51	1''54 × 1''17	9.7	29.19
NGC 4631	12 42 05.9	+32 32 22	1''85 × 1''76	14.3	597.52	2''29 × 1''83	12.9	16.71
NGC 4725	12 50 26.6	+25 30 06	1''85 × 1''76	13.5	561.64	1''33 × 1''26	9.0	29.20
NGC 4736	12 50 53.0	+41 07 14	1''72 × 1''55	13.9	706.09	2''25 × 2''06	13.4	15.67
NGC 4826	12 56 43.9	+21 41 00	1''97 × 1''75	14.3	559.38	1''46 × 1''33	10.1	28.20
NGC 5055	13 15 49.2	+42 01 49	1''76 × 1''60	12.8	619.07	1''51 × 1''17	9.7	29.58
NGC 5194	13 29 52.7	+47 11 43	1''79 × 1''57	17.0	820.75	1''54 × 1''15	9.3	28.43
NGC 5398	14 01 20.2	-33 04 09	6''62 × 1''76	20.6	239.46	3''98 × 1''03	8.4	11.09
NGC 5457	14 03 12.6	+54 20 57	1''82 × 1''67	13.9	619.05	1''55 × 1''10	8.6	27.29
NGC 5474	14 05 01.3	+53 39 44	1''83 × 1''71	14.3	616.05	1''49 × 1''07	11.9	40.40
NGC 5713	14 40 11.3	-00 17 27	2''55 × 1''77	17.6	526.76	2''35 × 1''80	15.4	19.67
NGC 5866	15 06 29.5	+55 45 48	1''92 × 1''63	13.8	595.03	1''62 × 1''20	15.4	42.92
NGC 6946	20 34 52.3	+60 09 14	2''03 × 1''64	16.1	655.75	2''15 × 1''12	9.5	21.44
NGC 7331	22 37 04.1	+34 24 56	1''82 × 1''67	15.1	672.97	1''51 × 1''21	10.0	29.80
NGC 7793	23 57 49.2	-32 35 24	4''77 × 1''62	14.0	245.06	4''47 × 1''08	9.4	10.50

NOTE—See Murphy et al. (2018a) for the 33 GHz imaging characteristics.

**Table 3.** Extranuclear Source Positions and Imaging Characteristics

Enuc. ID	R.A. Decl.		3 GHz			15 GHz		
			Synthesized	$\sigma$	$\sigma_{T_b}$	Synthesized	$\sigma$	$\sigma_{T_b}$
			Beam	( $\mu\text{Jy bm}^{-1}$ )	(mK)	Beam	( $\mu\text{Jy bm}^{-1}$ )	(mK)
NGC 0628 Enuc. 1	01 36 45.1	+15 47 51	1''96 × 1''78	14.0	542.77	1''56 × 1''21	9.8	28.16
NGC 0628 Enuc. 2	01 36 37.5	+15 45 12	1''96 × 1''78	14.0	544.62	1''57 × 1''22	9.6	27.27
NGC 0628 Enuc. 3	01 36 38.8	+15 44 25	1''96 × 1''78	14.0	542.12	1''57 × 1''23	9.6	26.82
NGC 0628 Enuc. 4	01 36 35.5	+15 50 11	1''96 × 1''78	13.8	537.98	1''56 × 1''20	8.0	23.07
NGC 1097 Enuc. 1	02 46 23.9	−30 17 51	5''76 × 1''80	41.2	537.94	3''76 × 0''95	11.8	17.84
NGC 1097 Enuc. 2	02 46 14.4	−30 15 05	5''76 × 1''80	38.3	500.07	3''80 × 0''98	11.4	16.42
NGC 2403 Enuc. 1	07 36 45.5	+65 37 00	2''21 × 1''53	13.7	548.00	1''86 × 1''16	9.4	23.61
NGC 2403 Enuc. 2	07 36 52.7	+65 36 46	2''21 × 1''53	13.7	547.71	1''85 × 1''15	9.5	23.96
NGC 2403 Enuc. 3	07 37 06.9	+65 36 39	2''21 × 1''53	13.7	548.41	1''84 × 1''16	9.7	24.51
NGC 2403 Enuc. 4	07 37 17.9	+65 33 46	2''21 × 1''53	13.7	546.14	1''80 × 1''15	9.5	24.86
NGC 2403 Enuc. 5	07 36 19.5	+65 37 04	2''21 × 1''53	13.5	541.72	1''79 × 1''15	9.5	24.84
NGC 2403 Enuc. 6	07 36 28.5	+65 33 50	2''21 × 1''53	13.5	541.23	1''77 × 1''13	9.7	26.15
NGC 2976 Enuc. 1	09 47 07.8	+67 55 52	2''83 × 1''66	14.5	415.03	1''99 × 1''13	9.8	23.62
NGC 2976 Enuc. 2	09 47 24.1	+67 53 57	2''83 × 1''66	14.4	412.17	1''97 × 1''13	10.0	24.19
NGC 3521 Enuc. 1	11 05 46.3	−00 04 10	3''07 × 1''95	19.4	436.89	1''92 × 1''22	14.0	32.41
NGC 3521 Enuc. 2	11 05 49.9	−00 03 40	3''07 × 1''95	19.8	445.88	2''05 × 1''11	11.7	27.66
NGC 3521 Enuc. 3	11 05 47.6	+00 00 33	3''07 × 1''95	18.9	425.62	2''21 × 1''13	11.6	25.02
NGC 3627 Enuc. 1	11 20 16.2	+12 57 50	1''95 × 1''77	15.4	604.26	1''50 × 1''22	9.0	26.70
NGC 3627 Enuc. 2	11 20 16.3	+12 58 44	1''95 × 1''77	15.7	614.25	1''92 × 1''41	15.7	31.48
NGC 3627 Enuc. 3	11 20 16.0	+12 59 52	1''95 × 1''77	15.7	616.15	1''51 × 1''17	13.4	40.92
NGC 3938 Enuc. 1	11 52 46.4	+44 07 01	3''13 × 1''73	15.0	374.91	1''27 × 1''12	8.3	31.38
NGC 3938 Enuc. 2	11 53 00.0	+44 07 55	3''13 × 1''73	14.8	368.03	1''27 × 1''12	8.3	31.40
NGC 4254 Enuc. 1	12 18 49.1	+14 23 59	1''99 × 1''81	15.1	567.30	1''55 × 1''14	8.5	26.05
NGC 4254 Enuc. 2	12 18 44.6	+14 24 25	1''99 × 1''81	15.3	575.22	1''51 × 1''16	9.6	29.55
NGC 4321 Enuc. 1	12 22 58.9	+15 49 35	1''89 × 1''72	14.9	620.02	1''53 × 1''18	9.8	29.30
NGC 4321 Enuc. 2	12 22 49.8	+15 50 29	1''89 × 1''72	14.9	618.78	1''52 × 1''18	9.9	29.98
NGC 4631 Enuc. 1	12 41 40.8	+32 31 51	1''87 × 1''75	14.0	577.02	1''66 × 1''27	9.1	23.44
NGC 4631 Enuc. 2	12 42 21.3	+32 33 07	1''85 × 1''76	13.9	578.32	1''61 × 1''28	9.0	23.48
NGC 4736 Enuc. 1	12 50 56.2	+41 07 20	1''72 × 1''55	13.9	705.86	1''54 × 1''17	12.9	38.89
NGC 5055 Enuc. 1	13 15 58.0	+42 00 26	1''76 × 1''60	13.1	630.58	1''50 × 1''17	9.9	30.50
NGC 5194 Enuc. 1	13 29 53.1	+47 12 40	1''79 × 1''57	16.8	810.49	1''53 × 1''14	9.1	28.20
NGC 5194 Enuc. 2	13 29 44.1	+47 10 21	1''74 × 1''52	17.0	863.15	1''52 × 1''14	8.9	27.62
NGC 5194 Enuc. 3	13 29 44.6	+47 09 55	1''74 × 1''52	16.9	858.25	1''52 × 1''14	9.1	28.37
NGC 5194 Enuc. 4	13 29 56.2	+47 14 07	1''79 × 1''57	16.0	768.85	1''52 × 1''14	9.5	29.61
NGC 5194 Enuc. 5	13 29 59.6	+47 14 01	1''79 × 1''57	16.1	773.77	1''52 × 1''14	9.7	30.21
NGC 5194 Enuc. 6	13 29 39.5	+47 08 35	1''74 × 1''52	15.8	805.61	1''51 × 1''12	8.7	27.81
NGC 5194 Enuc. 7	13 30 02.5	+47 09 52	1''74 × 1''52	17.8	904.22	1''52 × 1''11	9.3	29.80
NGC 5194 Enuc. 8	13 30 01.6	+47 12 52	1''79 × 1''57	16.7	803.48	1''58 × 1''18	9.7	28.04
NGC 5194 Enuc. 9	13 29 59.9	+47 11 12	1''79 × 1''57	17.0	819.52	1''59 × 1''16	10.7	31.20
NGC 5194 Enuc. 10	13 29 56.7	+47 10 46	1''74 × 1''52	18.1	921.23	1''59 × 1''16	10.8	31.55
NGC 5194 Enuc. 11	13 29 49.7	+47 13 29	1''79 × 1''57	16.3	783.23	1''57 × 1''21	12.8	36.27
NGC 5457 Enuc. 1	14 03 10.2	+54 20 58	1''82 × 1''67	13.8	615.51	1''55 × 1''10	8.4	26.65
NGC 5457 Enuc. 2	14 02 55.0	+54 22 27	1''81 × 1''63	14.1	643.39	1''54 × 1''09	8.5	27.14
NGC 5457 Enuc. 3	14 03 41.3	+54 19 05	1''82 × 1''67	14.1	627.94	4''68 × 2''20	25.0	13.13
NGC 5457 Enuc. 4	14 03 53.1	+54 22 06	1''82 × 1''73	13.8	590.56	1''54 × 1''08	9.5	30.71
NGC 5457 Enuc. 5	14 03 01.1	+54 14 29	1''81 × 1''63	13.8	629.72	1''49 × 1''07	10.8	36.48
NGC 5457 Enuc. 6	14 02 28.1	+54 16 26	1''86 × 1''67	13.7	596.38	1''53 × 1''06	11.9	39.68
NGC 5457 Enuc. 7	14 04 29.3	+54 23 46	1''82 × 1''73	13.7	589.02	1''50 × 1''04	13.0	44.82
NGC 5713 Enuc. 1	14 40 12.1	−00 17 47	2''55 × 1''77	17.6	525.60	2''35 × 1''80	15.9	20.36
NGC 5713 Enuc. 2	14 40 10.5	−00 17 47	2''55 × 1''77	17.6	527.29	2''35 × 1''80	15.9	20.36
NGC 6946 Enuc. 1	20 35 16.6	+60 10 57	2''03 × 1''64	15.2	616.55	2''07 × 1''10	8.3	19.75
NGC 6946 Enuc. 2	20 35 25.1	+60 10 03	2''03 × 1''64	15.0	609.01	2''00 × 1''09	9.8	24.32
NGC 6946 Enuc. 3	20 34 52.2	+60 12 41	2''03 × 1''64	15.0	608.66	2''09 × 1''09	8.7	20.65
NGC 6946 Enuc. 4	20 34 19.4	+60 10 09	2''03 × 1''64	14.8	603.01	2''45 × 1''90	10.1	11.78
NGC 6946 Enuc. 5	20 34 39.0	+60 04 53	2''06 × 1''63	15.1	604.38	1''91 × 1''11	8.8	22.34
NGC 6946 Enuc. 6	20 35 06.0	+60 11 01	2''03 × 1''64	15.7	636.59	1''95 × 1''11	8.6	21.28
NGC 6946 Enuc. 7	20 35 11.2	+60 08 60	2''03 × 1''64	15.7	636.59	2''14 × 1''13	8.8	19.64
NGC 6946 Enuc. 8	20 34 32.2	+60 10 20	2''05 × 1''63	15.8	639.98	1''99 × 1''11	8.7	21.20
NGC 6946 Enuc. 9	20 35 12.7	+60 08 53	2''03 × 1''64	15.7	636.59	2''14 × 1''13	8.8	19.64
NGC 7793 Enuc. 1	23 57 48.8	−32 36 59	4''77 × 1''62	13.9	243.82	4''62 × 1''09	9.6	10.26
NGC 7793 Enuc. 2	23 57 56.1	−32 35 40	4''77 × 1''62	14.0	244.33	4''71 × 1''11	9.8	10.09
NGC 7793 Enuc. 3	23 57 48.8	−32 34 53	4''77 × 1''62	14.0	245.29	4''47 × 1''08	8.8	9.84

NOTE—See Murphy et al. (2018a) for the 33 GHz imaging characteristics.

the CASA task IMSMOOTH to match all VLA images for each pointing to a common circularized, Gaussian, beam corresponding to the lowest angular resolution among all three frequency bands scaled by a factor of  $\sqrt{2} \times 0''.2$  (i.e., the pixel scale). This scaling factor eliminates cases for the convolution kernels used by IMSMOOTH to have length zero in any axis in units of pixels. We additionally crop all images to a common field-of-view (FOV) equal to the FOV of our 33 GHz observations (i.e., a primary beam FWHM of  $44''$ ).

### 3. ANCILLARY DATA AND PHOTOMETRY

In this section we provide a description of ancillary data used, as well as our procedure for extracting consistent aperture photometry across the full suite of multi-wavelength data available for galaxies in the SFRS.

#### 3.1. Ancillary Data

GALEX far-UV (FUV;  $1528\text{\AA}$ ) and near-UV (NUV;  $2271\text{\AA}$ ) data were taken from the GALEX Large Galaxy Atlas (Seibert 2007). The calibration uncertainty for these data is  $\sim 15\%$  in both bands. One galaxy, NGC 1377, does not have existing near- or far-UV imaging.

The  $H\alpha$  data used in this analysis is taken from the compilation presented in Leroy et al. (2012), where details about the data quality and preparation (e.g., correction for [NII] emission) can be found, as well as the SINGS archive. All  $H\alpha$  images were then further corrected for foreground stars. The typical resolution of the seeing-limited  $H\alpha$  images is  $\sim 1 - 2''$ , and the calibration uncertainty among these maps is taken to be  $\sim 20\%$ . Two galaxies, IC 342 and NGC 2146 do not have  $H\alpha$  imaging from SINGS.

Archival *Spitzer*  $8\mu\text{m}$  and  $24\mu\text{m}$  data were largely taken from the SINGS and Local Volume Legacy (LVL) legacy programs, and have a calibration uncertainty of  $\sim 5\%$ . Details on the associated observation strategies and data reduction steps can be found in Dale et al. (2007, 2009). Two galaxies, IC 342 and NGC 2146, were not a part of SINGS or LVL; their  $24\mu\text{m}$  imaging comes from Engelbracht et al. (2008).

Finally, in order to account for the significant differences between the point-spread functions (PSF) of the various telescopes used in this analysis, we implement the convolution kernels presented in Aniano et al. (2011) to convolve the instrumental PSF for each image, and produce a corrected Gaussian beam of  $7''$  at each wavelength.

#### 3.2. Region Identification and Aperture Photometry

To identify and characterize potential star-forming regions in the SFRS, we start by searching within an area

that is equal to twice the FWHM of the VLA primary beam at 33 GHz ( $\sim 160''$ ). Any region visually identified in least one radio band is retained for further investigation. The location of all radio-identified sources were compared with the  $8\mu\text{m}$  maps of each galaxy to determine if the source has a corresponding detection in the mid-IR, and is thus likely associated with a star-forming region. Sources characterized as potential background galaxies have no obvious  $8\mu\text{m}$  counterpart, and very rarely a 33 GHz counterpart. In total, we visually identified 389 regions for which we perform aperture photometry to determine those that are statistically significant detections. Of the 389 sources visually identified, 377 had a statistically significant detection (i.e.,  $S/N > 3$ ) in at least one band, which is given in Table 4. For completeness, the remaining 12 sources are still labeled in the panels of Figure 1 to demonstrate the full identification process we utilized.

Using the CASA task IMSTAT, we measured and report the 3–33 GHz flux densities for each region. The size of the apertures were hand-selected to fully encompass the visible extent of the 3–33 GHz radio flux density of each region, with an additional constraint of having a diameter equal to or larger than the FWHM of the synthesized beam for that pointing. We do not apply aperture corrections to our photometry given that we both convolve all images for a given pointing to common beam and use the same sized aperture at all wavelengths. Photometric uncertainties were conservatively estimated by taking the empirically measured noise from empty regions in each non primary beam corrected image, applying the empirical primary beam correction based on Equation 4 in EVLA Memo 195, and scaling by the ratio of the synthesized beam area to the adopted aperture area. This noise is then added in quadrature with the VLA calibration uncertainty ( $\sim 3\%$ ; Perley & Butler 2013). The median size of the apertures used for all 377 sources is  $164 \pm 6.3\text{pc}$  with a median absolute deviation of  $97\text{pc}$ . The aperture sizes used for each identified region is given in Table 4.

We additionally carried out photometry on the full VLA, GALEX,  $H\alpha$ , and *Spitzer*/MIPS  $24\mu\text{m}$  datasets after matching their resolution ( $7''$  FWHM), cropping each image to a common field of view, and re-gridding to a common pixel scale ( $0''.2$ ). In total, we identify 180 discrete sources, and critical apertures of  $7''$  were used in all cases. Unlike our native-resolution photometry, we report sources with upper-limits in all radio bands if a statistically significant detection exists in our ancillary GALEX and *Spitzer* imaging. The median size of the apertures used at  $7''$  resolution is  $259 \pm 7.2\text{pc}$  with a median absolute deviation of  $73\text{pc}$ . The UV and



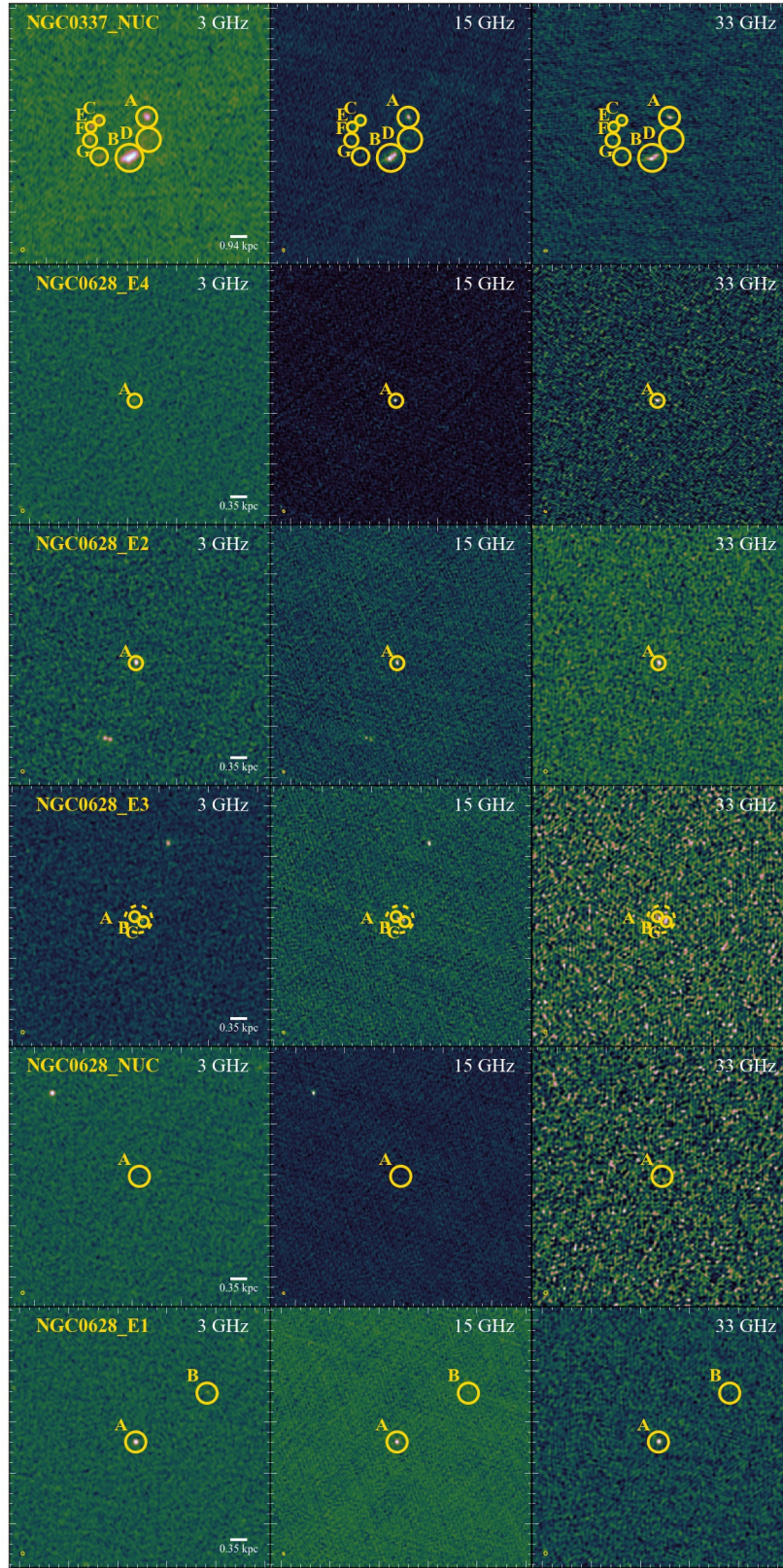


**Figure 1.** 3-panel images for all 56 galaxies in the SFRS showing the combination of our 3 GHz (left), 15 GHz (middle) and 33 GHz (right) observations. The color scale (Green 2011) is set to one of 4 power-law stretches:  $[a(p-p_{min})]/(p_{max}-p_{min})$ , where  $p$  is the pixel value and  $a = 1/3, 0.5, 1.0,$  and  $2.0$ . A cube-root stretch of  $a = 1/3$  was used when the brightest pixel in the image had a  $S/N > 500$ . A square-root stretch of  $a = 0.5$  was used when the brightest pixel in the image had an  $50 < S/N < 500$ . A linear stretch was used when the brightest pixel was between  $10 < S/N < 50$ , and a square stretch was used when the brightest pixel had a  $S/N < 10$ . A scalebar of  $10''$  is also given in the bottom right corner of each panel. To distinguish between individual sources identified in the full-resolution and  $7''$  smoothed maps, we use uppercase and lowercase letters as part of their names for reporting photometry in Tables 4 and 5, respectively. An extended version of this Figure is available in the Appendix.

H $\alpha$  photometry of each region was corrected for Milky Way extinction using [Schlegel et al. \(1998\)](#) assuming  $A_V/E(B - V) = 3.1$  and the modeled extinction curves of [Weingartner & Draine \(2001\)](#) and [Draine \(2003\)](#). The results from our radio photometry are given in Table 5. The GALEX, H $\alpha$ , and *Spitzer*/MIPS 24  $\mu$ m photometry results, which are presented in Table 6, are not used directly in the present analysis, but will be utilized for further studies.

Finally, in order to account for and remove any diffuse emission component that is most likely unassociated with the most recent star formation activity in the disks of these galaxies, we measure a local background value within the vicinity of each star-forming region. The local background was measured by placing an annulus a distance of 1.5 times the synthesized beam FWHM away from the center of the source position in both the full-resolution and smoothed maps. The median surface brightness within this annulus was then multiplied by the effective area of the beam to get an estimate of the local diffuse background emission. These values are given in Table 7. Further, we measure the frac-

tional contribution of the background emission for each region, and find that the median value is  $4.7 \pm 0.43\%$ ,  $6.6 \pm 0.79\%$ , and  $3.9 \pm 0.71\%$ , with median absolute deviations of 5.3%, 5.4%, and 4.5% for our 3, 15, and 33 GHz observations respectively. Importantly, these values are smaller than the 15 – 40% found for the regions studied at 25'' ( $\sim 1$  kpc) scales with the GBT ([Murphy et al. 2011](#)).

The regions, listed in Tables 4 and 5, are named according to the nearest 33 GHz image, with an alphabetical suffix if there are multiple regions corresponding to one image. For example, “NGC 2403 Enuc. 2 B” is the second of three regions within the VLA pointing of extranuclear region 2 in NGC 2403. We distinguish individual sources identified in the 7'' smoothed maps by instead using a lowercase letter. For example, “NGC 2403 Enuc. 2 b” is one of two regions in the image of extranuclear region 2 in NGC 2403, and is composed of the sum contribution of “NGC 2403 Enuc. 2 B” and “NGC 2403 Enuc. 2 C” in the full-resolution maps.

**Table 4.** Region Photometry and Derived Parameters

Source ID	R.A.	Decl.	$S_{3\text{ GHz}}$	$S_{15\text{ GHz}}$	$S_{33\text{ GHz}}$	$d_{\text{ap}}$	$r_G$	$\alpha$	$f_T^{33\text{ GHz}}$
	(J2000)	(J2000)	(mJy)	(mJy)	(mJy)	(pc)	(kpc)		
Star-Forming Regions									
NGC 0337 D	00 59 49.94	-07 34 47.60	$1.19 \pm 0.07$	$0.77 \pm 0.04$	$0.31 \pm 0.05$	655.	0.921	$-0.335 \pm 0.042$	$0.841 \pm 0.038$
NGC 0337 A	00 59 50.01	-07 34 34.33	$0.99 \pm 0.06$	$0.70 \pm 0.03$	$0.28 \pm 0.05$	561.	0.881	$-0.278 \pm 0.042$	$0.888 \pm 0.033$
NGC 0337 B	00 59 50.69	-07 34 58.26	$4.94 \pm 0.07$	$2.66 \pm 0.04$	$1.80 \pm 0.07$	749.	2.041	$-0.399 \pm 0.012$	$0.780 \pm 0.012$
NGC 0337 C	00 59 51.89	-07 34 36.20	$0.30 \pm 0.03$	$0.29 \pm 0.02$	$0.21 \pm 0.03$	281.	3.735	$-0.076 \pm 0.060$	$1.000 \pm 0.028$
NGC 0337 G	00 59 51.89	-07 34 57.50	$0.36 \pm 0.05$	$0.19 \pm 0.03$	$0.17 \pm 0.05$	468.	3.123	$-0.358 \pm 0.102$	$0.820 \pm 0.096$
NGC 0337 E	00 59 52.22	-07 34 40.10	$0.28 \pm 0.03$	$0.27 \pm 0.02$	$0.30 \pm 0.03$	281.	4.048	$0.022 \pm 0.059$	$1.000 \pm 0.022$
NGC 0337 F	00 59 52.26	-07 34 47.90	$0.28 \pm 0.04$	$0.19 \pm 0.02$	$0.22 \pm 0.04$	374.	3.753	$-0.159 \pm 0.087$	$0.968 \pm 0.051$
NGC 0628 Enuc. 4	01 36 35.69	+15 50 07.22	$0.27 \pm 0.03$	$0.26 \pm 0.02$	$0.23 \pm 0.03$	140.	7.614	$-0.043 \pm 0.065$	$1.000 \pm 0.029$
NGC 0628 Enuc. 2	01 36 37.64	+15 45 07.19	$0.51 \pm 0.03$	$0.35 \pm 0.02$	$0.29 \pm 0.04$	140.	4.468	$-0.233 \pm 0.044$	$0.921 \pm 0.031$
NGC 0628 Enuc. 3 C	01 36 38.63	+15 44 21.40	$0.28 \pm 0.02$	$0.21 \pm 0.02$	$0.23 \pm 0.04$	105.	5.798	$-0.149 \pm 0.057$	$0.974 \pm 0.033$
NGC 0628 Enuc. 3 A $^\dagger$	01 36 38.84	+15 44 22.90	$0.51 \pm 0.06$	$0.36 \pm 0.04$	$0.51 \pm 0.10$	279.	5.724	$-0.098 \pm 0.080$	$1.000 \pm 0.040$
NGC 0628 Enuc. 3 B	01 36 38.99	+15 44 24.40	$0.29 \pm 0.02$	$0.20 \pm 0.02$	$0.22 \pm 0.04$	105.	5.657	$-0.195 \pm 0.058$	$0.946 \pm 0.037$
NGC 0628 Enuc. 1 B	1 36 42.340	+15 48 16.84	$< 0.13$	$0.41 \pm 0.04$	$< 0.66$	209.	2.695	...	...
NGC 0628 Enuc. 1 A	01 36 45.25	+15 47 48.06	$0.27 \pm 0.04$	$0.26 \pm 0.04$	$0.26 \pm 0.07$	209.	2.466	$-0.010 \pm 0.111$	$1.000 \pm 0.045$
NGC 0855 C	02 14 03.56	+27 52 38.30	$1.81 \pm 0.06$	$1.06 \pm 0.04$	$0.74 \pm 0.07$	377.	0.072	$-0.346 \pm 0.027$	$0.831 \pm 0.025$
NGC 0855 A $^\dagger$	02 14 03.80	+27 52 37.85	$2.27 \pm 0.10$	$1.55 \pm 0.06$	$0.87 \pm 0.11$	613.	0.305	$-0.279 \pm 0.034$	$0.888 \pm 0.026$
NGC 0855 B	02 14 04.36	+27 52 36.80	$0.37 \pm 0.03$	$0.24 \pm 0.02$	$0.19 \pm 0.03$	189.	0.910	$-0.289 \pm 0.062$	$0.880 \pm 0.049$
NGC 0925 D	02 27 15.981	+33 33 38.58	$0.25 \pm 0.02$	$0.24 \pm 0.02$	$< 0.75$	133.	5.510	$-0.018 \pm 0.082$	$1.000 \pm 0.034$
NGC 0925 A	02 27 17.00	+33 34 43.00	$0.10 \pm 0.03$	$< 0.06$	$< 0.09$	177.	0.183	...	...
NGC 0925 B	02 27 20.62	+33 34 29.80	$0.22 \pm 0.02$	$0.17 \pm 0.02$	$< 0.21$	133.	2.097	$-0.174 \pm 0.095$	$0.959 \pm 0.057$
NGC 1097 Enuc. 2	02 46 14.40	-30 15 04.80	$1.32 \pm 0.25$	$< 0.16$	$0.26 \pm 0.08$	138.	7.378	$-0.684 \pm 0.147$	$0.358 \pm 0.301$
NGC 1097 D	02 46 18.34	-30 16 31.00	$11.86 \pm 0.10$	$2.97 \pm 0.04$	$2.23 \pm 0.07$	275.	0.813	$-0.809 \pm 0.009$	$0.059 \pm 0.024$
NGC 1097 B	02 46 18.96	-30 16 29.20	$7.10 \pm 0.10$	$3.35 \pm 0.04$	$3.03 \pm 0.07$	275.	0.052	$-0.409 \pm 0.010$	$0.769 \pm 0.010$

Table 4 continued



Table 4 (continued)

Source ID	R.A.	Decl.	$S_{3\text{ GHz}}$	$S_{15\text{ GHz}}$	$S_{33\text{ GHz}}$	$d_{\text{ap}}$	$r_G$	$\alpha$	$f_T^{33\text{ GHz}}$
	(J2000)	(J2000)	(mJy)	(mJy)	(mJy)	(pc)	(kpc)		
NGC 1097 A <sup>†</sup>	02 46 18.96	-30 16 29.20	104.78 ± 0.35	28.54 ± 0.15	21.13 ± 0.25	964.	0.052	-0.762 ± 0.003	0.183 ± 0.008
NGC 1097 E	02 46 19.08	-30 16 20.20	9.88 ± 0.10	2.96 ± 0.04	1.90 ± 0.07	275.	0.831	-0.733 ± 0.010	0.250 ± 0.022
NGC 1097 C	02 46 19.45	-30 16 33.70	12.16 ± 0.10	3.28 ± 0.04	2.35 ± 0.07	275.	0.514	-0.774 ± 0.008	0.152 ± 0.021
NGC 1097 Enuc. 1	02 46 23.90	-30 17 50.50	< 0.69	< 0.13	0.31 ± 0.05	688.	7.301	...	...
NGC 1266 C	03 16 00.76	-02 25 36.50	30.00 ± 0.03	8.94 ± 0.02	5.61 ± 0.07	445.	0.390	-0.749 ± 0.001	0.214 ± 0.003
NGC 1266 A <sup>†</sup>	03 16 00.76	-02 25 39.20	35.62 ± 0.08	6.89 ± 0.04	3.99 ± 0.16	1038.	0.267	-1.015 ± 0.004	0.234 ± 0.008
NGC 1266 B	03 16 00.76	-02 25 42.50	20.53 ± 0.03	4.63 ± 0.02	2.43 ± 0.07	445.	0.964	-0.924 ± 0.003	0.239 ± 0.006
NGC 1377	03 36 39.09	-20 54 06.60	0.20 ± 0.02	0.07 ± 0.02	0.06 ± 0.02	358.	0.344	-0.665 ± 0.141	0.396 ± 0.275
IC 342 B	03 46 47.80	+68 05 46.30	39.31 ± 0.12	18.40 ± 0.03	13.99 ± 0.08	64.	0.065	-0.458 ± 0.002	0.715 ± 0.002
IC 342 A <sup>†</sup>	03 46 48.45	+68 05 46.30	90.08 ± 0.30	36.82 ± 0.08	27.26 ± 0.20	159.	0.007	-0.539 ± 0.002	0.608 ± 0.003
IC 342 C	03 46 49.14	+68 05 48.40	23.28 ± 0.12	10.38 ± 0.03	8.02 ± 0.08	64.	0.074	-0.482 ± 0.003	0.685 ± 0.004
IC 342 D	03 46 50.918	+68 06 05.89	0.90 ± 0.12	0.13 ± 0.04	< 0.30	64.	0.404	-1.178 ± 0.184	0.227 ± 0.368
NGC 1482 C	03 54 38.73	-20 30 07.30	46.27 ± 0.03	12.80 ± 0.02	9.01 ± 0.15	438.	0.272	-0.795 ± 0.001	0.097 ± 0.003
NGC 1482 A <sup>†</sup>	03 54 38.97	-20 30 08.20	117.13 ± 0.09	24.25 ± 0.06	11.30 ± 0.40	1205.	0.104	-0.978 ± 0.002	0.236 ± 0.004
NGC 1482 B	03 54 39.22	-20 30 08.20	43.02 ± 0.03	12.63 ± 0.02	8.71 ± 0.14	438.	0.516	-0.759 ± 0.001	0.190 ± 0.003
NGC 2146 A	06 18 31.67	+78 21 43.84	6.15 ± 0.14	0.44 ± 0.06	2.29 ± 0.12	417.	3.862	-0.496 ± 0.024	0.667 ± 0.031
NGC 2146 B	06 18 33.90	+78 21 34.94	18.19 ± 0.08	1.15 ± 0.03	5.80 ± 0.06	250.	2.205	-0.542 ± 0.005	0.604 ± 0.007
NGC 2146 C	06 18 35.34	+78 21 30.75	36.86 ± 0.08	1.68 ± 0.03	9.97 ± 0.06	250.	1.322	-0.594 ± 0.002	0.523 ± 0.004
NGC 2146 D	06 18 38.35	+78 21 23.02	248.45 ± 0.22	21.18 ± 0.08	61.74 ± 0.15	667.	0.410	-0.700 ± 0.001	0.324 ± 0.002
NGC 2146 E	06 18 43.83	+78 21 11.70	13.61 ± 0.11	0.58 ± 0.04	3.59 ± 0.09	334.	3.245	-0.619 ± 0.011	0.480 ± 0.019
NGC 2403 Enuc. 5 C	07 36 19.35	+65 37 06.40	0.93 ± 0.03	0.75 ± 0.02	0.74 ± 0.02	62.	3.520	-0.101 ± 0.016	0.999 ± 0.008
NGC 2403 Enuc. 5 A <sup>†</sup>	07 36 19.84	+65 37 06.70	2.05 ± 0.06	2.09 ± 0.04	1.83 ± 0.05	140.	3.458	-0.038 ± 0.016	1.000 ± 0.007
NGC 2403 Enuc. 5 E	07 36 20.696	+65 38 04.84	0.24 ± 0.03	0.24 ± 0.03	< 0.47	62.	3.428	0.011 ± 0.098	1.000 ± 0.038
NGC 2403 Enuc. 5 B	07 36 22.99	+65 36 49.90	0.17 ± 0.03	0.17 ± 0.02	0.10 ± 0.03	62.	3.150	-0.109 ± 0.104	0.995 ± 0.053
NGC 2403 Enuc. 6 A	07 36 28.69	+65 33 49.95	0.87 ± 0.05	0.87 ± 0.04	0.78 ± 0.03	125.	5.369	-0.048 ± 0.029	1.000 ± 0.013
NGC 2403 Enuc. 6 B	07 36 29.56	+65 34 05.30	0.12 ± 0.03	< 0.06	0.05 ± 0.02	62.	4.933	-0.363 ± 0.165	0.815 ± 0.156
NGC 2403 Enuc. 1 E	07 36 38.042	+65 36 09.31	0.24 ± 0.03	0.29 ± 0.03	< 0.96	62.	1.529	0.110 ± 0.098	1.000 ± 0.030
NGC 2403 Enuc. 1 A	07 36 42.03	+65 36 51.67	0.51 ± 0.03	0.39 ± 0.02	0.25 ± 0.03	62.	1.085	-0.221 ± 0.040	0.929 ± 0.027
NGC 2403 C	07 36 42.562	+65 36 07.23	0.13 ± 0.03	0.14 ± 0.03	< 0.14	62.	0.952	0.038 ± 0.186	1.000 ± 0.067
NGC 2403 Enuc. 1 B	07 36 45.49	+65 37 01.39	1.52 ± 0.06	1.37 ± 0.04	1.14 ± 0.04	125.	1.203	-0.106 ± 0.021	0.997 ± 0.011
NGC 2403 Enuc. 1 C	07 36 45.74	+65 36 39.90	0.47 ± 0.03	0.10 ± 0.02	0.10 ± 0.03	62.	0.753	-0.799 ± 0.093	0.088 ± 0.249
NGC 2403 Enuc. 1 D	07 36 46.71	+65 36 37.50	0.20 ± 0.03	0.13 ± 0.02	0.11 ± 0.03	62.	0.697	-0.257 ± 0.103	0.904 ± 0.075
NGC 2403 Enuc. 2 B	07 36 49.15	+65 36 51.72	0.42 ± 0.04	0.32 ± 0.03	0.28 ± 0.04	94.	1.115	-0.167 ± 0.067	0.963 ± 0.040
NGC 2403 Enuc. 2 D	07 36 52.07	+65 36 48.40	0.64 ± 0.02	0.55 ± 0.02	0.56 ± 0.02	47.	1.258	-0.060 ± 0.018	1.000 ± 0.008
NGC 2403 Enuc. 2 A <sup>†</sup>	07 36 52.46	+65 36 45.70	2.14 ± 0.06	1.53 ± 0.04	1.48 ± 0.04	125.	1.229	-0.166 ± 0.016	0.964 ± 0.009
NGC 2403 Enuc. 2 C	07 36 52.80	+65 36 45.10	0.60 ± 0.02	0.45 ± 0.02	0.40 ± 0.02	47.	1.247	-0.170 ± 0.021	0.961 ± 0.013
NGC 2403 B	07 36 55.91	+65 35 38.49	0.19 ± 0.03	< 0.08	< 0.13	62.	0.699	...	...
NGC 2403 E	07 36 56.727	+65 35 12.17	0.14 ± 0.03	< 0.10	< 0.58	62.	1.101	...	...
NGC 2403 Enuc. 3 B	07 37 06.66	+65 36 38.40	3.81 ± 0.04	3.15 ± 0.03	2.89 ± 0.04	78.	2.763	-0.116 ± 0.006	0.992 ± 0.003
NGC 2403 Enuc. 4 B	07 37 16.55	+65 33 50.80	< 0.08	0.12 ± 0.02	0.07 ± 0.02	62.	3.305	-0.560 ± 0.358	0.577 ± 0.544
NGC 2403 Enuc. 4 C	07 37 18.14	+65 33 37.90	< 0.08	0.11 ± 0.02	0.08 ± 0.02	62.	3.556	-0.368 ± 0.359	0.810 ± 0.345
NGC 2403 Enuc. 4 A	07 37 18.30	+65 33 49.90	1.00 ± 0.06	0.99 ± 0.04	0.92 ± 0.03	125.	3.446	-0.037 ± 0.028	1.000 ± 0.012
Holmberg II B	08 19 12.69	+70 43 03.80	0.15 ± 0.02	0.14 ± 0.01	0.17 ± 0.02	44.	0.721	0.018 ± 0.078	1.000 ± 0.030
Holmberg II A	08 19 13.09	+70 43 08.90	0.33 ± 0.03	0.31 ± 0.02	0.34 ± 0.03	59.	0.739	-0.003 ± 0.048	1.000 ± 0.019
NGC 2798 B	09 17 22.56	+41 59 51.10	1.76 ± 0.02	0.61 ± 0.02	0.19 ± 0.03	375.	2.580	-0.693 ± 0.022	0.338 ± 0.045
NGC 2798 A	09 17 22.83	+42 00 01.00	11.23 ± 0.06	2.53 ± 0.06	0.93 ± 0.07	1001.	0.217	-0.945 ± 0.013	0.238 ± 0.027
NGC 2841 A	09 22 02.68	+50 58 35.74	0.64 ± 0.04	< 0.18	< 0.08	410.	0.171	...	...
NGC 2976 Enuc. 1 A	09 47 05.09	+67 55 51.70	1.14 ± 0.03	0.76 ± 0.02	0.75 ± 0.05	86.	1.432	-0.219 ± 0.020	0.930 ± 0.014
NGC 2976 Enuc. 1 D	09 47 07.64	+67 55 55.30	2.22 ± 0.02	1.80 ± 0.02	1.56 ± 0.03	69.	1.208	-0.136 ± 0.008	0.981 ± 0.004
NGC 2976 Enuc. 1 C	09 47 07.85	+67 55 48.10	0.48 ± 0.02	0.37 ± 0.01	0.33 ± 0.02	52.	1.111	-0.162 ± 0.027	0.966 ± 0.016
NGC 2976 Enuc. 1 B <sup>†</sup>	09 47 07.85	+67 55 53.98	3.26 ± 0.06	2.49 ± 0.05	2.01 ± 0.08	172.	1.178	-0.182 ± 0.014	0.954 ± 0.008
NGC 2976 B	09 47 13.54	+67 54 54.90	0.17 ± 0.02	0.16 ± 0.02	0.17 ± 0.03	69.	0.432	-0.017 ± 0.090	1.000 ± 0.037
NGC 2976 A	09 47 15.30	+67 55 00.00	< 0.07	0.15 ± 0.02	< 0.10	69.	0.000	...	...

Table 4 continued

Table 4 (continued)

Source ID	R.A.	Decl.	$S_{3\text{ GHz}}$	$S_{15\text{ GHz}}$	$S_{33\text{ GHz}}$	$d_{\text{ap}}$	$r_G$	$\alpha$	$f_T^{33\text{ GHz}}$
	(J2000)	(J2000)	(mJy)	(mJy)	(mJy)	(pc)	(kpc)		
NGC 2976 Enum. 2 A	09 47 23.94	+67 53 53.40	$1.67 \pm 0.04$	$1.46 \pm 0.03$	$1.25 \pm 0.06$	120.	1.421	$-0.098 \pm 0.018$	$1.000 \pm 0.009$
NGC 2976 Enum. 2 C	09 47 23.94	+67 54 05.40	$0.55 \pm 0.04$	$0.45 \pm 0.03$	$0.40 \pm 0.05$	103.	1.278	$-0.131 \pm 0.047$	$0.984 \pm 0.026$
NGC 2976 C	09 47 25.079	+67 55 09.45	$0.25 \pm 0.02$	< 0.07	< 0.48	69.	2.002	...	...
NGC 3049 A	09 54 49.56	+09 16 16.05	$1.47 \pm 0.04$	$0.53 \pm 0.04$	$0.47 \pm 0.04$	559.	0.110	$-0.546 \pm 0.032$	$0.598 \pm 0.048$
NGC 3049 B	09 54 50.05	+09 16 25.40	$0.32 \pm 0.03$	$0.22 \pm 0.02$	$0.16 \pm 0.03$	372.	1.033	$-0.272 \pm 0.070$	$0.893 \pm 0.053$
NGC 3049 C	09 54 51.46	+09 16 28.40	$0.21 \pm 0.02$	< 0.06	< 0.10	279.	3.622	...	...
NGC 3077 A	10 03 19.15	+68 43 59.90	$11.35 \pm 0.06$	$7.21 \pm 0.05$	$6.19 \pm 0.12$	186.	0.045	$-0.273 \pm 0.005$	$0.892 \pm 0.004$
NGC 3190 A	10 18 04.31	+21 49 31.79	$0.56 \pm 0.03$	$0.61 \pm 0.02$	$1.17 \pm 0.04$	374.	9.635	$0.315 \pm 0.024$	$1.000 \pm 0.005$
NGC 3184 B	10 18 11.442	+41 24 49.70	$0.33 \pm 0.04$	$0.20 \pm 0.04$	< 1.56	340.	4.382	$-0.323 \pm 0.153$	$0.851 \pm 0.132$
NGC 3184 A	10 18 16.91	+41 25 27.02	$0.65 \pm 0.04$	$0.33 \pm 0.03$	$0.30 \pm 0.03$	340.	0.057	$-0.363 \pm 0.044$	$0.815 \pm 0.042$
NGC 3198 B	10 19 50.990	+45 32 50.16	$0.21 \pm 0.04$	$0.14 \pm 0.03$	< 0.34	410.	5.622	$-0.233 \pm 0.193$	$0.921 \pm 0.134$
NGC 3198 A	10 19 55.02	+45 32 59.24	$0.49 \pm 0.04$	$0.28 \pm 0.03$	$0.19 \pm 0.05$	410.	0.180	$-0.354 \pm 0.074$	$0.824 \pm 0.068$
NGC 3198 C	10 19 57.979	+45 32 28.54	$0.17 \pm 0.04$	$0.17 \pm 0.03$	< 0.39	410.	8.035	$0.021 \pm 0.201$	$1.000 \pm 0.076$
IC 2574 D	10 28 40.72	+68 28 01.39	$0.98 \pm 0.03$	$0.31 \pm 0.02$	$0.48 \pm 0.08$	92.	5.606	$-0.596 \pm 0.040$	$0.520 \pm 0.066$
IC 2574 C	10 28 43.88	+68 28 26.90	$0.90 \pm 0.04$	$0.63 \pm 0.03$	$0.77 \pm 0.08$	129.	6.262	$-0.164 \pm 0.034$	$0.965 \pm 0.020$
IC 2574 A	10 28 48.41	+68 28 03.28	$0.60 \pm 0.03$	$0.50 \pm 0.02$	$0.48 \pm 0.03$	92.	5.247	$-0.105 \pm 0.031$	$0.997 \pm 0.016$
IC 2574 B	10 28 48.78	+68 28 35.90	$0.08 \pm 0.02$	$0.11 \pm 0.02$	< 0.13	73.	6.263	$0.157 \pm 0.195$	$1.000 \pm 0.053$
NGC 3265 A	10 31 06.77	+28 47 48.01	$2.76 \pm 0.05$	$0.67 \pm 0.03$	$0.43 \pm 0.04$	665.	0.090	$-0.849 \pm 0.024$	$0.245 \pm 0.053$
NGC 3351 C	10 43 55.25	+11 41 29.90	$2.20 \pm 0.04$	$1.04 \pm 0.04$	$1.21 \pm 0.19$	181.	2.844	$-0.439 \pm 0.024$	$0.737 \pm 0.028$
NGC 3351 A	10 43 57.67	+11 42 07.19	$7.20 \pm 0.06$	$2.75 \pm 0.04$	$1.95 \pm 0.05$	271.	0.267	$-0.572 \pm 0.009$	$0.558 \pm 0.013$
NGC 3351 B	10 43 57.77	+11 42 18.88	$8.84 \pm 0.06$	$3.55 \pm 0.04$	$2.26 \pm 0.05$	271.	0.271	$-0.567 \pm 0.007$	$0.566 \pm 0.011$
NGC 3521 Enum. 1	11 05 46.36	-00 04 10.10	$0.14 \pm 0.04$	$0.29 \pm 0.04$	< 0.15	271.	9.918	$0.469 \pm 0.194$	$1.000 \pm 0.025$
NGC 3521 Enum. 3 A	11 05 47.64	+00 00 32.80	< 0.20	$0.31 \pm 0.05$	< 0.18	489.	9.517	...	...
NGC 3521 Enum. 2 A	11 05 49.28	-00 03 26.70	$0.66 \pm 0.04$	$0.35 \pm 0.04$	$0.28 \pm 0.05$	271.	4.474	$-0.377 \pm 0.058$	$0.802 \pm 0.056$
NGC 3521 Enum. 3 C	11 05 49.421	-0 00 29.52	$0.99 \pm 0.07$	< 0.22	< 2.62	489.	6.970	...	...
NGC 3521 Enum. 2 B	11 05 51.04	-00 03 49.20	$0.30 \pm 0.04$	$0.36 \pm 0.04$	< 0.15	271.	5.824	$0.121 \pm 0.104$	$1.000 \pm 0.031$
NGC 3621 C	11 18 14.878	-32 47 35.40	$0.38 \pm 0.04$	$0.32 \pm 0.04$	< 2.10	191.	2.191	$-0.109 \pm 0.105$	$0.995 \pm 0.054$
NGC 3621 A	11 18 15.21	-32 48 39.60	$1.05 \pm 0.04$	$0.27 \pm 0.03$	< 0.16	191.	0.841	$-0.851 \pm 0.071$	$0.245 \pm 0.154$
NGC 3621 H	11 18 16.465	-32 48 56.84	$0.11 \pm 0.04$	< 0.09	< 0.17	191.	0.574	...	...
NGC 3621 G <sup>†</sup>	11 18 18.117	-32 49 39.41	$2.15 \pm 0.07$	$1.55 \pm 0.08$	< 2.71	381.	1.967	$-0.202 \pm 0.040$	$0.942 \pm 0.025$
NGC 3621 B	11 18 18.936	-32 47 44.04	$0.93 \pm 0.05$	$0.56 \pm 0.06$	< 2.97	254.	3.029	$-0.321 \pm 0.074$	$0.853 \pm 0.064$
NGC 3621 F	11 18 20.832	-32 48 53.41	$0.14 \pm 0.04$	< 0.12	< 1.22	191.	2.760	...	...
NGC 3621 E	11 18 21.542	-32 49 08.39	$0.62 \pm 0.04$	$0.19 \pm 0.05$	< 4.80	191.	3.143	$-0.722 \pm 0.162$	$0.277 \pm 0.362$
NGC 3627 Enum. 1 G	11 20 11.500	+12 57 55.42	$0.52 \pm 0.06$	< 0.33	< 2.45	318.	7.592	...	...
NGC 3627 Enum. 1 F	11 20 12.848	+12 57 56.98	$0.24 \pm 0.03$	< 0.15	< 0.32	182.	5.975	...	...
NGC 3627 Enum. 1 E	11 20 12.989	+12 57 36.49	$0.30 \pm 0.03$	< 0.15	$0.40 \pm 0.10$	182.	6.672	$0.124 \pm 0.116$	$1.000 \pm 0.034$
NGC 3627 B	11 20 13.34	+13 00 21.30	$3.99 \pm 0.07$	$2.42 \pm 0.10$	$1.46 \pm 0.37$	364.	3.072	$-0.319 \pm 0.028$	$0.855 \pm 0.024$
NGC 3627 A	11 20 15.01	+12 59 29.53	$1.95 \pm 0.05$	$1.10 \pm 0.06$	$0.69 \pm 0.05$	273.	0.023	$-0.397 \pm 0.026$	$0.781 \pm 0.027$
NGC 3627 Enum. 2 D	11 20 16.26	+12 58 44.30	$4.11 \pm 0.03$	$2.49 \pm 0.04$	$1.90 \pm 0.02$	136.	2.534	$-0.318 \pm 0.005$	$0.855 \pm 0.004$
NGC 3627 Enum. 1 A	11 20 16.33	+12 57 49.39	$2.42 \pm 0.05$	$1.44 \pm 0.06$	$1.26 \pm 0.05$	273.	4.706	$-0.282 \pm 0.017$	$0.885 \pm 0.013$
NGC 3627 Enum. 2 A <sup>†</sup>	11 20 16.53	+12 58 44.30	$7.18 \pm 0.09$	$4.22 \pm 0.12$	$3.51 \pm 0.08$	455.	2.781	$-0.304 \pm 0.010$	$0.868 \pm 0.008$
NGC 3627 Enum. 2 E	11 20 16.71	+12 58 43.40	$4.13 \pm 0.03$	$2.10 \pm 0.04$	$1.67 \pm 0.02$	136.	2.994	$-0.385 \pm 0.006$	$0.793 \pm 0.006$
NGC 3627 Enum. 2 C	11 20 17.98	+12 59 06.20	$0.43 \pm 0.03$	$0.43 \pm 0.05$	$0.24 \pm 0.05$	182.	4.390	$-0.124 \pm 0.072$	$0.987 \pm 0.038$
NGC 3627 Enum. 2 B	11 20 18.70	+12 59 24.20	$0.77 \pm 0.03$	$0.51 \pm 0.06$	< 0.38	182.	5.526	$-0.259 \pm 0.081$	$0.903 \pm 0.060$
NGC 3773	11 38 13.02	+12 06 44.10	$2.53 \pm 0.04$	$1.34 \pm 0.04$	$1.09 \pm 0.05$	481.	0.023	$-0.372 \pm 0.016$	$0.806 \pm 0.016$
NGC 3938 B	11 52 46.860	+44 08 07.38	$0.28 \pm 0.03$	< 0.08	< 0.59	434.	5.503	...	...
NGC 3938 Enum. 2 B	11 52 59.97	+44 08 00.00	$0.19 \pm 0.02$	$0.13 \pm 0.02$	$0.18 \pm 0.03$	347.	11.079	$-0.069 \pm 0.080$	$1.000 \pm 0.037$
NGC 3938 Enum. 2 A	11 53 00.20	+44 07 48.07	$0.34 \pm 0.03$	$0.28 \pm 0.02$	$0.23 \pm 0.04$	434.	11.048	$-0.139 \pm 0.061$	$0.979 \pm 0.034$
NGC 4254 Enum. 2 D	12 18 45.82	+14 24 09.80	< 0.09	$0.10 \pm 0.03$	$0.17 \pm 0.02$	279.	5.332	$0.670 \pm 0.371$	$1.000 \pm 0.029$
NGC 4254 Enum. 2 C	12 18 46.19	+14 24 11.90	< 0.07	< 0.06	$0.08 \pm 0.02$	209.	4.931	...	...
NGC 4254 Enum. 1 E	12 18 46.77	+14 23 51.00	$0.29 \pm 0.03$	$0.11 \pm 0.02$	< 0.14	279.	5.622	$-0.602 \pm 0.132$	$0.509 \pm 0.223$
NGC 4254 Enum. 2 E	12 18 47.495	+14 24 41.83	$0.14 \pm 0.03$	< 0.09	< 0.14	279.	2.617	...	...
NGC 4254	12 18 49.54	+14 25 01.40	$0.41 \pm 0.06$	$0.52 \pm 0.04$	$0.36 \pm 0.05$	559.	0.124	$-0.008 \pm 0.085$	$1.000 \pm 0.034$

Table 4 continued

Table 4 (continued)

Source ID	R.A.	Decl.	$S_{3\text{ GHz}}$	$S_{15\text{ GHz}}$	$S_{33\text{ GHz}}$	$d_{\text{ap}}$	$r_G$	$\alpha$	$f_T^{33\text{ GHz}}$
	(J2000)	(J2000)	(mJy)	(mJy)	(mJy)	(pc)	(kpc)		
NGC 4254 Enuc. 1 D	12 18 50.03	+14 24 17.10	0.79 ± 0.04	0.23 ± 0.02	0.35 ± 0.04	349.	3.167	-0.487 ± 0.047	0.678 ± 0.060
NGC 4254 Enuc. 1 B	12 18 50.07	+14 24 06.60	0.21 ± 0.05	0.12 ± 0.03	0.41 ± 0.05	419.	3.924	0.321 ± 0.100	1.000 ± 0.018
NGC 4254 Enuc. 1 C	12 18 50.44	+14 24 22.50	0.21 ± 0.02	< 0.05	0.13 ± 0.03	209.	2.953	-0.204 ± 0.110	0.941 ± 0.071
NGC 4321 Enuc. 2	12 22 49.90	+15 50 28.70	0.17 ± 0.04	< 0.08	0.11 ± 0.03	347.	8.026	-0.176 ± 0.132	0.958 ± 0.080
NGC 4321 C	12 22 54.46	+15 49 21.30	2.57 ± 0.03	1.09 ± 0.02	0.59 ± 0.03	277.	0.500	-0.560 ± 0.014	0.577 ± 0.021
NGC 4321 F	12 22 54.63	+15 49 14.70	0.93 ± 0.02	0.45 ± 0.02	0.31 ± 0.02	208.	0.514	-0.451 ± 0.024	0.723 ± 0.028
NGC 4321 H	12 22 54.92	+15 49 09.90	0.65 ± 0.02	0.31 ± 0.02	0.27 ± 0.02	208.	0.810	-0.401 ± 0.032	0.778 ± 0.033
NGC 4321 A <sup>†</sup>	12 22 54.92	+15 49 21.00	23.09 ± 0.12	8.99 ± 0.09	5.06 ± 0.11	1040.	0.024	-0.603 ± 0.006	0.508 ± 0.010
NGC 4321 B	12 22 54.94	+15 49 20.40	2.47 ± 0.02	0.79 ± 0.02	0.45 ± 0.02	208.	0.069	-0.707 ± 0.013	0.308 ± 0.028
NGC 4321 G	12 22 54.94	+15 49 29.40	1.77 ± 0.03	0.63 ± 0.02	0.38 ± 0.03	277.	0.605	-0.644 ± 0.022	0.435 ± 0.041
NGC 4321 D	12 22 55.29	+15 49 15.30	3.26 ± 0.03	1.27 ± 0.02	0.83 ± 0.03	277.	0.653	-0.578 ± 0.011	0.549 ± 0.017
NGC 4321 E	12 22 55.38	+15 49 23.40	3.94 ± 0.03	1.39 ± 0.02	0.87 ± 0.03	277.	0.547	-0.641 ± 0.010	0.442 ± 0.018
NGC 4321 Enuc. 1 B	12 22 58.82	+15 48 50.60	0.28 ± 0.02	0.17 ± 0.02	< 0.12	208.	5.246	-0.321 ± 0.094	0.853 ± 0.081
NGC 4536 C	12 34 26.94	+02 11 19.40	33.72 ± 0.03	12.67 ± 0.02	8.01 ± 0.03	281.	0.243	-0.605 ± 0.001	0.504 ± 0.002
NGC 4536 A <sup>†</sup>	12 34 27.08	+02 11 17.30	88.63 ± 0.10	28.11 ± 0.06	16.57 ± 0.09	844.	0.030	-0.710 ± 0.001	0.303 ± 0.003
NGC 4536 B	12 34 27.34	+02 11 15.50	27.18 ± 0.03	9.90 ± 0.02	6.51 ± 0.03	281.	0.330	-0.617 ± 0.001	0.483 ± 0.002
NGC 4559 E	12 35 55.427	+27 58 01.88	0.15 ± 0.04	0.12 ± 0.04	< 0.15	203.	1.703	-0.106 ± 0.245	0.997 ± 0.125
NGC 4559 C	12 35 56.27	+27 57 40.80	0.20 ± 0.04	0.18 ± 0.03	0.21 ± 0.03	203.	1.294	0.014 ± 0.100	1.000 ± 0.038
NGC 4559 D	12 35 57.59	+27 57 36.90	< 0.12	0.12 ± 0.03	< 0.07	203.	0.090	...	...
NGC 4559 B	12 35 58.36	+27 57 33.90	0.09 ± 0.03	0.16 ± 0.02	0.13 ± 0.02	135.	0.599	0.088 ± 0.123	1.000 ± 0.040
NGC 4559 A	12 35 58.45	+27 57 27.90	0.16 ± 0.02	0.10 ± 0.02	0.14 ± 0.01	102.	0.563	-0.051 ± 0.065	1.000 ± 0.029
NGC 4569 A	12 36 49.84	+13 09 46.59	2.89 ± 0.07	1.44 ± 0.07	0.88 ± 0.08	430.	0.051	-0.460 ± 0.026	0.711 ± 0.031
NGC 4579	12 37 43.52	+11 49 05.50	2.04 ± 0.13	2.76 ± 0.22	0.60 ± 0.18	795.	0.103	0.077 ± 0.060	1.000 ± 0.020
NGC 4594	12 39 59.43	-11 37 23.03	0.86 ± 0.09	0.46 ± 0.06	0.83 ± 0.08	440.	0.046	-0.048 ± 0.061	1.000 ± 0.027
NGC 4631 Enuc. 1	12 41 40.47	+32 31 50.00	0.51 ± 0.05	0.66 ± 0.04	0.61 ± 0.04	296.	13.669	0.058 ± 0.050	1.000 ± 0.017
NGC 4625 A	12 41 52.27	+41 16 25.50	< 0.12	0.11 ± 0.03	< 0.06	271.	0.190	...	...
NGC 4631 A	12 42 03.59	+32 32 16.28	7.26 ± 0.03	2.46 ± 0.04	1.51 ± 0.04	148.	3.389	-0.666 ± 0.008	0.393 ± 0.015
NGC 4631 H	12 42 04.17	+32 32 16.60	0.98 ± 0.03	1.31 ± 0.03	0.85 ± 0.04	148.	3.276	0.031 ± 0.019	1.000 ± 0.007
NGC 4631 B	12 42 04.38	+32 32 25.08	5.50 ± 0.04	3.32 ± 0.04	3.07 ± 0.04	185.	1.712	-0.265 ± 0.006	0.898 ± 0.004
NGC 4631 G	12 42 05.07	+32 32 12.40	0.91 ± 0.04	0.73 ± 0.04	0.62 ± 0.04	185.	4.464	-0.155 ± 0.029	0.970 ± 0.017
NGC 4631 Enuc. 2 B	12 42 22.22	+32 32 46.33	1.56 ± 0.07	1.40 ± 0.05	1.39 ± 0.06	369.	6.825	-0.052 ± 0.026	1.000 ± 0.012
NGC 4631 Enuc. 2 C	12 42 23.985	+32 32 08.65	< 0.11	0.22 ± 0.03	< 0.92	185.	12.785	...	...
NGC 4725 C	12 50 24.87	+25 29 22.80	0.22 ± 0.02	0.08 ± 0.02	< 0.12	173.	2.693	-0.597 ± 0.136	0.518 ± 0.226
NGC 4725 A	12 50 26.57	+25 30 02.72	0.07 ± 0.02	0.17 ± 0.01	0.30 ± 0.01	173.	0.034	0.641 ± 0.078	1.000 ± 0.007
NGC 4736 K	12 50 49.204	+41 07 33.20	0.61 ± 0.05	0.78 ± 0.08	< 0.42	136.	1.102	0.154 ± 0.078	1.000 ± 0.021
NGC 4736 J	12 50 49.219	+41 07 23.09	1.01 ± 0.05	0.49 ± 0.08	< 0.36	136.	1.017	-0.447 ± 0.100	0.727 ± 0.116
NGC 4736 I	12 50 49.604	+41 07 09.41	1.27 ± 0.05	0.65 ± 0.07	< 0.29	136.	0.922	-0.416 ± 0.073	0.762 ± 0.079
NGC 4736 G	12 50 49.935	+41 06 41.41	0.27 ± 0.05	< 0.24	< 0.43	136.	1.248	...	...
NGC 4736 L	12 50 50.030	+41 07 50.00	0.56 ± 0.05	< 0.24	< 0.48	136.	1.222	...	...
NGC 4736 H	12 50 50.045	+41 06 53.23	1.28 ± 0.05	1.08 ± 0.07	0.35 ± 0.10	136.	1.002	-0.159 ± 0.045	0.968 ± 0.026
NGC 4736 M	12 50 50.746	+41 07 38.18	0.16 ± 0.05	< 0.21	< 0.25	136.	0.872	...	...
NGC 4736 F	12 50 51.201	+41 06 49.50	1.35 ± 0.05	0.89 ± 0.07	< 0.23	136.	0.846	-0.262 ± 0.053	0.900 ± 0.040
NGC 4736 N	12 50 51.776	+41 07 48.36	0.26 ± 0.05	1.07 ± 0.07	< 0.27	136.	0.991	0.878 ± 0.117	1.000 ± 0.006
NGC 4736 A	12 50 53.050	+41 07 12.50	6.19 ± 0.05	2.13 ± 0.06	1.23 ± 0.05	136.	0.020	-0.668 ± 0.013	0.389 ± 0.025
NGC 4736 O	12 50 53.190	+41 07 46.40	0.17 ± 0.05	0.44 ± 0.07	0.38 ± 0.08	136.	0.914	0.345 ± 0.137	1.000 ± 0.024
NGC 4736 E	12 50 54.070	+41 06 29.06	< 0.14	0.77 ± 0.08	< 0.41	136.	1.200	...	...
NGC 4736 P	12 50 54.541	+41 07 48.36	1.06 ± 0.05	0.30 ± 0.07	0.61 ± 0.10	136.	1.069	-0.316 ± 0.064	0.857 ± 0.054
NGC 4736 D	12 50 54.565	+41 06 36.52	0.59 ± 0.05	1.05 ± 0.08	0.43 ± 0.11	136.	1.029	0.259 ± 0.061	1.000 ± 0.013
NGC 4736 Enuc. 1 D	12 50 55.99	+41 07 26.60	0.16 ± 0.03	0.33 ± 0.05	0.27 ± 0.03	90.	0.869	0.203 ± 0.091	1.000 ± 0.022
NGC 4736 Enuc. 1 A	12 50 56.35	+41 07 17.00	1.55 ± 0.05	1.06 ± 0.08	0.88 ± 0.04	136.	0.860	-0.238 ± 0.022	0.918 ± 0.015
NGC 4736 Enuc. 1 B	12 50 56.65	+41 07 04.40	2.79 ± 0.05	1.59 ± 0.08	1.03 ± 0.05	136.	0.928	-0.399 ± 0.017	0.780 ± 0.018
NGC 4736 Enuc. 1 C	12 50 56.83	+41 06 47.52	1.37 ± 0.05	1.13 ± 0.08	0.64 ± 0.07	136.	1.133	-0.228 ± 0.036	0.924 ± 0.025
NGC 4736 Enuc. 1 E	12 50 56.84	+41 07 23.00	0.09 ± 0.02	< 0.12	0.14 ± 0.02	68.	1.033	0.205 ± 0.126	1.000 ± 0.030

Table 4 continued

Table 4 (continued)

Source ID	R.A.	Decl.	$S_{3\text{ GHz}}$	$S_{15\text{ GHz}}$	$S_{33\text{ GHz}}$	$d_{\text{ap}}$	$r_G$	$\alpha$	$f_{\text{T}}^{33\text{ GHz}}$
	(J2000)	(J2000)	(mJy)	(mJy)	(mJy)	(pc)	(kpc)		
NGC 4826 C	12 56 43.11	+21 40 54.79	$0.72 \pm 0.02$	$0.48 \pm 0.02$	$0.22 \pm 0.02$	77.	0.427	$-0.344 \pm 0.028$	$0.833 \pm 0.026$
NGC 4826 B	12 56 43.11	+21 41 06.79	$0.72 \pm 0.02$	$0.53 \pm 0.02$	$0.25 \pm 0.02$	77.	0.295	$-0.295 \pm 0.027$	$0.874 \pm 0.021$
NGC 4826 A	12 56 43.61	+21 41 00.41	$12.21 \pm 0.04$	$4.55 \pm 0.04$	$2.83 \pm 0.04$	153.	0.034	$-0.611 \pm 0.005$	$0.494 \pm 0.008$
NGC 4826 F <sup>†</sup>	12 56 43.73	+21 41 00.90	$10.97 \pm 0.12$	$9.71 \pm 0.12$	$3.61 \pm 0.10$	409.	0.049	$-0.212 \pm 0.009$	$0.935 \pm 0.006$
NGC 4826 E	12 56 43.84	+21 41 11.40	$0.43 \pm 0.02$	$0.46 \pm 0.02$	$0.14 \pm 0.02$	77.	0.558	$-0.095 \pm 0.039$	$1.000 \pm 0.020$
NGC 4826 D	12 56 44.34	+21 40 55.99	$0.57 \pm 0.02$	$0.33 \pm 0.02$	$0.31 \pm 0.02$	77.	0.250	$-0.268 \pm 0.029$	$0.896 \pm 0.021$
NGC 5055 C	13 15 46.766	+42 02 01.43	$0.14 \pm 0.03$	$< 0.07$	$< 0.11$	154.	1.349	...	...
NGC 5055 D	13 15 47.919	+42 01 41.96	$0.22 \pm 0.03$	$0.19 \pm 0.02$	$< 0.08$	154.	0.722	$-0.070 \pm 0.104$	$1.000 \pm 0.049$
NGC 5055 A	13 15 49.29	+42 01 45.82	$1.99 \pm 0.04$	$1.01 \pm 0.03$	$0.33 \pm 0.04$	231.	0.054	$-0.475 \pm 0.022$	$0.693 \pm 0.027$
NGC 5055 B	13 15 50.20	+42 01 01.90	$1.20 \pm 0.03$	$0.29 \pm 0.03$	$< 0.24$	154.	2.805	$-0.875 \pm 0.057$	$0.243 \pm 0.123$
NGC 5055 E nuc. 1	13 15 58.32	+42 00 27.10	$0.47 \pm 0.04$	$0.43 \pm 0.03$	$0.40 \pm 0.03$	231.	5.645	$-0.060 \pm 0.048$	$1.000 \pm 0.022$
NGC 5194 E nuc. 6	13 29 39.32	+47 08 38.90	$0.68 \pm 0.06$	$0.53 \pm 0.03$	$0.56 \pm 0.02$	222.	12.377	$-0.066 \pm 0.038$	$1.000 \pm 0.018$
NGC 5194 E nuc. 3 B	13 29 43.77	+47 10 00.65	$< 0.19$	$0.35 \pm 0.03$	$0.13 \pm 0.03$	222.	7.645	$-1.260 \pm 0.290$	$0.224 \pm 0.574$
NGC 5194 E nuc. 3 A	13 29 45.06	+47 09 58.43	$0.81 \pm 0.08$	$0.55 \pm 0.04$	$0.58 \pm 0.03$	259.	7.051	$-0.130 \pm 0.045$	$0.985 \pm 0.024$
NGC 5194 E nuc. 11 G	13 29 45.117	+47 13 32.37	$0.29 \pm 0.04$	$< 0.11$	$0.30 \pm 0.05$	148.	5.358	$0.017 \pm 0.095$	$1.000 \pm 0.036$
NGC 5194 E nuc. 11 A	13 29 47.07	+47 13 40.72	$0.47 \pm 0.04$	$< 0.10$	$0.22 \pm 0.03$	148.	4.942	$-0.318 \pm 0.063$	$0.855 \pm 0.054$
NGC 5194 E nuc. 11 B	13 29 47.52	+47 13 25.14	$< 0.13$	$0.16 \pm 0.03$	$0.18 \pm 0.02$	148.	4.365	$0.203 \pm 0.299$	$1.000 \pm 0.073$
NGC 5194 E nuc. 11 C	13 29 49.56	+47 13 28.04	$< 0.13$	$0.10 \pm 0.03$	$0.15 \pm 0.02$	148.	4.057	$0.508 \pm 0.422$	$1.000 \pm 0.049$
NGC 5194 E nuc. 11 D	13 29 49.57	+47 14 00.06	$0.85 \pm 0.04$	$0.27 \pm 0.03$	$0.11 \pm 0.03$	148.	5.220	$-0.761 \pm 0.068$	$0.185 \pm 0.168$
NGC 5194 H	13 29 49.96	+47 11 25.90	$2.92 \pm 0.09$	$1.22 \pm 0.06$	$0.29 \pm 0.08$	296.	1.968	$-0.569 \pm 0.034$	$0.563 \pm 0.052$
NGC 5194 L	13 29 50.26	+47 11 46.90	$1.66 \pm 0.07$	$0.66 \pm 0.04$	$0.17 \pm 0.05$	222.	1.450	$-0.614 \pm 0.044$	$0.490 \pm 0.076$
NGC 5194 M	13 29 50.32	+47 11 37.90	$0.68 \pm 0.03$	$0.25 \pm 0.02$	$0.13 \pm 0.02$	111.	1.520	$-0.642 \pm 0.051$	$0.439 \pm 0.094$
NGC 5194 E nuc. 11 E	13 29 50.48	+47 13 45.15	$0.20 \pm 0.03$	$0.23 \pm 0.02$	$0.16 \pm 0.02$	111.	4.641	$-0.118 \pm 0.077$	$0.991 \pm 0.041$
NGC 5194 A	13 29 50.69	+47 11 55.79	$1.41 \pm 0.05$	$0.55 \pm 0.03$	$0.26 \pm 0.03$	148.	1.185	$-0.624 \pm 0.032$	$0.473 \pm 0.056$
NGC 5194 E nuc. 11 F	13 29 50.92	+47 13 43.64	$0.24 \pm 0.03$	$0.14 \pm 0.02$	$0.14 \pm 0.02$	111.	4.592	$-0.251 \pm 0.073$	$0.908 \pm 0.053$
NGC 5194 K	13 29 51.43	+47 12 00.40	$0.86 \pm 0.05$	$0.66 \pm 0.03$	$0.22 \pm 0.03$	148.	0.876	$-0.263 \pm 0.039$	$0.899 \pm 0.029$
NGC 5194 B	13 29 51.57	+47 12 08.43	$1.96 \pm 0.05$	$0.64 \pm 0.03$	$0.38 \pm 0.04$	148.	1.045	$-0.695 \pm 0.025$	$0.335 \pm 0.053$
NGC 5194 G	13 29 51.79	+47 11 38.50	$1.14 \pm 0.05$	$0.48 \pm 0.03$	$0.10 \pm 0.03$	148.	0.629	$-0.580 \pm 0.040$	$0.546 \pm 0.063$
NGC 5194 J	13 29 52.23	+47 12 03.40	$0.59 \pm 0.03$	$0.14 \pm 0.02$	$0.07 \pm 0.02$	111.	0.777	$-0.888 \pm 0.079$	$0.242 \pm 0.170$
NGC 5194 E	13 29 52.59	+47 11 52.90	$12.56 \pm 0.09$	$4.37 \pm 0.05$	$1.69 \pm 0.05$	296.	0.379	$-0.705 \pm 0.008$	$0.313 \pm 0.016$
NGC 5194 O	13 29 52.61	+47 11 22.90	$0.38 \pm 0.07$	$0.47 \pm 0.04$	$< 0.13$	222.	0.813	$0.131 \pm 0.125$	$1.000 \pm 0.036$
NGC 5194 I	13 29 52.76	+47 11 42.40	$5.37 \pm 0.03$	$1.42 \pm 0.02$	$0.70 \pm 0.02$	111.	0.037	$-0.835 \pm 0.008$	$0.246 \pm 0.016$
NGC 5194 C <sup>†</sup>	13 29 52.77	+47 11 40.90	$10.73 \pm 0.06$	$2.82 \pm 0.03$	$1.21 \pm 0.03$	185.	0.082	$-0.855 \pm 0.007$	$0.245 \pm 0.014$
NGC 5194 E nuc. 1 A	13 29 53.22	+47 12 40.00	$0.33 \pm 0.04$	$0.10 \pm 0.02$	$0.26 \pm 0.03$	148.	2.368	$-0.102 \pm 0.071$	$0.999 \pm 0.036$
NGC 5194 E nuc. 4 D	13 29 53.90	+47 14 04.90	$< 0.09$	$< 0.05$	$0.12 \pm 0.02$	111.	5.873	...	...
NGC 5194 N	13 29 54.14	+47 11 27.40	$1.33 \pm 0.07$	$0.27 \pm 0.04$	$< 0.14$	222.	0.919	$-0.996 \pm 0.098$	$0.235 \pm 0.203$
NGC 5194 F	13 29 55.12	+47 11 34.39	$0.76 \pm 0.06$	$0.51 \pm 0.03$	$0.31 \pm 0.04$	185.	1.412	$-0.305 \pm 0.053$	$0.867 \pm 0.043$
NGC 5194 E nuc. 4 C	13 29 55.73	+47 13 48.40	$0.16 \pm 0.03$	$0.11 \pm 0.02$	$0.11 \pm 0.02$	111.	5.770	$-0.149 \pm 0.099$	$0.974 \pm 0.056$
NGC 5194 P	13 29 55.85	+47 11 55.90	$0.71 \pm 0.05$	$0.28 \pm 0.03$	$0.16 \pm 0.04$	148.	2.119	$-0.586 \pm 0.066$	$0.536 \pm 0.107$
NGC 5194 E nuc. 4 E	13 29 56.20	+47 14 08.50	$< 0.09$	$< 0.05$	$0.05 \pm 0.01$	111.	6.690	...	...
NGC 5194 E nuc. 10	13 29 56.73	+47 10 45.70	$0.71 \pm 0.07$	$0.35 \pm 0.04$	$0.35 \pm 0.04$	222.	2.829	$-0.326 \pm 0.063$	$0.849 \pm 0.055$
NGC 5194 E nuc. 4 B	13 29 57.62	+47 13 54.82	$0.11 \pm 0.03$	$< 0.05$	$0.07 \pm 0.02$	111.	6.717	$-0.217 \pm 0.156$	$0.932 \pm 0.104$
NGC 5194 E nuc. 5 B	13 29 58.92	+47 14 09.40	$0.27 \pm 0.04$	$0.18 \pm 0.03$	$0.15 \pm 0.03$	148.	7.776	$-0.264 \pm 0.100$	$0.899 \pm 0.075$
NGC 5194 E nuc. 4 F	13 29 59.00	+47 14 09.10	$0.21 \pm 0.03$	$0.15 \pm 0.02$	$0.09 \pm 0.02$	111.	7.798	$-0.298 \pm 0.095$	$0.873 \pm 0.077$
NGC 5194 E nuc. 4 G	13 29 59.59	+47 13 59.50	$0.56 \pm 0.04$	$0.29 \pm 0.03$	$0.14 \pm 0.03$	148.	7.726	$-0.456 \pm 0.064$	$0.717 \pm 0.076$
NGC 5194 E nuc. 5 A	13 29 59.64	+47 13 59.43	$0.64 \pm 0.05$	$0.35 \pm 0.03$	$0.38 \pm 0.04$	185.	7.748	$-0.252 \pm 0.051$	$0.908 \pm 0.037$
NGC 5194 E nuc. 9	13 29 59.84	+47 11 12.60	$0.40 \pm 0.06$	$0.36 \pm 0.03$	$0.38 \pm 0.04$	185.	4.166	$-0.021 \pm 0.073$	$1.000 \pm 0.030$
NGC 5194 E nuc. 8 C	13 30 00.33	+47 13 19.90	$0.34 \pm 0.04$	$0.27 \pm 0.02$	$< 0.13$	148.	6.815	$-0.132 \pm 0.097$	$0.983 \pm 0.053$
NGC 5194 E nuc. 8 B	13 30 00.69	+47 13 06.93	$0.67 \pm 0.07$	$0.64 \pm 0.03$	$0.22 \pm 0.05$	222.	6.622	$-0.128 \pm 0.065$	$0.985 \pm 0.035$
NGC 5194 E nuc. 7 E	13 30 01.00	+47 09 28.90	$< 0.14$	$0.19 \pm 0.02$	$0.27 \pm 0.04$	148.	6.204	$0.479 \pm 0.250$	$1.000 \pm 0.031$
NGC 5194 E nuc. 8 A	13 30 01.39	+47 12 51.33	$0.55 \pm 0.07$	$0.53 \pm 0.03$	$0.39 \pm 0.04$	222.	6.591	$-0.119 \pm 0.065$	$0.990 \pm 0.034$
NGC 5194 E nuc. 7 A	13 30 02.28	+47 09 47.77	$1.20 \pm 0.07$	$0.40 \pm 0.03$	$0.34 \pm 0.05$	222.	6.301	$-0.612 \pm 0.047$	$0.493 \pm 0.081$
NGC 5194 E nuc. 7 C	13 30 02.76	+47 09 56.80	$0.41 \pm 0.05$	$0.18 \pm 0.02$	$0.17 \pm 0.03$	148.	6.369	$-0.428 \pm 0.077$	$0.748 \pm 0.085$

Table 4 continued

Table 4 (continued)

Source ID	R.A.	Decl.	$S_{3\text{ GHz}}$	$S_{15\text{ GHz}}$	$S_{33\text{ GHz}}$	$d_{\text{ap}}$	$r_G$	$\alpha$	$f_T^{33\text{ GHz}}$
	(J2000)	(J2000)	(mJy)	(mJy)	(mJy)	(pc)	(kpc)		
NGC 5194 E nuc. 7 B	13 30 03.50	+47 09 41.14	$0.32 \pm 0.06$	$0.16 \pm 0.03$	$< 0.13$	185.	6.961	$-0.420 \pm 0.146$	$0.758 \pm 0.159$
NGC 5194 E nuc. 7 F	13 30 05.06	+47 10 34.90	$5.47 \pm 0.05$	$1.81 \pm 0.03$	$< 0.32$	148.	7.231	$-0.688 \pm 0.010$	$0.349 \pm 0.021$
NGC 5194 E nuc. 8 D	13 30 07.391	+47 13 22.05	$0.29 \pm 0.04$	$0.20 \pm 0.03$	$< 0.98$	148.	10.734	$-0.238 \pm 0.141$	$0.918 \pm 0.099$
NGC 5398	14 01 20.11	-33 04 10.66	$2.40 \pm 0.06$	$1.71 \pm 0.03$	$1.68 \pm 0.03$	334.	1.417	$-0.152 \pm 0.013$	$0.972 \pm 0.007$
NGC 5457 E nuc. 6 A	14 02 28.23	+54 16 26.55	$1.05 \pm 0.04$	$0.94 \pm 0.04$	$0.55 \pm 0.04$	195.	15.711	$-0.179 \pm 0.028$	$0.956 \pm 0.017$
NGC 5457 E nuc. 6 E	14 02 28.34	+54 16 36.20	$0.67 \pm 0.04$	$0.45 \pm 0.03$	$0.45 \pm 0.03$	162.	15.525	$-0.183 \pm 0.035$	$0.954 \pm 0.022$
NGC 5457 E nuc. 6 B	14 02 29.59	+54 16 15.85	$2.34 \pm 0.05$	$1.57 \pm 0.04$	$0.76 \pm 0.05$	227.	15.552	$-0.323 \pm 0.019$	$0.851 \pm 0.016$
NGC 5457 E nuc. 6 C	14 02 30.59	+54 16 09.84	$1.01 \pm 0.03$	$0.74 \pm 0.03$	$0.57 \pm 0.03$	130.	15.416	$-0.214 \pm 0.022$	$0.934 \pm 0.015$
NGC 5457 E nuc. 6 D	14 02 30.64	+54 16 01.20	$0.58 \pm 0.03$	$0.37 \pm 0.03$	$0.32 \pm 0.04$	130.	15.563	$-0.260 \pm 0.044$	$0.902 \pm 0.032$
NGC 5457 E nuc. 6 F	14 02 31.08	+54 15 49.70	$0.21 \pm 0.02$	$0.11 \pm 0.02$	$< 0.15$	97.	15.678	$-0.402 \pm 0.137$	$0.776 \pm 0.142$
NGC 5457 E nuc. 2 B	14 02 51.05	+54 22 09.50	$0.13 \pm 0.02$	$0.12 \pm 0.01$	$< 0.11$	97.	7.282	$-0.086 \pm 0.127$	$1.000 \pm 0.062$
NGC 5457 E nuc. 2 C	14 02 59.329	+54 23 23.97	$0.16 \pm 0.02$	$0.06 \pm 0.02$	$< 0.78$	97.	6.670	$-0.631 \pm 0.213$	$0.459 \pm 0.384$
NGC 5457 E nuc. 5 B	14 03 01.10	+54 14 30.50	$1.48 \pm 0.03$	$1.20 \pm 0.02$	$1.13 \pm 0.02$	130.	13.068	$-0.118 \pm 0.012$	$0.991 \pm 0.006$
NGC 5457 E nuc. 5 A <sup>†</sup>	14 03 01.17	+54 14 26.90	$2.11 \pm 0.06$	$2.16 \pm 0.04$	$1.28 \pm 0.05$	260.	13.180	$-0.114 \pm 0.017$	$0.993 \pm 0.009$
NGC 5457 E nuc. 5 C	14 03 01.24	+54 14 23.60	$0.88 \pm 0.03$	$0.62 \pm 0.02$	$0.68 \pm 0.02$	130.	13.282	$-0.123 \pm 0.020$	$0.988 \pm 0.010$
NGC 5457 E nuc. 1	14 03 10.17	+54 20 58.10	$0.10 \pm 0.02$	$< 0.04$	$0.08 \pm 0.01$	97.	0.756	$-0.106 \pm 0.109$	$0.997 \pm 0.056$
NGC 5457	14 03 12.50	+54 20 56.40	$0.87 \pm 0.05$	$0.24 \pm 0.03$	$0.37 \pm 0.03$	195.	0.036	$-0.445 \pm 0.041$	$0.729 \pm 0.047$
NGC 5457 E nuc. 3 E	14 03 34.039	+54 18 36.69	$0.23 \pm 0.03$	$0.19 \pm 0.05$	$< 1.61$	130.	8.447	$-0.121 \pm 0.197$	$0.989 \pm 0.105$
NGC 5457 E nuc. 3 D	14 03 38.63	+54 18 49.30	$0.60 \pm 0.03$	$0.35 \pm 0.04$	$< 0.15$	130.	9.430	$-0.329 \pm 0.072$	$0.846 \pm 0.063$
NGC 5457 E nuc. 3 A	14 03 39.85	+54 18 56.58	$0.91 \pm 0.04$	$0.87 \pm 0.04$	$0.67 \pm 0.05$	162.	9.645	$-0.093 \pm 0.030$	$1.000 \pm 0.015$
NGC 5457 E nuc. 3 B	14 03 41.46	+54 19 04.95	$11.51 \pm 0.07$	$9.26 \pm 0.08$	$7.34 \pm 0.08$	292.	9.971	$-0.170 \pm 0.004$	$0.962 \pm 0.003$
NGC 5457 E nuc. 3 C	14 03 42.98	+54 19 24.77	$0.97 \pm 0.04$	$0.56 \pm 0.06$	$0.41 \pm 0.07$	195.	10.132	$-0.352 \pm 0.052$	$0.825 \pm 0.048$
NGC 5457 E nuc. 4 A	14 03 51.86	+54 21 52.80	$0.42 \pm 0.04$	$0.25 \pm 0.03$	$0.23 \pm 0.03$	162.	12.097	$-0.271 \pm 0.061$	$0.893 \pm 0.047$
NGC 5457 E nuc. 4 B	14 03 53.04	+54 21 56.31	$0.34 \pm 0.04$	$0.28 \pm 0.03$	$0.26 \pm 0.03$	162.	12.463	$-0.109 \pm 0.062$	$0.996 \pm 0.032$
NGC 5457 E nuc. 4 C	14 03 53.17	+54 22 06.29	$0.83 \pm 0.04$	$0.56 \pm 0.03$	$0.46 \pm 0.03$	162.	12.530	$-0.249 \pm 0.029$	$0.910 \pm 0.021$
NGC 5457 E nuc. 4 D	14 03 54.01	+54 22 11.21	$1.01 \pm 0.04$	$0.58 \pm 0.03$	$0.36 \pm 0.03$	162.	12.801	$-0.385 \pm 0.029$	$0.794 \pm 0.029$
NGC 5457 E nuc. 7 D <sup>†</sup>	14 04 29.03	+54 23 48.80	$5.95 \pm 0.07$	$4.35 \pm 0.07$	$3.82 \pm 0.06$	325.	23.774	$-0.187 \pm 0.008$	$0.951 \pm 0.005$
NGC 5457 E nuc. 7 B	14 04 29.24	+54 23 52.98	$2.14 \pm 0.02$	$0.75 \pm 0.02$	$0.73 \pm 0.02$	97.	23.859	$-0.496 \pm 0.010$	$0.667 \pm 0.013$
NGC 5713 A	14 40 10.28	-00 17 20.25	$1.84 \pm 0.03$	$0.95 \pm 0.04$	$0.60 \pm 0.03$	415.	2.130	$-0.445 \pm 0.018$	$0.730 \pm 0.020$
NGC 5713 F	14 40 10.34	-00 17 29.10	$0.38 \pm 0.02$	$0.32 \pm 0.03$	$0.20 \pm 0.02$	311.	2.197	$-0.212 \pm 0.046$	$0.935 \pm 0.030$
NGC 5713 B	14 40 10.74	-00 17 19.74	$3.75 \pm 0.02$	$1.70 \pm 0.03$	$1.32 \pm 0.02$	311.	1.329	$-0.449 \pm 0.006$	$0.724 \pm 0.007$
NGC 5713 E nuc. 2	14 40 10.78	-00 17 50.00	$1.22 \pm 0.05$	$0.77 \pm 0.05$	$0.28 \pm 0.04$	623.	3.320	$-0.426 \pm 0.040$	$0.751 \pm 0.044$
NGC 5713 E nuc. 2 A	14 40 10.83	-00 17 36.01	$1.93 \pm 0.04$	$1.08 \pm 0.05$	$0.62 \pm 0.03$	519.	1.999	$-0.431 \pm 0.020$	$0.745 \pm 0.022$
NGC 5713 C	14 40 11.05	-00 17 19.08	$5.39 \pm 0.02$	$1.99 \pm 0.03$	$1.48 \pm 0.02$	311.	0.795	$-0.558 \pm 0.005$	$0.579 \pm 0.008$
NGC 5713 G <sup>†</sup>	14 40 11.40	-00 17 20.10	$11.25 \pm 0.12$	$6.76 \pm 0.14$	$2.16 \pm 0.10$	1556.	0.174	$-0.447 \pm 0.012$	$0.727 \pm 0.014$
NGC 5713 D	14 40 11.41	-00 17 19.41	$7.56 \pm 0.02$	$3.24 \pm 0.03$	$2.39 \pm 0.02$	311.	0.163	$-0.493 \pm 0.003$	$0.671 \pm 0.004$
NGC 5713 E nuc. 1 A	14 40 12.10	-00 17 47.20	$< 0.10$	$0.19 \pm 0.04$	$< 0.06$	415.	3.058	...	...
NGC 5713 E	14 40 12.74	-00 17 18.60	$1.38 \pm 0.04$	$0.86 \pm 0.05$	$0.58 \pm 0.04$	519.	2.158	$-0.337 \pm 0.026$	$0.839 \pm 0.024$
NGC 5866	15 06 29.50	+55 45 47.56	$6.88 \pm 0.05$	$4.97 \pm 0.03$	$2.18 \pm 0.03$	297.	0.071	$-0.331 \pm 0.005$	$0.844 \pm 0.004$
NGC 6946 E nuc. 4 A	20 34 19.08	+60 10 09.81	$0.38 \pm 0.03$	$0.34 \pm 0.02$	$0.39 \pm 0.02$	132.	9.282	$0.017 \pm 0.037$	$1.000 \pm 0.014$
NGC 6946 E nuc. 4 B	20 34 19.20	+60 10 03.69	$0.18 \pm 0.02$	$0.21 \pm 0.01$	$0.20 \pm 0.01$	99.	9.172	$0.038 \pm 0.056$	$1.000 \pm 0.020$
NGC 6946 E nuc. 4 H	20 34 21.880	+60 10 47.83	$0.09 \pm 0.03$	$0.12 \pm 0.02$	$0.16 \pm 0.04$	132.	9.199	$0.216 \pm 0.172$	$1.000 \pm 0.041$
NGC 6946 E nuc. 8 A	20 34 32.29	+60 10 18.61	$2.25 \pm 0.05$	$0.73 \pm 0.03$	$0.82 \pm 0.05$	198.	6.106	$-0.550 \pm 0.021$	$0.591 \pm 0.031$
NGC 6946 E nuc. 5 A	20 34 37.14	+60 05 10.18	$< 0.08$	$< 0.04$	$0.10 \pm 0.02$	99.	9.238	...	...
NGC 6946 E nuc. 8 B	20 34 37.489	+60 09 36.47	$< 0.11$	$0.22 \pm 0.02$	$< 0.58$	132.	6.106	...	...
NGC 6946 E nuc. 5 B	20 34 39.31	+60 04 52.72	$0.33 \pm 0.04$	$0.38 \pm 0.02$	$0.38 \pm 0.02$	165.	9.695	$0.054 \pm 0.059$	$1.000 \pm 0.020$
NGC 6946 E nuc. 3 A	20 34 49.85	+60 12 40.69	$0.10 \pm 0.03$	$0.20 \pm 0.02$	$0.22 \pm 0.02$	132.	7.743	$0.259 \pm 0.118$	$1.000 \pm 0.025$
NGC 6946 E nuc. 3 B	20 34 51.22	+60 12 42.36	$0.12 \pm 0.03$	$0.21 \pm 0.02$	$0.20 \pm 0.02$	132.	7.727	$0.139 \pm 0.108$	$1.000 \pm 0.031$
NGC 6946 A	20 34 52.18	+60 09 14.60	$21.08 \pm 0.08$	$8.50 \pm 0.05$	$4.42 \pm 0.15$	297.	0.041	$-0.570 \pm 0.004$	$0.561 \pm 0.007$
NGC 6946 E nuc. 3 C	20 34 52.32	+60 12 44.00	$0.49 \pm 0.05$	$0.47 \pm 0.03$	$0.43 \pm 0.03$	198.	7.736	$-0.057 \pm 0.050$	$1.000 \pm 0.023$
NGC 6946 B	20 34 52.90	+60 08 51.80	$0.45 \pm 0.03$	$0.39 \pm 0.02$	$0.27 \pm 0.06$	99.	0.857	$-0.101 \pm 0.046$	$1.000 \pm 0.023$
NGC 6946 C	20 34 53.59	+60 09 18.80	$0.74 \pm 0.03$	$0.62 \pm 0.02$	$0.32 \pm 0.05$	99.	0.356	$-0.134 \pm 0.028$	$0.982 \pm 0.015$
NGC 6946 E nuc. 6 J	20 35 03.14	+60 10 56.40	$0.11 \pm 0.03$	$0.07 \pm 0.01$	$0.11 \pm 0.03$	99.	4.357	$-0.099 \pm 0.144$	$1.000 \pm 0.072$

Table 4 continued



Table 4 (continued)

Source ID	R.A.	Decl.	$S_{3\text{ GHz}}$	$S_{15\text{ GHz}}$	$S_{33\text{ GHz}}$	$d_{\text{ap}}$	$r_G$	$\alpha$	$f_T^{33\text{ GHz}}$
	(J2000)	(J2000)	(mJy)	(mJy)	(mJy)	(pc)	(kpc)		
NGC 6946 Enuc. 6 I	20 35 03.75	+60 10 59.40	$0.22 \pm 0.03$	$0.10 \pm 0.01$	$0.10 \pm 0.03$	99.	4.524	$-0.399 \pm 0.091$	$0.780 \pm 0.094$
NGC 6946 Enuc. 6 H	20 35 04.19	+60 10 54.60	$0.19 \pm 0.03$	$0.11 \pm 0.01$	$0.15 \pm 0.03$	99.	4.457	$-0.154 \pm 0.087$	$0.971 \pm 0.050$
NGC 6946 Enuc. 6 F	20 35 05.20	+60 10 56.40	$0.24 \pm 0.03$	$0.06 \pm 0.01$	$0.12 \pm 0.02$	99.	4.659	$-0.406 \pm 0.089$	$0.772 \pm 0.094$
NGC 6946 Enuc. 6 E	20 35 06.68	+60 11 12.00	$< 0.11$	$0.15 \pm 0.02$	$0.16 \pm 0.03$	132.	5.295	$0.085 \pm 0.298$	$1.000 \pm 0.097$
NGC 6946 Enuc. 6 B	20 35 07.01	+60 10 45.30	$0.34 \pm 0.03$	$0.29 \pm 0.01$	$0.19 \pm 0.03$	99.	4.709	$-0.151 \pm 0.052$	$0.973 \pm 0.029$
NGC 6946 Enuc. 6 C	20 35 07.81	+60 10 47.10	$0.11 \pm 0.03$	$0.06 \pm 0.01$	$< 0.08$	99.	4.899	$-0.407 \pm 0.210$	$0.772 \pm 0.221$
NGC 6946 Enuc. 9 E	20 35 09.04	+60 09 22.95	$0.13 \pm 0.03$	$0.08 \pm 0.02$	$< 0.12$	99.	4.361	$-0.277 \pm 0.178$	$0.889 \pm 0.137$
NGC 6946 Enuc. 9 D	20 35 10.28	+60 09 22.35	$0.19 \pm 0.04$	$0.22 \pm 0.02$	$< 0.14$	132.	4.689	$0.081 \pm 0.132$	$1.000 \pm 0.043$
NGC 6946 Enuc. 9 A	20 35 11.24	+60 08 57.42	$0.86 \pm 0.06$	$0.74 \pm 0.03$	$0.61 \pm 0.05$	198.	5.111	$-0.125 \pm 0.039$	$0.987 \pm 0.021$
NGC 6946 Enuc. 6 L	20 35 11.31	+60 10 32.99	$0.72 \pm 0.04$	$0.24 \pm 0.02$	$0.36 \pm 0.10$	132.	5.374	$-0.585 \pm 0.059$	$0.538 \pm 0.095$
NGC 6946 Enuc. 9 C	20 35 11.49	+60 09 12.45	$0.12 \pm 0.03$	$0.20 \pm 0.01$	$0.11 \pm 0.03$	99.	5.054	$0.101 \pm 0.136$	$1.000 \pm 0.042$
NGC 6946 Enuc. 9 B	20 35 11.69	+60 09 05.85	$0.16 \pm 0.03$	$0.17 \pm 0.01$	$0.13 \pm 0.02$	99.	5.154	$-0.046 \pm 0.100$	$1.000 \pm 0.044$
NGC 6946 Enuc. 7 A	20 35 12.96	+60 08 50.95	$0.19 \pm 0.05$	$0.75 \pm 0.02$	$0.48 \pm 0.04$	165.	5.630	$-0.098 \pm 0.089$	$1.000 \pm 0.044$
NGC 6946 Enuc. 7 B	20 35 14.11	+60 08 51.79	$0.13 \pm 0.03$	$0.21 \pm 0.01$	$0.16 \pm 0.03$	99.	5.918	$0.089 \pm 0.114$	$1.000 \pm 0.037$
NGC 6946 Enuc. 1 A	20 35 16.79	+60 11 00.23	$0.69 \pm 0.03$	$0.64 \pm 0.02$	$0.66 \pm 0.03$	132.	6.989	$-0.027 \pm 0.027$	$1.000 \pm 0.012$
NGC 6946 Enuc. 2 C	20 35 21.36	+60 09 51.93	$0.17 \pm 0.03$	$0.17 \pm 0.03$	$< 0.14$	132.	7.548	$-0.003 \pm 0.157$	$1.000 \pm 0.063$
NGC 7331 G	22 37 02.38	+34 24 59.90	$0.70 \pm 0.07$	$< 0.43$	$< 0.38$	562.	4.675	...	...
NGC 7331 F	22 37 02.52	+34 25 17.90	$0.69 \pm 0.05$	$0.43 \pm 0.11$	$< 0.34$	422.	3.998	$-0.296 \pm 0.169$	$0.874 \pm 0.137$
NGC 7331 H	22 37 03.11	+34 24 43.40	$1.33 \pm 0.07$	$1.18 \pm 0.16$	$< 0.40$	633.	3.296	$-0.073 \pm 0.091$	$1.000 \pm 0.043$
NGC 7331 I	22 37 03.83	+34 24 29.30	$1.23 \pm 0.06$	$1.47 \pm 0.13$	$< 0.38$	492.	2.483	$0.112 \pm 0.062$	$1.000 \pm 0.019$
NGC 7331 A	22 37 04.10	+34 24 56.00	$0.16 \pm 0.03$	$0.37 \pm 0.07$	$< 0.16$	281.	0.000	$0.516 \pm 0.175$	$1.000 \pm 0.020$
NGC 7331 E	22 37 05.00	+34 25 08.90	$0.91 \pm 0.07$	$< 0.48$	$0.49 \pm 0.13$	633.	3.053	$-0.257 \pm 0.118$	$0.904 \pm 0.086$
NGC 7331 B	22 37 05.36	+34 24 53.90	$0.52 \pm 0.05$	$0.80 \pm 0.11$	$< 0.26$	422.	3.445	$0.276 \pm 0.102$	$1.000 \pm 0.021$
NGC 7331 D	22 37 05.77	+34 24 44.90	$0.15 \pm 0.03$	$0.45 \pm 0.07$	$< 0.20$	281.	4.371	$0.673 \pm 0.170$	$1.000 \pm 0.013$
NGC 7793 Enuc. 1 E	23 57 48.222	-32 36 15.38	$0.12 \pm 0.02$	$0.07 \pm 0.01$	$< 0.35$	95.	1.430	$-0.390 \pm 0.188$	$0.789 \pm 0.190$
NGC 7793 Enuc. 3	23 57 48.87	-32 34 52.80	$0.21 \pm 0.02$	$0.20 \pm 0.01$	$< 0.14$	95.	0.992	$-0.044 \pm 0.083$	$1.000 \pm 0.036$
NGC 7793 Enuc. 1 A	23 57 48.89	-32 36 58.60	$0.09 \pm 0.03$	$0.07 \pm 0.01$	$< 0.17$	114.	2.587	$-0.172 \pm 0.232$	$0.961 \pm 0.139$
NGC 7793 C	23 57 48.94	-32 34 54.60	$0.19 \pm 0.02$	$0.17 \pm 0.01$	$0.12 \pm 0.04$	95.	0.941	$-0.096 \pm 0.089$	$1.000 \pm 0.045$
NGC 7793 A	23 57 49.41	-32 35 26.70	$0.23 \pm 0.04$	$0.20 \pm 0.02$	$0.16 \pm 0.04$	152.	0.097	$-0.118 \pm 0.109$	$0.991 \pm 0.058$
NGC 7793 Enuc. 1 B	23 57 49.68	-32 37 13.00	$< 0.09$	$0.11 \pm 0.02$	$< 0.19$	114.	2.962	...	...
NGC 7793 Enuc. 1 C	23 57 51.10	-32 36 49.00	$0.18 \pm 0.02$	$0.14 \pm 0.01$	$< 0.21$	95.	2.268	$-0.153 \pm 0.105$	$0.972 \pm 0.060$
NGC 7793 Enuc. 2	23 57 56.15	-32 35 40.60	$< 0.13$	$< 0.08$	$0.14 \pm 0.05$	171.	1.540	...	...
Likely Background Galaxies									
NGC 0925 C	02 27 15.30	+33 35 28.60	$1.37 \pm 0.02$	$0.68 \pm 0.02$	$0.29 \pm 0.08$	133.	3.375	$-0.445 \pm 0.020$	$0.730 \pm 0.023$
IC 342 E	03 46 45.793	+68 05 29.95	$0.79 \pm 0.12$	$0.28 \pm 0.04$	$< 0.29$	64.	0.373	$-0.637 \pm 0.122$	$0.448 \pm 0.223$
Holmberg II C	08 19 12.69	+70 43 03.80	$0.15 \pm 0.02$	$0.14 \pm 0.01$	$0.17 \pm 0.02$	44.	2.067	$0.018 \pm 0.078$	$1.000 \pm 0.030$
NGC 2841 B	09 22 00.988	+50 59 05.13	$0.11 \pm 0.02$	$< 0.10$	$< 0.07$	205.	2.374	...	...
NGC 2976 Enuc. 1 E	09 47 04.737	+67 56 41.47	$0.17 \pm 0.02$	$< 0.07$	$< 0.39$	69.	2.080	...	...
NGC 3077 B	10 03 16.379	+68 43 42.53	$0.06 \pm 0.02$	$0.12 \pm 0.02$	$< 0.14$	56.	0.456	$0.419 \pm 0.205$	$1.000 \pm 0.030$
NGC 3190 B	10 18 05.64	+21 49 55.91	$2.11 \pm 0.03$	$0.67 \pm 0.02$	$0.50 \pm 0.03$	374.	0.082	$-0.664 \pm 0.015$	$0.398 \pm 0.030$
NGC 3265 B	10 31 11.125	+28 48 07.09	$0.36 \pm 0.03$	$0.08 \pm 0.02$	$< 0.52$	380.	5.817	$-0.965 \pm 0.194$	$0.237 \pm 0.406$
NGC 3351 D	10 43 55.136	+11 42 05.36	$0.32 \pm 0.04$	$0.10 \pm 0.03$	$< 0.21$	181.	2.472	$-0.738 \pm 0.222$	$0.240 \pm 0.516$
NGC 3627 Enuc. 1 B	11 20 17.291	+12 56 57.67	$0.14 \pm 0.03$	$< 0.16$	$< 0.44$	182.	7.224	...	...
NGC 4569 B	12 36 47.368	+13 10 27.07	$0.50 \pm 0.03$	$< 0.12$	$< 0.46$	191.	5.433	...	...
NGC 4625 B	12 41 52.424	+41 17 17.64	$0.97 \pm 0.03$	$0.27 \pm 0.02$	$0.34 \pm 0.05$	180.	2.434	$-0.654 \pm 0.043$	$0.417 \pm 0.082$
NGC 6946 Enuc. 4 F	20 34 23.90	+60 10 42.90	$5.79 \pm 0.04$	$1.73 \pm 0.03$	$0.93 \pm 0.08$	198.	8.611	$-0.751 \pm 0.012$	$0.208 \pm 0.029$
NGC 6946 Enuc. 4 G	20 34 26.24	+60 10 30.59	$2.50 \pm 0.04$	$0.88 \pm 0.03$	$0.49 \pm 0.10$	165.	7.811	$-0.652 \pm 0.022$	$0.420 \pm 0.042$
Likely Associated with Supernovae									
NGC 2403 Enuc. 3 D	07 37 17.034	+65 35 57.79	$< 0.09$	$1.73 \pm 0.04$	$< 2.94$	62.	3.525	...	...

Table 4 continued

Table 4 (continued)

Source ID	R.A.	Decl.	$S_{3\text{ GHz}}$	$S_{15\text{ GHz}}$	$S_{33\text{ GHz}}$	$d_{\text{ap}}$	$r_G$	$\alpha$	$f_T^{33\text{ GHz}}$
	(J2000)	(J2000)	(mJy)	(mJy)	(mJy)	(pc)	(kpc)		
NGC 4736 B	12 50 52.026	+41 07 15.63	$0.16 \pm 0.05$	$< 0.19$	$< 0.15$	136.	0.280	...	...
NGC 4736 C	12 50 52.522	+41 07 01.94	$0.16 \pm 0.05$	$< 0.20$	$< 0.15$	136.	0.350	...	...
NGC 5194 D	13 29 55.79	+47 11 45.19	$1.22 \pm 0.06$	$0.63 \pm 0.03$	$0.82 \pm 0.05$	185.	1.909	$-0.221 \pm 0.030$	$0.929 \pm 0.020$
NGC 5194 Enuc. 7 D	13 30 05.12	+47 10 10.90	$1.54 \pm 0.05$	$0.17 \pm 0.02$	$< 0.15$	148.	7.398	$-1.377 \pm 0.084$	$0.221 \pm 0.165$
NGC 6946 F	20 34 50.927	+60 10 20.35	$0.20 \pm 0.04$	$0.11 \pm 0.03$	$< 2.45$	132.	2.527	$-0.386 \pm 0.223$	$0.792 \pm 0.223$
NGC 6946 Enuc. 6 D	20 35 08.09	+60 11 13.50	$0.28 \pm 0.04$	$0.35 \pm 0.02$	$0.22 \pm 0.04$	132.	5.557	$0.032 \pm 0.078$	$1.000 \pm 0.029$
NGC 6946 Enuc. 2 B	20 35 25.29	+60 09 58.64	$1.23 \pm 0.06$	$1.42 \pm 0.04$	$1.89 \pm 0.05$	231.	8.572	$0.187 \pm 0.023$	$1.000 \pm 0.006$
NGC 7331 C	22 37 05.60	+34 24 32.90	$0.79 \pm 0.07$	$1.85 \pm 0.15$	$0.72 \pm 0.15$	562.	3.813	$0.349 \pm 0.065$	$1.000 \pm 0.011$
NGC 7793 B	23 57 47.35	-32 35 24.60	$0.14 \pm 0.02$	$< 0.04$	$< 0.11$	95.	0.591	...	...
Likely AME Candidates									
NGC 2403 Enuc. 5 D	07 36 20.57	+65 37 08.50	$0.64 \pm 0.03$	$0.63 \pm 0.02$	$0.62 \pm 0.02$	62.	3.362	$-0.014 \pm 0.022$	$1.000 \pm 0.009$
NGC 2403 Enuc. 2 E	07 36 57.88	+65 37 24.39	$1.17 \pm 0.03$	$0.96 \pm 0.03$	$1.19 \pm 0.08$	62.	2.684	$-0.075 \pm 0.019$	$1.000 \pm 0.009$
NGC 2403 Enuc. 3 A	07 37 05.20	+65 36 41.74	$0.39 \pm 0.03$	$0.40 \pm 0.02$	$0.52 \pm 0.03$	62.	2.637	$0.108 \pm 0.039$	$1.000 \pm 0.012$
NGC 2403 Enuc. 3 C	07 37 07.86	+65 36 38.56	$2.51 \pm 0.03$	$1.91 \pm 0.02$	$1.89 \pm 0.03$	62.	2.921	$-0.135 \pm 0.007$	$0.982 \pm 0.004$
NGC 3627 Enuc. 1 D	11 20 13.857	+12 57 09.26	$0.41 \pm 0.03$	$0.56 \pm 0.05$	$0.61 \pm 0.13$	182.	7.171	$0.185 \pm 0.067$	$1.000 \pm 0.017$
NGC 3627 Enuc. 1 C	11 20 14.093	+12 56 59.60	$0.45 \pm 0.05$	$0.63 \pm 0.08$	$0.96 \pm 0.30$	273.	7.467	$0.248 \pm 0.094$	$1.000 \pm 0.021$
NGC 4254 Enuc. 2 A	12 18 46.14	+14 24 19.18	$0.12 \pm 0.03$	$0.15 \pm 0.03$	$0.21 \pm 0.02$	279.	4.669	$0.252 \pm 0.109$	$1.000 \pm 0.024$
NGC 4254 Enuc. 1 A	12 18 49.21	+14 23 57.78	$0.34 \pm 0.03$	$0.14 \pm 0.02$	$0.23 \pm 0.03$	279.	4.437	$-0.225 \pm 0.059$	$0.926 \pm 0.040$
NGC 4631 C	12 42 05.62	+32 32 29.46	$1.75 \pm 0.03$	$0.87 \pm 0.03$	$1.25 \pm 0.03$	148.	1.354	$-0.174 \pm 0.012$	$0.959 \pm 0.007$
NGC 4631 D	12 42 06.24	+32 32 31.70	$1.54 \pm 0.03$	$0.53 \pm 0.03$	$0.94 \pm 0.03$	148.	1.525	$-0.248 \pm 0.015$	$0.911 \pm 0.011$
NGC 4631 E	12 42 07.18	+32 32 33.90	$0.94 \pm 0.02$	$0.46 \pm 0.03$	$0.79 \pm 0.03$	111.	1.740	$-0.109 \pm 0.016$	$0.995 \pm 0.008$
NGC 4631 F	12 42 07.89	+32 32 33.42	$6.83 \pm 0.04$	$3.27 \pm 0.05$	$3.98 \pm 0.06$	222.	1.366	$-0.285 \pm 0.006$	$0.882 \pm 0.005$
NGC 4631 Enuc. 2 A	12 42 21.41	+32 33 06.38	$0.60 \pm 0.04$	$0.23 \pm 0.02$	$0.43 \pm 0.02$	185.	9.993	$-0.171 \pm 0.034$	$0.961 \pm 0.020$
NGC 4725 B	12 50 28.49	+25 30 22.26	$0.15 \pm 0.02$	$0.18 \pm 0.01$	$0.35 \pm 0.02$	173.	1.930	$0.414 \pm 0.052$	$1.000 \pm 0.008$
NGC 5194 Enuc. 2	13 29 44.09	+47 10 22.86	$1.33 \pm 0.08$	$0.46 \pm 0.03$	$0.58 \pm 0.04$	259.	6.852	$-0.399 \pm 0.035$	$0.780 \pm 0.037$
NGC 5194 Enuc. 1 C	13 29 49.39	+47 12 40.90	$0.54 \pm 0.05$	$0.46 \pm 0.03$	$0.72 \pm 0.05$	148.	2.587	$0.089 \pm 0.045$	$1.000 \pm 0.015$
NGC 5194 Enuc. 1 B	13 29 51.98	+47 12 43.90	$0.50 \pm 0.05$	$0.48 \pm 0.02$	$0.55 \pm 0.03$	148.	2.327	$0.048 \pm 0.043$	$1.000 \pm 0.015$
NGC 5194 Enuc. 4 A	13 29 55.50	+47 14 01.50	$0.71 \pm 0.04$	$0.29 \pm 0.02$	$0.40 \pm 0.02$	148.	6.192	$-0.253 \pm 0.031$	$0.907 \pm 0.023$
NGC 5457 Enuc. 2 A	14 02 55.08	+54 22 27.44	$0.40 \pm 0.04$	$0.27 \pm 0.02$	$0.37 \pm 0.03$	162.	6.429	$-0.060 \pm 0.052$	$1.000 \pm 0.024$
NGC 5457 Enuc. 7 A	14 04 28.61	+54 23 52.40	$1.07 \pm 0.02$	$0.55 \pm 0.02$	$0.71 \pm 0.02$	97.	23.668	$-0.197 \pm 0.013$	$0.945 \pm 0.008$
NGC 5457 Enuc. 7 C	14 04 29.45	+54 23 47.11	$3.56 \pm 0.03$	$1.80 \pm 0.03$	$1.93 \pm 0.02$	130.	23.894	$-0.285 \pm 0.006$	$0.883 \pm 0.005$
NGC 6946 Enuc. 4 C	20 34 19.88	+60 10 06.42	$1.58 \pm 0.03$	$1.42 \pm 0.02$	$1.56 \pm 0.02$	132.	9.032	$0.001 \pm 0.009$	$1.000 \pm 0.004$
NGC 6946 Enuc. 4 D	20 34 21.39	+60 10 17.87	$0.11 \pm 0.03$	$0.81 \pm 0.02$	$0.69 \pm 0.02$	132.	8.808	$-0.076 \pm 0.043$	$1.000 \pm 0.021$
NGC 6946 Enuc. 4 E	20 34 22.72	+60 10 34.04	$1.35 \pm 0.03$	$1.34 \pm 0.02$	$1.29 \pm 0.03$	132.	8.741	$-0.015 \pm 0.013$	$1.000 \pm 0.005$
NGC 6946 E	20 34 51.30	+60 09 38.30	$0.73 \pm 0.05$	$0.71 \pm 0.03$	$1.27 \pm 0.11$	165.	0.972	$0.121 \pm 0.040$	$1.000 \pm 0.012$
NGC 6946 D	20 34 52.78	+60 09 30.50	$0.40 \pm 0.04$	$0.51 \pm 0.02$	$0.54 \pm 0.07$	132.	0.601	$0.132 \pm 0.058$	$1.000 \pm 0.017$
NGC 6946 Enuc. 6 M	20 35 00.77	+60 11 30.29	$0.50 \pm 0.04$	$0.09 \pm 0.02$	$0.45 \pm 0.10$	132.	5.163	$-0.301 \pm 0.088$	$0.870 \pm 0.072$
NGC 6946 Enuc. 6 G	20 35 06.00	+60 11 00.60	$0.79 \pm 0.03$	$0.49 \pm 0.01$	$0.54 \pm 0.02$	99.	4.894	$-0.204 \pm 0.021$	$0.941 \pm 0.014$
NGC 6946 Enuc. 6 K	20 35 06.20	+60 10 55.50	$0.70 \pm 0.03$	$0.38 \pm 0.01$	$0.45 \pm 0.02$	99.	4.801	$-0.246 \pm 0.025$	$0.912 \pm 0.018$
NGC 6946 Enuc. 6 A <sup>†</sup>	20 35 06.24	+60 10 58.32	$1.84 \pm 0.05$	$1.08 \pm 0.03$	$1.20 \pm 0.05$	198.	4.876	$-0.232 \pm 0.019$	$0.922 \pm 0.013$
NGC 6946 Enuc. 1 B	20 35 11.25	+60 10 33.89	$0.72 \pm 0.03$	$0.36 \pm 0.02$	$0.66 \pm 0.08$	132.	5.374	$-0.287 \pm 0.039$	$0.881 \pm 0.031$
NGC 6946 Enuc. 2 A	20 35 23.61	+60 09 48.93	$0.11 \pm 0.03$	$0.31 \pm 0.02$	$0.36 \pm 0.04$	132.	8.130	$0.379 \pm 0.112$	$1.000 \pm 0.018$
NGC 7793 Enuc. 1 D	23 57 46.742	-32 36 07.00	$0.23 \pm 0.02$	$0.10 \pm 0.02$	$< 0.81$	95.	1.393	$-0.486 \pm 0.122$	$0.680 \pm 0.155$

NOTE—<sup>†</sup>The aperture used for this region contained multiple smaller individual regions.

**Table 5.** Region Photometry and Derived Parameters at 7'' Angular Resolution

Source ID	R.A.	Decl.	$S_{3\text{ GHz}}$	$S_{15\text{ GHz}}$	$S_{33\text{ GHz}}$	$d_{\text{ap}}$	$r_{\text{G}}$	$\alpha$	$f_{\text{T}}^{33\text{ GHz}}$
	(J2000)	(J2000)	(mJy)	(mJy)	(mJy)	(pc)	(kpc)		
Star-Forming Regions									
NGC 0337 a	00 59 50.018	-07 34 33.9	$0.53 \pm 0.02$	$0.37 \pm 0.01$	$0.23 \pm 0.01$	655.	0.945	$-0.30 \pm 0.03$	$0.87 \pm 0.02$
NGC 0337 b	00 59 50.683	-07 34 57.6	$1.70 \pm 0.05$	$0.91 \pm 0.03$	$0.61 \pm 0.02$	655.	1.966	$-0.42 \pm 0.02$	$0.76 \pm 0.02$
NGC 0337 c	00 59 51.995	-07 34 54.9	$0.13 \pm 0.01$	$0.12 \pm 0.01$	$0.10 \pm 0.02$	655.	3.227	$-0.10 \pm 0.07$	$1.00 \pm 0.03$
NGC 0337 d	00 59 52.156	-07 34 38.2	$0.25 \pm 0.02$	$0.25 \pm 0.01$	$0.21 \pm 0.02$	655.	4.061	$-0.05 \pm 0.04$	$1.00 \pm 0.02$
NGC 0628 Enuc. 4	01 36 35.718	+15 50 07.25	$0.14 \pm 0.01$	$0.13 \pm 0.01$	$0.12 \pm 0.01$	244.	7.608	$-0.04 \pm 0.04$	$1.00 \pm 0.02$
NGC 0628 Enuc. 2	01 36 37.645	+15 45 07.2	$0.26 \pm 0.01$	$0.15 \pm 0.01$	$0.18 \pm 0.01$	244.	4.468	$-0.22 \pm 0.03$	$0.93 \pm 0.02$
NGC 0628 Enuc. 3	01 36 38.779	+15 44 23.2	$0.27 \pm 0.01$	$0.21 \pm 0.01$	$0.19 \pm 0.02$	244.	5.720	$-0.16 \pm 0.03$	$0.97 \pm 0.02$
NGC 0628	01 36 41.7	+15 46 59	$< 0.03$	$< 0.02$	$< 0.04$	244.	0.071	...	...
NGC 0628 Enuc. 1	01 36 45.266	+15 47 48.3	$0.55 \pm 0.02$	$0.42 \pm 0.01$	$0.29 \pm 0.02$	244.	2.478	$-0.22 \pm 0.02$	$0.93 \pm 0.02$
NGC 0855	02 14 03.677	+27 52 37.85	$0.47 \pm 0.02$	$0.28 \pm 0.01$	$0.22 \pm 0.01$	330.	0.202	$-0.31 \pm 0.02$	$0.86 \pm 0.02$
NGC 0925	02 27 17	+33 34 43	$0.06 \pm 0.01$	$0.04 \pm 0.01$	$< 0.03$	310.	0.183	$-0.30 \pm 0.14$	$0.87 \pm 0.12$
NGC 1097 Enuc. 2	02 46 14.4	-30 15 03.992	$< 0.19$	$< 0.04$	$< 0.06$	482.	7.435	...	...
NGC 1097	02 46 18.984	-30 16 28.8	$5.57 \pm 0.18$	$2.55 \pm 0.08$	$2.29 \pm 0.09$	482.	0.020	$-0.40 \pm 0.02$	$0.78 \pm 0.02$
NGC 1097 Enuc. 1 a	02 46 22.557	-30 17 29.9	$< 0.21$	$0.08 \pm 0.01$	$0.08 \pm 0.02$	482.	5.416	$-0.07 \pm 0.41$	$1.00 \pm 0.20$
NGC 1097 Enuc. 1 b	02 46 22.927	-30 17 48.1	$0.33 \pm 0.07$	$< 0.04$	$0.11 \pm 0.02$	482.	6.817	$-0.48 \pm 0.11$	$0.69 \pm 0.14$
NGC 1097 Enuc. 1 c	02 46 24.062	-30 17 50.9	$< 0.21$	$< 0.04$	$0.07 \pm 0.02$	482.	7.392	...	...
NGC 1266	03 16 00.76	-02 25 37.1	$23.46 \pm 0.70$	$6.94 \pm 0.21$	$4.13 \pm 0.13$	1038.	0.270	$-0.73 \pm 0.02$	$0.26 \pm 0.04$
NGC 1377	03 36 38.9	-20 54 06	$< 0.06$	$< 0.03$	$< 0.06$	835.	0.580	...	...
NGC 1482	03 54 38.966	-20 30 07.8	$33.61 \pm 1.01$	$9.61 \pm 0.29$	$6.78 \pm 0.21$	767.	0.124	$-0.69 \pm 0.02$	$0.35 \pm 0.04$
NGC 2403 Enuc. 6	07 36 28.693	+65 33 49.4	$0.34 \pm 0.01$	$0.32 \pm 0.01$	$0.30 \pm 0.01$	109.	5.380	$-0.06 \pm 0.02$	$1.00 \pm 0.01$
NGC 2403 Enuc. 1 a	07 36 42.061	+65 36 51.898	$0.26 \pm 0.01$	$0.20 \pm 0.01$	$0.13 \pm 0.01$	109.	1.087	$-0.22 \pm 0.04$	$0.93 \pm 0.02$
NGC 2403 Enuc. 1 b	07 36 45.5	+65 37 00.9	$0.66 \pm 0.02$	$0.59 \pm 0.02$	$0.55 \pm 0.02$	109.	1.192	$-0.07 \pm 0.02$	$1.00 \pm 0.01$
NGC 2403 Enuc. 2 a	07 36 49.115	+65 36 51.697	$0.35 \pm 0.01$	$0.30 \pm 0.01$	$0.25 \pm 0.01$	109.	1.113	$-0.13 \pm 0.03$	$0.98 \pm 0.01$
NGC 2403	07 36 50	+65 36 04	$< 0.03$	$< 0.02$	$< 0.02$	109.	0.000	...	...
NGC 2403 Enuc. 2 b	07 36 52.361	+65 36 46.9	$0.64 \pm 0.02$	$0.50 \pm 0.02$	$0.49 \pm 0.02$	109.	1.249	$-0.12 \pm 0.02$	$0.99 \pm 0.01$
NGC 2403 Enuc. 4	07 37 18.19	+65 33 48.1	$0.34 \pm 0.01$	$0.33 \pm 0.01$	$0.33 \pm 0.01$	109.	3.455	$-0.01 \pm 0.02$	$1.00 \pm 0.01$
Holmberg II	08 19 13.058	+70 43 08	$0.20 \pm 0.01$	$0.19 \pm 0.01$	$0.21 \pm 0.01$	104.	0.738	$0.01 \pm 0.04$	$1.00 \pm 0.01$
NGC 2798	09 17 22.854	+42 00 00.4	$15.27 \pm 0.46$	$5.71 \pm 0.17$	$2.06 \pm 0.06$	876.	0.144	$-0.80 \pm 0.02$	$0.08 \pm 0.05$
NGC 2841	09 22 02.668	+50 58 35.7	$0.92 \pm 0.03$	$0.89 \pm 0.03$	$0.56 \pm 0.02$	479.	0.155	$-0.18 \pm 0.02$	$0.95 \pm 0.01$
NGC 2976 Enuc. 1 a	09 47 05.192	+67 55 51.999	$0.54 \pm 0.02$	$0.36 \pm 0.01$	$0.35 \pm 0.02$	120.	1.420	$-0.21 \pm 0.02$	$0.94 \pm 0.01$
NGC 2976 Enuc. 1 b	09 47 07.64	+67 55 54.7	$1.23 \pm 0.04$	$1.01 \pm 0.03$	$0.86 \pm 0.03$	120.	1.201	$-0.14 \pm 0.02$	$0.98 \pm 0.01$
NGC 2976	09 47 13.491	+67 54 53.999	$0.11 \pm 0.01$	$0.08 \pm 0.01$	$0.09 \pm 0.01$	120.	0.462	$-0.12 \pm 0.07$	$0.99 \pm 0.04$
NGC 2976 Enuc. 2 a	09 47 23.834	+67 53 54.9	$0.59 \pm 0.02$	$0.51 \pm 0.02$	$0.45 \pm 0.02$	120.	1.394	$-0.11 \pm 0.02$	$0.99 \pm 0.01$
NGC 2976 Enuc. 2 b	09 47 23.941	+67 54 02.1	$0.28 \pm 0.01$	$0.23 \pm 0.01$	$0.21 \pm 0.02$	120.	1.310	$-0.13 \pm 0.03$	$0.98 \pm 0.02$
NGC 3049	09 54 49.559	+09 16 16.1	$1.35 \pm 0.04$	$0.75 \pm 0.02$	$0.55 \pm 0.02$	652.	0.103	$-0.38 \pm 0.02$	$0.80 \pm 0.02$
NGC 3077	10 03 19.15	+68 43 59.90	$3.62 \pm 0.11$	$2.31 \pm 0.07$	$1.89 \pm 0.06$	130.	0.045	$-0.27 \pm 0.02$	$0.89 \pm 0.01$
NGC 3190	10 18 05.643	+21 49 55.9	$1.08 \pm 0.03$	$0.50 \pm 0.02$	$0.27 \pm 0.01$	655.	0.098	$-0.55 \pm 0.02$	$0.59 \pm 0.03$
NGC 3184	10 18 16.94	+41 25 27	$0.35 \pm 0.01$	$0.18 \pm 0.01$	$0.14 \pm 0.01$	397.	0.063	$-0.40 \pm 0.03$	$0.78 \pm 0.03$
NGC 3198	10 19 54.986	+45 32 59.3	$0.63 \pm 0.02$	$0.31 \pm 0.01$	$0.12 \pm 0.01$	479.	0.116	$-0.51 \pm 0.03$	$0.65 \pm 0.04$
IC 2574 a	10 28 43.712	+68 28 26.296	$0.29 \pm 0.01$	$0.20 \pm 0.01$	$0.28 \pm 0.02$	129.	6.253	$-0.11 \pm 0.03$	$0.99 \pm 0.02$
IC 2574 b	10 28 48.4	+68 28 03.5	$0.29 \pm 0.01$	$0.23 \pm 0.01$	$0.24 \pm 0.01$	129.	5.254	$-0.10 \pm 0.03$	$1.00 \pm 0.01$
NGC 3265	10 31 06.768	+28 47 48	$1.97 \pm 0.06$	$0.77 \pm 0.02$	$0.44 \pm 0.02$	665.	0.087	$-0.62 \pm 0.02$	$0.48 \pm 0.03$
NGC 3351 a	10 43 57.677	+11 42 08	$2.84 \pm 0.09$	$1.14 \pm 0.04$	$0.78 \pm 0.03$	317.	0.230	$-0.54 \pm 0.02$	$0.60 \pm 0.03$
NGC 3351 b	10 43 57.8	+11 42 18.5	$3.28 \pm 0.10$	$1.37 \pm 0.04$	$0.91 \pm 0.03$	317.	0.258	$-0.54 \pm 0.02$	$0.61 \pm 0.03$
NGC 3521 Enuc. 1	11 05 46.3	-00 04 08.992	$0.05 \pm 0.02$	$0.13 \pm 0.02$	$< 0.07$	380.	9.929	$0.56 \pm 0.21$	$1.00 \pm 0.02$
NGC 3521 Enuc. 3	11 05 47.6	+00 00 33.004	$< 0.05$	$0.08 \pm 0.01$	$< 0.05$	380.	9.509	...	...
NGC 3521	11 05 48.9	-00 02 06	$< 0.06$	$< 0.10$	$< 0.05$	380.	0.625	...	...
NGC 3521 Enuc. 2 a	11 05 49.34	-00 03 24.2	$0.29 \pm 0.02$	$0.13 \pm 0.02$	$0.13 \pm 0.03$	380.	4.302	$-0.39 \pm 0.07$	$0.79 \pm 0.07$

*Table 5 continued*

Table 5 (continued)

Source ID	R.A.	Decl.	$S_{3\text{ GHz}}$	$S_{15\text{ GHz}}$	$S_{33\text{ GHz}}$	$d_{\text{ap}}$	$r_{\text{G}}$	$\alpha$	$f_{\text{T}}^{33\text{ GHz}}$
	(J2000)	(J2000)	(mJy)	(mJy)	(mJy)	(pc)	(kpc)		
NGC 3521 E nuc. 2 b	11 05 49.94	-00 03 55.9	< 0.06	< 0.06	0.11 ± 0.03	380.	6.044	...	...
NGC 3621	11 18 16	-32 48 42	0.06 ± 0.02	< 0.04	< 0.07	222.	0.348	...	...
NGC 3627	11 20 15	+12 59 29.4	4.75 ± 0.14	1.73 ± 0.05	1.09 ± 0.04	318.	0.028	-0.62 ± 0.02	0.48 ± 0.03
NGC 3627 E nuc. 1	11 20 16.323	+12 57 49.2	1.33 ± 0.04	1.03 ± 0.03	0.86 ± 0.03	318.	4.712	-0.18 ± 0.02	0.96 ± 0.01
NGC 3627 E nuc. 2	11 20 16.464	+12 58 43.4	4.56 ± 0.14	2.52 ± 0.08	1.97 ± 0.06	318.	2.746	-0.35 ± 0.02	0.82 ± 0.02
NGC 3773	11 38 13.02	+12 06 43.8	0.85 ± 0.03	0.45 ± 0.02	0.39 ± 0.02	421.	0.023	-0.34 ± 0.02	0.84 ± 0.02
NGC 3938 b	11 52 48.191	+44 07 05.9	< 0.03	< 0.02	0.08 ± 0.01	607.	1.407	...	...
NGC 3938 a	11 52 49.5	+44 07 14	< 0.03	< 0.02	< 0.03	607.	0.140	...	...
NGC 3938 E nuc. 2 a	11 53 00.056	+44 08 00	0.09 ± 0.01	0.06 ± 0.01	0.10 ± 0.01	607.	11.158	0.00 ± 0.07	1.00 ± 0.03
NGC 3938 E nuc. 2 b	11 53 00.195	+44 07 48.3	0.15 ± 0.01	0.13 ± 0.01	0.11 ± 0.01	607.	11.049	-0.11 ± 0.05	0.99 ± 0.03
NGC 4254 E nuc. 2 a	12 18 45.777	+14 24 10.4	0.04 ± 0.01	0.05 ± 0.01	0.09 ± 0.01	489.	5.342	0.46 ± 0.12	1.00 ± 0.02
NGC 4254 E nuc. 2 b	12 18 46.128	+14 24 18.8	0.06 ± 0.01	0.07 ± 0.01	0.12 ± 0.01	489.	4.698	0.32 ± 0.08	1.00 ± 0.01
NGC 4254 a	12 18 48.677	+14 24 42.5	0.17 ± 0.01	0.04 ± 0.01	0.07 ± 0.01	489.	1.553	-0.52 ± 0.07	0.64 ± 0.09
NGC 4254 b	12 18 49.668	+14 24 59	0.14 ± 0.01	0.11 ± 0.01	0.11 ± 0.01	489.	0.111	-0.09 ± 0.05	1.00 ± 0.02
NGC 4254 E nuc. 1 b	12 18 50.009	+14 24 06.9	0.07 ± 0.01	0.05 ± 0.01	0.15 ± 0.01	489.	3.886	0.38 ± 0.07	1.00 ± 0.01
NGC 4254 c	12 18 50.102	+14 25 11.6	0.04 ± 0.01	0.09 ± 0.01	0.07 ± 0.01	489.	0.960	0.14 ± 0.13	1.00 ± 0.04
NGC 4254 E nuc. 1 c	12 18 50.194	+14 24 18.6	0.35 ± 0.01	0.12 ± 0.01	0.18 ± 0.01	489.	3.116	-0.41 ± 0.03	0.77 ± 0.03
NGC 4254 d	12 18 51.63	+14 25 08.599	0.30 ± 0.01	0.04 ± 0.01	0.12 ± 0.02	489.	2.344	-0.52 ± 0.05	0.64 ± 0.07
NGC 4254 e	12 18 51.899	+14 24 49.699	0.08 ± 0.01	0.02 ± 0.01	0.13 ± 0.02	489.	2.813	0.17 ± 0.08	1.00 ± 0.02
NGC 4254 f	12 18 51.919	+14 24 40.099	0.04 ± 0.01	< 0.02	0.14 ± 0.02	489.	3.149	0.55 ± 0.14	1.00 ± 0.01
NGC 4321 E nuc. 2 a	12 22 48.844	+15 50 12.8	0.06 ± 0.01	0.05 ± 0.01	0.05 ± 0.01	485.	8.305	-0.10 ± 0.10	1.00 ± 0.05
NGC 4321 E nuc. 2 b	12 22 49.904	+15 50 27.8	0.06 ± 0.01	0.03 ± 0.01	0.05 ± 0.01	485.	7.979	-0.13 ± 0.10	0.98 ± 0.05
NGC 4321 E nuc. 2	12 22 50.652	+15 50 27.2	< 0.03	< 0.02	0.04 ± 0.01	485.	7.285	...	...
NGC 4321 a	12 22 54.651	+15 49 19.8	2.03 ± 0.06	0.81 ± 0.03	0.46 ± 0.02	485.	0.284	-0.61 ± 0.02	0.50 ± 0.03
NGC 4321 b	12 22 55.129	+15 49 20.4	3.01 ± 0.09	1.07 ± 0.03	0.64 ± 0.02	485.	0.270	-0.64 ± 0.02	0.44 ± 0.03
NGC 4321 E nuc. 1	12 22 58.9	+15 49 35.003	< 0.03	< 0.02	< 0.02	485.	4.520	...	...
NGC 4536	12 34 27.06	+02 11 18.2	21.45 ± 0.64	7.81 ± 0.23	4.90 ± 0.15	492.	0.126	-0.62 ± 0.02	0.48 ± 0.03
NGC 4559 a	12 35 56.273	+27 57 40.5	0.08 ± 0.01	0.07 ± 0.01	0.08 ± 0.01	237.	1.304	-0.01 ± 0.08	1.00 ± 0.03
NGC 4559 b	12 35 56.455	+27 57 21.3	0.05 ± 0.01	0.07 ± 0.01	0.05 ± 0.01	237.	1.880	0.05 ± 0.12	1.00 ± 0.04
NGC 4559 c	12 35 58.47	+27 57 29.7	0.10 ± 0.01	0.10 ± 0.01	0.11 ± 0.01	237.	0.608	0.02 ± 0.06	1.00 ± 0.02
NGC 4569	12 36 49.8	+13 09 46.6	2.99 ± 0.09	0.92 ± 0.03	0.52 ± 0.02	335.	0.037	-0.73 ± 0.02	0.26 ± 0.04
NGC 4579	12 37 43.518	+11 49 05.6	21.36 ± 0.64	24.39 ± 0.73	30.71 ± 0.92	557.	0.105	0.14 ± 0.02	1.00 ± 0.01
NGC 4594 a	12 39 59.42	-11 37 23	38.94 ± 1.17	45.37 ± 1.36	36.58 ± 1.10	308.	0.052	-0.01 ± 0.02	1.00 ± 0.01
NGC 4631 E nuc. 1	12 41 40.468	+32 31 49.1	0.16 ± 0.01	0.16 ± 0.01	0.14 ± 0.01	259.	13.762	-0.04 ± 0.04	1.00 ± 0.02
NGC 4625	12 41 52.4	+41 16 24	< 0.03	0.04 ± 0.01	0.02 ± 0.01	316.	0.139	-0.91 ± 0.39	0.24 ± 0.82
NGC 4631 a	12 42 03.433	+32 32 17.198	3.50 ± 0.11	1.05 ± 0.03	0.72 ± 0.03	259.	3.189	-0.68 ± 0.02	0.37 ± 0.04
NGC 4631 b	12 42 03.978	+32 32 15.999	1.62 ± 0.05	1.06 ± 0.03	0.58 ± 0.02	259.	3.435	-0.39 ± 0.02	0.79 ± 0.02
NGC 4631 c	12 42 04.31	+32 32 25.299	2.35 ± 0.07	1.36 ± 0.04	1.29 ± 0.04	259.	1.734	-0.26 ± 0.02	0.90 ± 0.01
NGC 4631 d	12 42 05.093	+32 32 10.6	0.36 ± 0.01	0.27 ± 0.01	0.26 ± 0.01	259.	4.988	-0.14 ± 0.03	0.98 ± 0.01
NGC 4631 e	12 42 05.568	+32 32 29.5	0.91 ± 0.03	0.44 ± 0.02	0.61 ± 0.02	259.	1.387	-0.20 ± 0.02	0.94 ± 0.01
NGC 4631 E nuc. 2 b	12 42 21.988	+32 32 45	0.47 ± 0.02	0.33 ± 0.01	0.36 ± 0.01	259.	6.651	-0.14 ± 0.02	0.98 ± 0.01
NGC 4725 a	12 50 26.556	+25 30 03	0.05 ± 0.01	0.10 ± 0.01	0.16 ± 0.01	404.	0.044	0.50 ± 0.07	1.00 ± 0.01
NGC 4736	12 50 53.053	+41 07 12.8	3.83 ± 0.12	1.60 ± 0.05	1.02 ± 0.03	158.	0.014	-0.55 ± 0.02	0.59 ± 0.03
NGC 4736 E nuc. 1 a	12 50 56.412	+41 07 14.3	0.69 ± 0.02	0.45 ± 0.03	0.35 ± 0.02	158.	0.864	-0.29 ± 0.02	0.88 ± 0.02
NGC 4736 E nuc. 1 b	12 50 56.704	+41 07 05	1.08 ± 0.03	0.62 ± 0.03	0.39 ± 0.02	158.	0.939	-0.41 ± 0.02	0.77 ± 0.02
NGC 4736 E nuc. 1 c	12 50 56.784	+41 06 47.6	0.64 ± 0.02	0.46 ± 0.03	0.26 ± 0.02	158.	1.123	-0.31 ± 0.03	0.86 ± 0.03
NGC 4826	12 56 43.556	+21 41 00.6	4.39 ± 0.13	1.62 ± 0.05	1.00 ± 0.03	179.	0.055	-0.62 ± 0.02	0.48 ± 0.03
NGC 5055	13 15 49.308	+42 01 45.1	0.71 ± 0.02	0.35 ± 0.01	0.12 ± 0.01	269.	0.009	-0.55 ± 0.03	0.59 ± 0.04
NGC 5055 E nuc. 1	13 15 58.323	+42 00 27.4	0.18 ± 0.01	0.15 ± 0.01	0.15 ± 0.01	269.	5.630	-0.07 ± 0.04	1.00 ± 0.02
NGC 5194 E nuc. 6 a	13 29 39.324	+47 08 40.7	0.26 ± 0.02	0.20 ± 0.01	0.21 ± 0.01	259.	12.321	-0.09 ± 0.03	1.00 ± 0.01
NGC 5194 E nuc. 3	13 29 45.13	+47 09 57.4	0.33 ± 0.02	0.25 ± 0.01	0.26 ± 0.01	259.	7.048	-0.10 ± 0.03	1.00 ± 0.01
NGC 5194 E nuc. 11 a	13 29 47.138	+47 13 41.298	0.26 ± 0.02	0.06 ± 0.01	0.10 ± 0.01	259.	4.941	-0.42 ± 0.04	0.75 ± 0.05
NGC 5194 E nuc. 11 b	13 29 47.58	+47 13 24.799	< 0.04	0.11 ± 0.01	0.09 ± 0.01	259.	4.340	-0.25 ± 0.17	0.91 ± 0.12

Table 5 continued

Table 5 (continued)

Source ID	R.A.	Decl.	$S_{3\text{ GHz}}$	$S_{15\text{ GHz}}$	$S_{33\text{ GHz}}$	$d_{\text{ap}}$	$r_{\text{G}}$	$\alpha$	$f_{\text{T}}^{33\text{ GHz}}$
	(J2000)	(J2000)	(mJy)	(mJy)	(mJy)	(pc)	(kpc)		
NGC 5194 Enum. 11 d	13 29 49.582	+47 13 28.7	< 0.04	0.04 ± 0.01	0.07 ± 0.01	259.	4.078	0.74 ± 0.34	1.00 ± 0.02
NGC 5194 Enum. 11 c	13 29 49.671	+47 14 00.2	0.42 ± 0.02	0.14 ± 0.01	0.06 ± 0.01	259.	5.221	-0.75 ± 0.05	0.22 ± 0.11
NGC 5194c	13 29 50.022	+47 11 31.898	0.76 ± 0.03	0.42 ± 0.02	0.16 ± 0.01	259.	1.804	-0.48 ± 0.03	0.69 ± 0.04
NGC 5194 Enum. 11 e	13 29 50.642	+47 13 44.9	0.20 ± 0.01	0.18 ± 0.01	0.13 ± 0.01	259.	4.633	-0.18 ± 0.04	0.96 ± 0.02
NGC 5194 b	13 29 51.64	+47 12 06.7	1.09 ± 0.04	0.41 ± 0.02	0.22 ± 0.01	259.	0.977	-0.64 ± 0.02	0.44 ± 0.04
NGC 5194 e	13 29 52.553	+47 11 52.6	3.17 ± 0.10	1.13 ± 0.04	0.46 ± 0.02	259.	0.365	-0.77 ± 0.02	0.17 ± 0.05
NGC 5194 d	13 29 52.729	+47 11 40.6	4.68 ± 0.14	1.24 ± 0.04	0.53 ± 0.02	259.	0.092	-0.89 ± 0.02	0.24 ± 0.04
NGC 5194 Enum. 1c	13 29 53.129	+47 12 39.4	0.18 ± 0.02	0.06 ± 0.01	0.14 ± 0.01	259.	2.323	-0.13 ± 0.04	0.98 ± 0.02
NGC 5194 Enum. 4 a	13 29 53.932	+47 14 04.899	< 0.04	< 0.02	0.08 ± 0.01	259.	5.880	...	...
NGC 5194 Enum. 10 a	13 29 55.346	+47 10 47.199	0.12 ± 0.02	0.07 ± 0.01	0.09 ± 0.01	259.	2.336	-0.16 ± 0.07	0.97 ± 0.04
NGC 5194 Enum. 4c	13 29 55.611	+47 13 50.2	0.16 ± 0.01	0.06 ± 0.01	0.09 ± 0.01	259.	5.798	-0.29 ± 0.05	0.88 ± 0.04
NGC 5194 a	13 29 55.791	+47 11 45.097	0.55 ± 0.02	0.32 ± 0.01	0.35 ± 0.02	259.	1.906	-0.22 ± 0.03	0.93 ± 0.02
NGC 5194 Enum. 10 b	13 29 56.523	+47 10 46.9	0.25 ± 0.02	0.15 ± 0.01	0.14 ± 0.01	259.	2.723	-0.24 ± 0.04	0.91 ± 0.03
NGC 5194 Enum. 4 d	13 29 58.733	+47 14 09.398	0.13 ± 0.01	0.08 ± 0.01	0.07 ± 0.01	259.	7.696	-0.28 ± 0.06	0.89 ± 0.05
NGC 5194 Enum. 5 a	13 29 59.6	+47 13 59.8	0.26 ± 0.02	0.15 ± 0.01	0.17 ± 0.01	259.	7.742	-0.20 ± 0.04	0.94 ± 0.02
NGC 5194 Enum. 9	13 29 59.782	+47 11 12.3	0.19 ± 0.02	0.17 ± 0.01	0.21 ± 0.01	259.	4.131	0.03 ± 0.04	1.00 ± 0.02
NGC 5194 Enum. 7 a	13 30 01.029	+47 09 28.599	0.07 ± 0.02	0.11 ± 0.01	0.12 ± 0.02	259.	6.221	0.22 ± 0.11	1.00 ± 0.03
NGC 5194 Enum. 8	13 30 01.482	+47 12 51.7	0.46 ± 0.02	0.38 ± 0.01	0.29 ± 0.01	259.	6.650	-0.17 ± 0.03	0.96 ± 0.01
NGC 5194 Enum. 7 b	13 30 02.382	+47 09 48.7	0.45 ± 0.02	0.21 ± 0.01	0.20 ± 0.01	259.	6.329	-0.38 ± 0.03	0.80 ± 0.03
NGC 5194 Enum. 7 c	13 30 03.471	+47 09 40.3	0.18 ± 0.02	0.07 ± 0.01	0.05 ± 0.01	259.	6.962	-0.55 ± 0.08	0.59 ± 0.11
NGC 5398	14 01 20.105	-33 04 09.2	0.86 ± 0.03	0.62 ± 0.02	0.64 ± 0.02	260.	1.381	-0.13 ± 0.02	0.98 ± 0.01
NGC 5457 Enum. 6 a	14 02 28.203	+54 16 27.2	0.68 ± 0.02	0.39 ± 0.01	0.40 ± 0.01	227.	15.707	-0.24 ± 0.02	0.91 ± 0.01
NGC 5457 Enum. 6 b	14 02 29.607	+54 16 15.799	1.02 ± 0.03	0.56 ± 0.02	0.45 ± 0.02	227.	15.550	-0.34 ± 0.02	0.83 ± 0.02
NGC 5457 Enum. 6 c	14 02 30.566	+54 16 09.798	0.58 ± 0.02	0.42 ± 0.02	0.30 ± 0.02	227.	15.422	-0.25 ± 0.02	0.91 ± 0.02
NGC 5457 Enum. 5 a	14 03 01.203	+54 14 28.4	0.96 ± 0.03	0.68 ± 0.02	0.72 ± 0.02	227.	13.129	-0.14 ± 0.02	0.98 ± 0.01
NGC 5457 Enum. 1	14 03 10.2	+54 20 57.8	0.08 ± 0.01	< 0.02	0.05 ± 0.01	227.	0.744	-0.15 ± 0.07	0.97 ± 0.04
NGC 5457	14 03 12.531	+54 20 55.2	0.34 ± 0.01	0.09 ± 0.01	0.15 ± 0.01	227.	0.062	-0.41 ± 0.03	0.77 ± 0.03
NGC 5457 Enum. 3 a	14 03 38.317	+54 18 51.398	0.30 ± 0.02	0.17 ± 0.02	< 0.10	227.	9.307	-0.36 ± 0.10	0.82 ± 0.09
NGC 5457 Enum. 3 b	14 03 39.894	+54 18 56.799	0.48 ± 0.02	0.44 ± 0.03	0.35 ± 0.03	227.	9.655	-0.10 ± 0.03	1.00 ± 0.02
NGC 5457 Enum. 3 c	14 03 41.437	+54 19 04.9	4.27 ± 0.13	3.33 ± 0.10	2.91 ± 0.09	227.	9.964	-0.16 ± 0.02	0.97 ± 0.01
NGC 5457 Enum. 3 d	14 03 42.912	+54 19 24.699	0.42 ± 0.02	0.24 ± 0.02	0.21 ± 0.03	227.	10.113	-0.31 ± 0.05	0.86 ± 0.04
NGC 5457 Enum. 4 a	14 03 52.036	+54 21 52.5	0.18 ± 0.01	0.12 ± 0.01	0.10 ± 0.01	227.	12.149	-0.24 ± 0.04	0.91 ± 0.03
NGC 5457 Enum. 4 b	14 03 52.997	+54 21 57.3	0.20 ± 0.01	0.15 ± 0.01	0.14 ± 0.01	227.	12.453	-0.16 ± 0.04	0.97 ± 0.02
NGC 5457 Enum. 4 c	14 03 53.203	+54 22 06.3	0.46 ± 0.02	0.26 ± 0.01	0.28 ± 0.01	227.	12.540	-0.22 ± 0.02	0.93 ± 0.01
NGC 5457 Enum. 4 d	14 03 53.993	+54 22 10.8	0.50 ± 0.02	0.26 ± 0.01	0.25 ± 0.01	227.	12.795	-0.32 ± 0.02	0.86 ± 0.02
NGC 5474	14 05 01.3	+53 39 44	< 0.03	< 0.02	< 0.02	231.	0.070	...	...
NGC 5713 Enum. 2 a	14 40 10.8	-00 17 35.5	0.82 ± 0.03	0.48 ± 0.02	0.26 ± 0.01	726.	1.984	-0.44 ± 0.02	0.74 ± 0.03
NGC 5713 Enum. 2 b	14 40 10.86	-00 17 50.2	0.41 ± 0.02	0.27 ± 0.02	0.09 ± 0.01	726.	3.295	-0.42 ± 0.04	0.75 ± 0.04
NGC 5713	14 40 11.3	-00 17 27	1.42 ± 0.04	0.82 ± 0.03	0.35 ± 0.01	726.	0.795	-0.52 ± 0.02	0.63 ± 0.03
NGC 5713 Enum. 1	14 40 11.36	-00 17 18.2	5.54 ± 0.17	2.28 ± 0.07	1.44 ± 0.04	726.	0.313	-0.56 ± 0.02	0.57 ± 0.03
NGC 5866	15 06 29.5	+55 45 47.7	5.48 ± 0.17	3.57 ± 0.11	2.01 ± 0.06	519.	0.051	-0.40 ± 0.02	0.78 ± 0.02
NGC 6946 Enum. 4 c	20 34 22.738	+60 10 34.197	0.68 ± 0.02	0.70 ± 0.02	0.62 ± 0.02	231.	8.739	-0.03 ± 0.02	1.00 ± 0.01
NGC 6946 Enum. 8	20 34 32.28	+60 10 19.3	1.16 ± 0.04	0.56 ± 0.02	0.58 ± 0.02	231.	6.122	-0.32 ± 0.02	0.85 ± 0.02
NGC 6946 Enum. 5 a	20 34 37.155	+60 05 10.099	< 0.03	< 0.02	0.07 ± 0.01	231.	9.239	...	...
NGC 6946 Enum. 5 b	20 34 39.361	+60 04 52.4	0.14 ± 0.01	0.16 ± 0.01	0.16 ± 0.01	231.	9.704	0.06 ± 0.04	1.00 ± 0.01
NGC 6946 Enum. 3 a	20 34 49.865	+60 12 40.699	0.04 ± 0.01	0.11 ± 0.01	0.10 ± 0.01	231.	7.742	0.18 ± 0.09	1.00 ± 0.02
NGC 6946 Enum. 3 b	20 34 52.24	+60 12 43.7	0.19 ± 0.01	0.18 ± 0.01	0.17 ± 0.01	231.	7.729	-0.04 ± 0.03	1.00 ± 0.01
NGC 6946 b	20 34 52.26	+60 09 14.3	19.95 ± 0.60	8.56 ± 0.26	5.55 ± 0.17	231.	0.016	-0.53 ± 0.02	0.62 ± 0.03
NGC 6946 Enum. 6 b	20 35 06.965	+60 10 46.5	0.21 ± 0.01	0.19 ± 0.01	0.12 ± 0.01	231.	4.728	-0.14 ± 0.04	0.98 ± 0.02
NGC 6946 Enum. 9	20 35 11.086	+60 08 57.45	0.83 ± 0.03	0.73 ± 0.02	0.71 ± 0.02	231.	5.071	-0.07 ± 0.02	1.00 ± 0.01
NGC 6946 Enum. 7	20 35 12.974	+60 08 50.55	0.26 ± 0.01	0.43 ± 0.01	0.34 ± 0.01	231.	5.637	0.13 ± 0.03	1.00 ± 0.01
NGC 6946 Enum. 1	20 35 16.801	+60 11 00	0.34 ± 0.01	0.31 ± 0.01	0.34 ± 0.01	231.	6.989	-0.01 ± 0.03	1.00 ± 0.01
NGC 7331	22 37 04.1	+34 24 56	0.05 ± 0.01	0.23 ± 0.03	< 0.07	492.	0.000	0.90 ± 0.18	1.00 ± 0.01

Table 5 continued



Table 5 (continued)

Source ID	R.A.	Decl.	$S_{3\text{ GHz}}$	$S_{15\text{ GHz}}$	$S_{33\text{ GHz}}$	$d_{\text{ap}}$	$r_{\text{G}}$	$\alpha$	$f_{\text{T}}^{33\text{ GHz}}$
	(J2000)	(J2000)	(mJy)	(mJy)	(mJy)	(pc)	(kpc)		
NGC 7793 Enum. 1	23 57 48.8	-32 36 57.991	$0.05 \pm 0.01$	$0.02 \pm 0.01$	$< 0.07$	133.	2.574	$-0.42 \pm 0.25$	$0.76 \pm 0.27$
NGC 7793 Enum. 3	23 57 48.8	-32 34 51.995	$0.10 \pm 0.01$	$0.10 \pm 0.01$	$< 0.08$	133.	1.016	$-0.03 \pm 0.09$	$1.00 \pm 0.04$
NGC 7793 a	23 57 49.2	-32 35 24	$0.06 \pm 0.01$	$0.04 \pm 0.01$	$0.05 \pm 0.01$	133.	0.174	$-0.18 \pm 0.14$	$0.95 \pm 0.09$
NGC 7793 b	23 57 49.58	-32 35 25.6	$0.10 \pm 0.01$	$0.05 \pm 0.01$	$0.07 \pm 0.01$	133.	0.081	$-0.26 \pm 0.09$	$0.90 \pm 0.07$
NGC 7793 Enum. 2	23 57 56.1	-32 35 40	$< 0.04$	$< 0.02$	$< 0.04$	133.	1.526	...	...
Likely Associated with Supernovae									
NGC 6946 Enum. 6 a	20 35 06.08	+60 10 58.5	$0.72 \pm 0.02$	$0.42 \pm 0.01$	$0.48 \pm 0.02$	231.	4.855	$-0.20 \pm 0.02$	$0.94 \pm 0.01$
Likely AME Candidates									
NGC 2403 Enum. 5	07 36 19.839	+65 37 05.5	$0.64 \pm 0.02$	$0.59 \pm 0.02$	$0.56 \pm 0.02$	109.	3.464	$-0.06 \pm 0.02$	$1.00 \pm 0.01$
NGC 2403 Enum. 3	07 37 06.948	+65 36 39	$2.01 \pm 0.06$	$1.63 \pm 0.05$	$1.62 \pm 0.05$	109.	2.811	$-0.10 \pm 0.02$	$1.00 \pm 0.01$
NGC 4254 Enum. 1 a	12 18 49.203	+14 23 57.9	$0.16 \pm 0.01$	$0.07 \pm 0.01$	$0.12 \pm 0.01$	489.	4.428	$-0.18 \pm 0.04$	$0.95 \pm 0.03$
NGC 4631 f	12 42 06.256	+32 32 31.9	$0.79 \pm 0.03$	$0.27 \pm 0.01$	$0.51 \pm 0.02$	259.	1.566	$-0.23 \pm 0.02$	$0.92 \pm 0.01$
NGC 4631 g	12 42 07.466	+32 32 31.599	$1.65 \pm 0.05$	$0.88 \pm 0.03$	$0.97 \pm 0.03$	259.	0.960	$-0.25 \pm 0.02$	$0.91 \pm 0.01$
NGC 4631 h	12 42 08.059	+32 32 34.899	$2.07 \pm 0.06$	$0.97 \pm 0.03$	$1.29 \pm 0.04$	259.	1.769	$-0.24 \pm 0.02$	$0.92 \pm 0.01$
NGC 4631 Enum. 2 a	12 42 21.419	+32 33 06.3	$0.28 \pm 0.01$	$0.11 \pm 0.01$	$0.18 \pm 0.01$	259.	9.974	$-0.22 \pm 0.03$	$0.93 \pm 0.02$
NGC 4725 b	12 50 28.484	+25 30 21.899	$0.08 \pm 0.01$	$0.11 \pm 0.01$	$0.19 \pm 0.01$	404.	1.921	$0.37 \pm 0.06$	$1.00 \pm 0.01$
NGC 5194 Enum. 2	13 29 44.1	+47 10 23.4	$0.66 \pm 0.02$	$0.37 \pm 0.01$	$0.39 \pm 0.01$	259.	6.834	$-0.24 \pm 0.02$	$0.92 \pm 0.01$
NGC 5194 Enum. 1 a	13 29 49.508	+47 12 40.296	$0.29 \pm 0.02$	$0.24 \pm 0.01$	$0.38 \pm 0.02$	259.	2.534	$0.09 \pm 0.03$	$1.00 \pm 0.01$
NGC 5194 Enum. 1 b	13 29 52.07	+47 12 43.6	$0.28 \pm 0.02$	$0.24 \pm 0.01$	$0.27 \pm 0.01$	259.	2.322	$-0.02 \pm 0.03$	$1.00 \pm 0.01$
NGC 5194 Enum. 4 b	13 29 55.493	+47 14 01.6	$0.35 \pm 0.02$	$0.13 \pm 0.01$	$0.19 \pm 0.01$	259.	6.193	$-0.28 \pm 0.03$	$0.89 \pm 0.02$
NGC 5457 Enum. 2	14 02 55	+54 22 27.5	$0.18 \pm 0.01$	$0.11 \pm 0.01$	$0.17 \pm 0.01$	227.	6.451	$-0.05 \pm 0.04$	$1.00 \pm 0.02$
NGC 5457 Enum. 7	14 04 29.334	+54 23 47.6	$2.15 \pm 0.07$	$1.07 \pm 0.03$	$1.14 \pm 0.03$	227.	23.861	$-0.29 \pm 0.02$	$0.88 \pm 0.01$
NGC 6946 Enum. 4 a	20 34 19.842	+60 10 06.6	$0.92 \pm 0.03$	$0.75 \pm 0.02$	$0.83 \pm 0.03$	231.	9.044	$-0.06 \pm 0.02$	$1.00 \pm 0.01$
NGC 6946 Enum. 4 b	20 34 21.41	+60 10 17.699	$0.06 \pm 0.01$	$0.42 \pm 0.01$	$0.34 \pm 0.01$	231.	8.801	$0.13 \pm 0.05$	$1.00 \pm 0.01$
NGC 6946 a	20 34 51.295	+60 09 39.2	$0.35 \pm 0.02$	$0.35 \pm 0.01$	$0.51 \pm 0.03$	231.	1.004	$0.09 \pm 0.03$	$1.00 \pm 0.01$
NGC 6946 c	20 34 52.742	+60 09 30.5	$0.27 \pm 0.01$	$0.34 \pm 0.01$	$0.25 \pm 0.03$	231.	0.601	$0.08 \pm 0.04$	$1.00 \pm 0.01$
NGC 6946 Enum. 2 a	20 35 23.572	+60 09 48.899	$0.05 \pm 0.01$	$0.16 \pm 0.01$	$0.15 \pm 0.01$	231.	8.120	$0.30 \pm 0.08$	$1.00 \pm 0.01$
NGC 6946 Enum. 2 b	20 35 25.381	+60 09 58.8	$1.03 \pm 0.03$	$0.76 \pm 0.02$	$0.70 \pm 0.02$	231.	8.595	$-0.17 \pm 0.02$	$0.96 \pm 0.01$

#### 4. RESULTS

Using the 3, 15, and 33 GHz photometry, along with the  $8\ \mu\text{m}$  imaging from *Spitzer*, we classify each region as either a star-forming region (SF), a background galaxy candidate (BG), a likely supernova remnant (SNe/R: see Section 5.4), or an anomalous microwave emission candidate (AME: see Section 5.5). In total we have identified 320 star-forming regions, 14 likely background galaxies, 10 likely supernovae/supernova remnants, and 33 AME candidates. Given that we are primarily interested in emission arising from our sample galaxies, the potential background galaxies have been removed from all plots, and are discussed as a separate population of sources in Section 5.3. Regions identified at  $7''$  which include emission from potential AME and SNe/R candidates are correspondingly classified in Table 5.

We present results for the spectral index and thermal fraction distributions only including regions identified in

the SFRs that have a  $S/N \geq 3$  measured in at least two radio bands. This ensures that our fit results are not biased by single detections at one frequency, and allows us to make accurate comparisons with the regions identified in M18a, for which a detection at 33 GHz was required. This requirement removes 4 likely background galaxies, 4 likely supernova remnants, and 34 star-forming regions. These single-band detections are distributed almost uniformly across all three frequency bands: 19, 11, and 12 at 3, 15, and 33 GHz, respectively. Accordingly, in the sample used to study the radio spectral indices and thermal fractions, we have retained 335 (286 SF, 10 BG, 6 SNe/R, and 33 AME) of the 377 sources with a statistically significant detection in at least one band. The median  $S/N$  of these 335 sources is 18, 15, and 9 for detections at 3, 15, and 33 GHz, respectively.

We apply the same criteria for sources included in the spectral index and thermal fraction analysis using the  $7''$  smoothed images. This removes 17 star-forming regions. These single-band detections are also distributed

uniformly across all three bands: 7, 4, and 6 at 3, 15, and 33 GHz, respectively. Accordingly, we have retained 163 (142 SF, 0 BG, 1 SNe/R, and 20 AME) of the 180 sources with a statistically significant detection in at least one band. The median  $S/N$  of these 163 sources is 24, 23, and 19 for detections at 3, 15, and 33 GHz, respectively.

#### 4.1. Spectral Indices

The simplest approach to modeling the radio spectra of galaxies is by adopting a two-component power-law, with the thermal/nonthermal ratio as well as the non-thermal spectral index allowed to vary as free parameters. For many star-forming galaxies in the local Universe, this model adequately describes the dominant physical processes occurring at radio frequencies (Condon 1992). However, a robust interpretation of the radio spectrum can be complex. For example: the thermal and nonthermal fractions may vary with galaxy mass (e.g. Hughes et al. 2007; Bell 2003), the nonthermal index can vary within galaxies (Tabatabaei et al. 2017), and AME may add an additional component to the radio spectra at high frequencies in some regions (e.g. Murphy et al. 2010, 2018b).

To measure the 3 – 33 GHz spectral indices, we performed a linear least-squares fit to the data with a single power-law representing the combination of thermal and nonthermal emission. The distributions of the measured spectral slopes with the 10 likely background galaxies removed are given in the top panel of Figure 2 (325 total regions). The median spectral indices we measure from 3 – 15, 15 – 33, and 3 – 33 GHz are  $-0.25 \pm 0.024$ ,  $-0.20 \pm 0.043$ , and  $-0.23 \pm 0.018$ , respectively. The median absolute deviation of these distributions is 0.34, 0.61, and 0.27 respectively. Interestingly, we do not see particularly steep spectral indices from 3 – 15 GHz, indicating that the contribution of non-thermal emission to the radio flux density of individual star-forming regions is marginal on  $\sim 100$  pc scales in these galaxies. This is consistent with the results presented in Murphy et al. (2012), where they show that the thermal fraction at 33 GHz increased as function of decreasing linear resolution. Despite the relatively flat spectral slopes from 3 – 15 GHz, we do see evidence that the spectrum continues to flatten from 15 – 33 GHz, on average. This is consistent with expectations for star-forming regions, where the radio spectrum is synchrotron-dominated at low frequencies, and flattens at higher frequencies as the contribution of thermal emission increases (Condon et al. 2012; Clemens et al. 2010; Murphy et al. 2013). Finally, we do not see any significant evidence for free-free absorption, which is known to affect the compact cen-

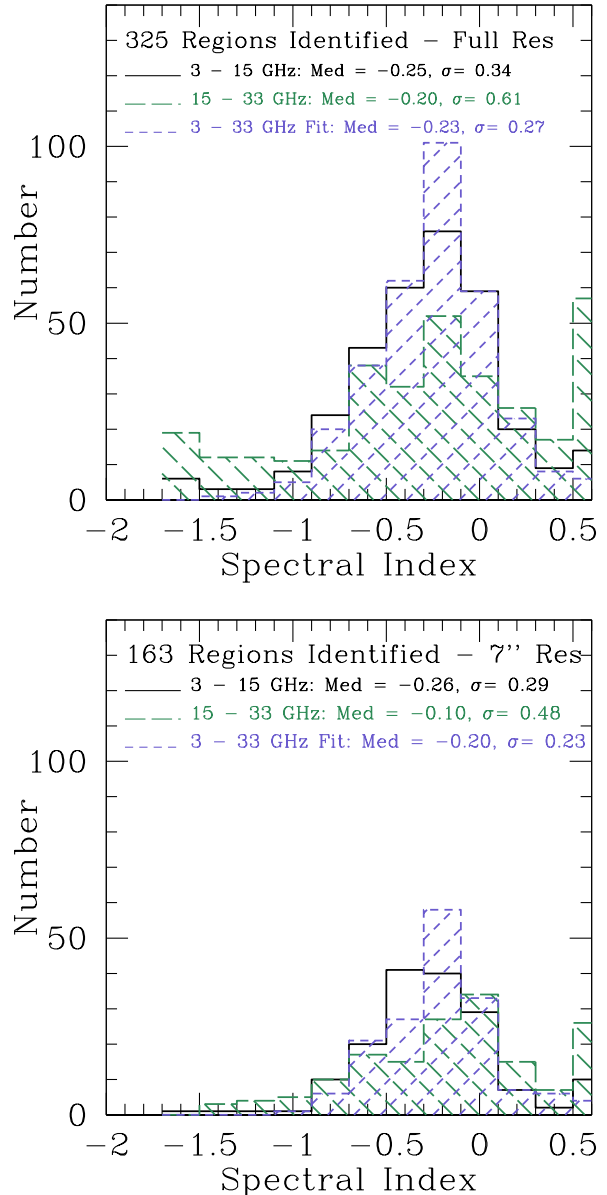


**Figure 2.** Top: The 3–15 GHz (black), 15–33 GHz (green), and 3–33 GHz (purple) radio spectral index distributions for 325 regions identified in the SFRS. The median size of the apertures used is  $162 \pm 6.5$  pc. Bottom: The spectral index distributions for 163  $7''$  regions identified in M18a. The median size of the apertures used at  $7''$  resolution is  $259 \pm 7.2$  pc. Overall, we find that the 3 – 33 GHz distributions measured at  $\sim 2''$  and  $7''$  are consistent with one another, implying that free-free emission dominates the radio spectra of star-forming regions on scales up to  $\sim 500$  pc. Not included in any of these plots are the likely background galaxy candidates identified.

tral regions of local star-forming and starburst galaxies, and would result in steep spectral indices even at high frequencies (Condon & Yin 1990; Clemens et al. 2008; Murphy et al. 2013).

In the nearby Universe, the typical radio spectrum of normal star-forming galaxies is well-described by a power-law spectrum with a spectral index of  $-0.7$ , and a thermal fraction of  $\sim 10\%$  at  $\sim 1$  GHz (Klein et al. 1988; Condon & Yin 1990), whereas studies of local luminous infrared galaxies (LIRGs) find a flat spectrum around 1 GHz and a steepening spectrum above 10 GHz (Clemens et al. 2008; Leroy et al. 2011; Murphy et al. 2013). New high-resolution observations of a large sample of LIRGs in the Great Observatories All-Sky LIRG Survey (GOALS) have revealed that the steep spectrum seen in highly star-forming galaxies are attributed solely to the nucleus, and that in extranuclear regions the spectral shape is typical of the star-forming regions identified in this study (Linden et al. 2019).

#### 4.2. Thermal Fractions

Given the results above, we now calculate the thermal fraction of each region by using the spectral index, measured in Section 4.1, from 3 – 15 GHz ( $\alpha_{3-15\text{ GHz}}$ ) to set the lower-limit on the nonthermal spectral index ( $\alpha^{\text{NT}}$ ) such that  $\alpha^{\text{NT}} = -0.83$  if  $\alpha_{3-15\text{ GHz}} \geq -0.83$ , and  $\alpha^{\text{NT}} = \alpha_{3-15\text{ GHz}}$  if  $\alpha_{3-15\text{ GHz}} < -0.83$ . A constant nonthermal radio spectral index of  $-0.83$  is assumed based on the average non-thermal spectral index found among the 10 star-forming regions studied in NGC 6946 by Murphy et al. (2011). Furthermore, this value is consistent with the results of Niklas & Beck (1997, i.e.,  $\alpha^{\text{NT}} = -0.83$  with a scatter of  $\sigma_{\alpha^{\text{NT}}} = 0.13$ ) for a sample of 74 nearby galaxies. Finally, we adopt a single power-law exponent for the free-free emission ( $\sim -0.1$ ), and use the fit from 3 to 33 GHz to set the overall radio spectral index. Then, using the prescription in Klein et al. (1984), we can calculate the thermal fraction at 33 GHz such that,

$$f_{\text{T}}^{\nu_1} = \frac{\left(\frac{\nu_2}{\nu_1}\right)^{-\alpha} - \left(\frac{\nu_2}{\nu_1}\right)^{-\alpha^{\text{NT}}}}{\left(\frac{\nu_2}{\nu_1}\right)^{-0.1} - \left(\frac{\nu_2}{\nu_1}\right)^{-\alpha^{\text{NT}}}} \quad (1)$$

where  $\nu_1$  is the target frequency (33 GHz),  $\alpha$  is the observed slope from 3 to 33 GHz, and  $\alpha^{\text{NT}}$  is the non-thermal spectral index. In the top Panel of Figure 3 we show the resulting thermal fractions of the star-forming regions in our sample using the empirically measured values from Equation 1. We find that the median value is  $92 \pm 0.8\%$  with a median absolute deviation of 11%. This demonstrates that we can reliably use the 33 GHz flux density to infer the total free-free emission, and thus current star formation activity, on the scales of individ-

ual HII and star-forming regions. While this result had been suggested by our previous GBT and VLA campaigns (e.g., Murphy et al. 2011, 2012, 2018a), this is the first measurement of the 33 GHz thermal fraction based on the shape of the radio spectrum at these frequencies and spatial scales in nearby galaxies.

Further, by restricting our analysis such that we remove all non-SF regions, all apertures containing multiple smaller individual regions, and require  $r_{\text{G}} \geq 250\text{pc}$  (238 regions), we mitigate contamination from any central AGN and can determine broad population statistics for extragalactic HII regions using our cleanest sample of extranuclear star-forming regions. In Figure 4 we find that the median thermal fraction is  $93 \pm 0.8\%$  with a median absolute deviation of 10%. This value is consistent with the results presented in Figures 2, and 3, and confirms that supernova remnants, ultra-compact HII regions, and/or AME candidates do not bias our results.

Finally, we measure the thermal fraction at 33 GHz for 163 regions identified at  $7''$  resolution in M18a to be  $94 \pm 0.8\%$  with a median absolute deviation of 8%. This result is consistent with the measurements at  $2''$  and confirms that free-free emission dominates the radio spectra of star-forming regions on scales up to  $\sim 500\text{pc}$ . Further, when we apply the same radial cut (i.e.,  $r_{\text{G}} > 250\text{pc}$ ) and remove all non-SF regions, retaining 111/163 regions, the median thermal fraction at 33 GHz is  $97 \pm 0.5\%$  with a median absolute deviation of 4.6%. Thus, it is clear that regardless of the size of the photometric apertures used, isolating extranuclear SF regions in nearby galaxies results in a higher thermal fraction at 33 GHz and a smaller median absolute deviation in the overall distribution.

#### 4.3. MCMC Parameter Estimation

From Equation 1 it is clear that reliable estimates for the 33 GHz thermal fraction are sensitive to the value adopted for the nonthermal spectral index ( $\alpha^{\text{NT}}$ ). While the median 3 – 15 GHz spectral index observed for our sample is well below the canonical value (i.e.,  $-0.83$ ), degeneracies may still exist between  $\alpha^{\text{NT}}$  and  $f_{\text{T}}$ . In this case classical  $\chi^2$  fitting methods may underestimate the true uncertainties associated with modeling the radio spectrum as a two-component power-law [i.e.,  $S(\nu) = A\nu^{\alpha^{\text{NT}}} + B\nu^{-0.1}$ ]. Here, we explore whether the marginalized posterior distributions from a Monte-Carlo Markov Chain (MCMC) analysis better reflect the uncertainties associated with this decomposition (Hogg et al. 2010).

For this exercise, we use the Python package EMCEE (Foreman-Mackey et al. 2013) to generate posterior

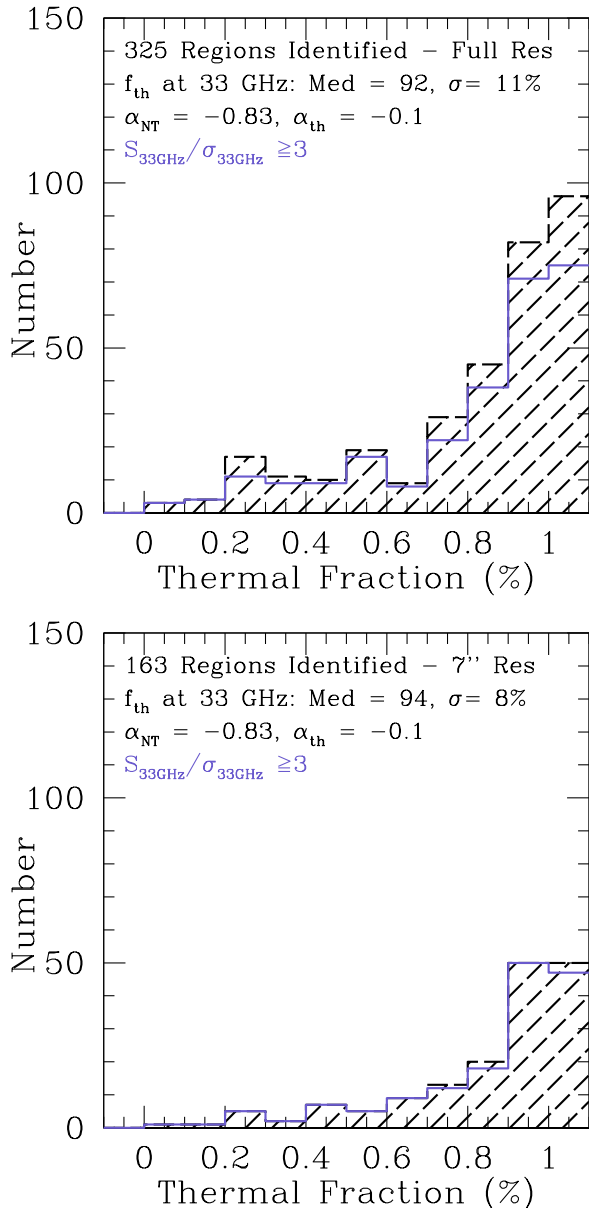


**Figure 3.** Top: The thermal fraction distribution at 33 GHz for 325 star-forming regions in the SFRS (black). In purple we show the distribution for regions with a  $S/N \geq 3$  at 33 GHz, demonstrating that the lack of a significant 33 GHz detection does not bias our results. The median size of the apertures used is  $162 \pm 6.5$  pc. Bottom: The thermal fraction distribution for 163  $7''$  regions identified in M18a with a  $S/N > 3$  in two radio bands. The median size of the apertures used at  $7''$  resolution is  $259 \pm 7.2$  pc. Overall, we find that the median thermal fraction at 33 GHz is  $\sim 93\%$ , and that this value does not vary significantly from 100 up to  $\sim 500$  pc scales in our galaxy sample.

probability distributions for each of the fitted parameters ( $\alpha^{\text{NT}}$ ,  $f_{\text{T}}$ , and  $A/B$ ) given the typical  $S/N$  ratio of our three-band observations. Following Westcott et al. (2018), we parameterize our two-component power-law model at a reference frequency of 1 GHz to avoid dependencies in frequency space. Further, we adopt a gaussian probability distribution function for the nonthermal spectral index whose mean and standard deviation are consistent with the values obtained in Niklas & Beck (1997). Finally, we make a slight modification to Equation 9 presented in Westcott et al. (2018),

$$P(\theta) \propto H(A, B) e^{-\frac{(\alpha - 0.83)^2}{0.13^2}} \quad (2)$$

such that  $H$  is equal to 1 when the values of  $A$  and  $B$  are greater than zero. This is done in order to constrain the nonthermal spectral index, thermal fraction, and normalization constants of each component simultaneously. We make 1000 realizations of this model at three different  $S/N$  ratios (5, 10, and 50) by randomly selecting a nonthermal spectral index ( $-2 < \alpha^{\text{NT}} < 0$ ) and values of  $A(B)$  [ $0 < A(B) < 1$ ], to represent the typical variance in the values observed for our sample.

In Figure 5 we plot the relative difference in the input and output thermal fraction as a function of the input nonthermal spectral index. For a fixed  $S/N$  per region of 10, and with only three data points, our MCMC modeling can recover the input nonthermal spectral index to within  $1\sigma$  for  $-1.25 < \alpha^{\text{NT}} < 0.25$ . Importantly, we find that the best-constrained spectra have nonthermal indices very close to the fixed-value adopted for our  $\chi^2$ -minimization ( $-0.83$ ). This result demonstrates that adopting fixed values for the  $\alpha^{\text{NT}}$  does not introduce systematic biases into the derived 33 GHz thermal fractions, over a reasonable set of input conditions for our two-component power-law model. This is an important result for calibrations of the total star-formation rate, which rely on using the observed radio continuum (Murphy et al. 2011, 2012).

## 5. DISCUSSION

### 5.1. Trends with Galactocentric Radius

Following the same procedure as M18a, we use the measured position angle (PA) and inclination of each galaxy to convert the angular separation of each star-forming region from the nucleus into a de-projected galactocentric radius ( $r_{\text{G}}$ ). In M18a we found that the median 33 GHz continuum-to- $\text{H}\alpha$  line flux ratio was statistically larger within  $r_{\text{G}} < 250$  pc relative to the outer disk regions by a factor of  $1.82 \pm 0.39$ , while the ratio of 33 GHz-to- $24\mu\text{m}$  flux densities is lower by a factor of  $0.45 \pm 0.08$ . Such a situation may arise if the circum-

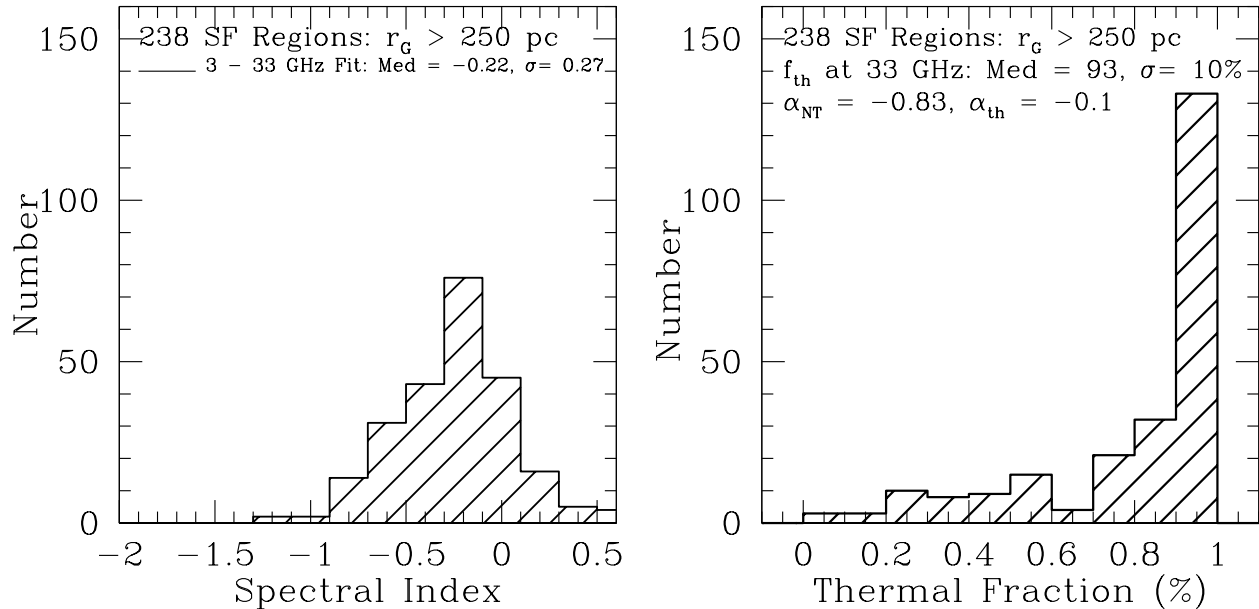


**Figure 4.** The spectral index and thermal fraction distributions for all 238 SF regions with the likely supernova remnants and AME candidates removed, and a requirement of  $r_G \geq 250$ pc (The same cut adopted in M18a). This represents the cleanest sample of extranuclear star-forming regions for which we can determine broad population statistics for extragalactic HII regions. Ultimately we find that the median spectral index and thermal fraction distributions at 33 GHz are consistent with the results presented in Figures 2 and 3, confirming that supernova remnants, ultra-compact HII regions, and AME candidates do not bias our results.

nuclear regions of these galaxies have extended star formation histories in which star formation that has taken place over a longer period of time, resulting in an accumulation of young dust-heating stars in addition to much older bulge stars that boost the  $24 \mu\text{m}$  flux density relative to what is seen in the extranuclear regions. This is largely opposite to what we would expect if there was an additional nonthermal component powering the 33 GHz emission in the central regions of these galaxies, unless the excess dust-heating at  $24 \mu\text{m}$  far exceeds any additional nonthermal emission contribution at 33 GHz.

Therefore, these results suggested that the larger ratio of 33 GHz flux density to H $\alpha$  line flux found in the central regions of these galaxies may primarily arise from increased extinction. We can now test this picture for 325 discrete regions (background galaxies removed) with detailed radio spectral fitting and thermal fraction estimates, which do not suffer from the effects of variable dust extinction in galaxies. In Figure 6 it is clear that the overall dispersion in the measured spectral index and thermal fraction at 33 GHz increases significantly for regions that lie within the 250 pc galactocentric radius cut used in M18a to distinguish extranuclear from nuclear/circumnuclear star-forming regions. In fact, limiting the analysis to sources with  $r_G < 250$ pc results in a value for the median 33 GHz thermal fraction of  $\sim 71 \pm 3.5\%$  with a median absolute deviation of  $\sim 18\%$

relative to  $\sim 95 \pm 2.2\%$  with a median absolute deviation of  $\sim 11\%$  for regions with  $r_G \geq 250$ pc. Additionally, the scatter of the thermal fraction distribution increases by nearly a factor of 2 within  $r_G < 250$ pc. This confirms that while extinction may play a role in driving the previously seen correlations, excess nonthermal emission is indeed present in many of the circumnuclear star-forming regions observed in the SFRS.

## 5.2. Model Age Fitting

By making use of differences in the timescales associated with thermal (free-free) and synchrotron emission, we can place estimates on the age of star-forming regions by examining how these processes affect the radio spectral index from 3 – 33 GHz. Since free-free emission is directly associated with ionizing photons that are only produced by the shortest-lived ( $\leq 10$  Myr) massive stars, its presence in large quantities relative to synchrotron emission is indicative of very young star formation.

To better-quantify these different timescales, we use a Starburst 99 (SB99) model of a single instantaneous burst with default inputs (solar metallicity and 2-component Kroupa IMF) run for 1 Gyr (Leitherer et al. 1999). However, in order to take into account the fact that at the median physical scales we are probing, ( $\sim 100$  pc), a single, instantaneous starburst may not



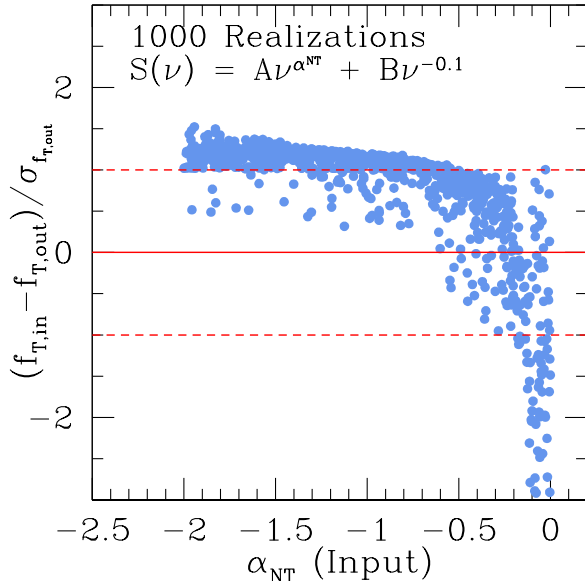


**Figure 5.** The results from our MCMC analysis of 1000 random realizations of 3 - 33 GHz spectra using as a model  $S(\nu) = A\nu^{\alpha_{\text{NT}}} + B\nu^{-0.1}$ . For these realizations we fix  $S/N = 10$  and vary the thermal fraction at 33 GHz by randomly assigning a non-thermal spectral index from 0 to 2, and an A (B) values between 0 and 1. It is clear from this exercise that by fitting our data using an MCMC approach, our ability to recover the true value for the 33 GHz thermal fraction peaks at  $\alpha_{\text{NT},\text{in}} \sim -0.8$ , which closely resembles the canonical value for the nonthermal spectral index.

be representative, we also include SB99 models with a continuous star formation history of  $\text{SFR} = 1 M_{\odot} \text{yr}^{-1}$  using the same metallicity and IMF input as in the instantaneous burst model (Figure 7 - Left Panel). The details of these models, and their application to extranuclear star-forming regions identified in LIRGs is presented in Linden et al. (2019).

For both models we then perform a  $\chi^2$  minimization to the observed spectral indices for each star-forming region in the sample. We stress that without including cosmic-ray propagation, which will affect the relative ratio of free-free and non-thermal emission on these scales, this exercise is simply meant to understand how the observed distribution of spectral indices can be represented as a distribution of ages. In the left panel of Figure 7 it is clear that our models are insensitive to HII regions with ages  $\tau_{\text{HII}} < 3 \text{ Myr}$  and  $\tau_{\text{HII}} > 40 \text{ Myr}$ . However, in the intermediate age range we find that a typical uncertainty of 4–6% on the observed spectral index corresponds to a 0.1–0.2 dex uncertainty in age. Therefore while the age of any individual region may be uncertain, the increase in the number of young ( $3 < \tau_{\text{HII}} < 10 \text{ Myr}$ ) relative to old ( $\tau_{\text{HII}} \sim 20 - 30 \text{ Myr}$ ) star-forming regions is robust.

The right panel of Figure 7 shows the distribution of fitted ages for the instantaneous burst model in blue and the continuous model in green. Overall, we find that the majority ( $\sim 70\%$ ) of our regions are best-modeled by a continuous burst, with a median age of  $\sim 10 \text{ Myr}$  (grey distribution). Further we find that when all regions are modeled using a continuous SFH, an age-gradient emerges in Figure 6. At small  $r_{\text{G}}$ , the regions with low thermal fractions, which drive the observed scatter, are preferentially older ( $\tau_{\text{HII}} \sim 20 - 30 \text{ Myr}$ ). This further supports the notion that the central star-forming regions are, on average, older, and that the associated cosmic ray population in the inner disk of these galaxies is being continuously replenished by ongoing star-formation.

### 5.3. Likely Background Galaxies

For the 10 likely background sources (BG) identified (i.e. sources with no obvious  $8 \mu\text{m}$  counterpart), which have a  $S/N \geq 3$  in at least two radio bands, the median 3 - 33 GHz spectral index is  $-0.65 \pm 0.04$  with a median absolute deviation of 0.3. This value is significantly steeper than the average value measured for the SF regions, and indicates that these sources are primarily dominated by synchrotron emission. This result further suggests that our visual classification scheme involving both radio and near-IR imaging appears to be an effective discriminator for various types of radio sources in surveys of nearby galaxies. Finally, a cross-reference with NED suggests that none of these sources have been previously identified in the literature.

### 5.4. Supernova and Supernova Remnants

In order to identify possible supernova remnants, we cross-correlated our sample of 377 regions against the Open Supernova Catalog (OSC: Guillochon et al. 2017). In total we identify 6 sources as being spatially coincident (within  $2''$ ) to an identified radio source with a  $S/N \geq 3$  in at least two radio bands. The 3 - 33 GHz spectral slopes measured are uniformly distributed from  $-1$  to  $0.5$ . This scatter is likely driven by SNe/R at various stages of their evolution, and therefore a large range in the degree of energy loss of the CRs as they propagate through the ISM. For one region identified in NGC 7331, the measured 15 GHz flux density is larger by over an order of magnitude due to a supernova, SN2014C, which was discovered in January of 2014, between the time our 3 and 15 GHz observations of this source were taken (Shivvers et al. 2019).

### 5.5. Anomalous Microwave Emission

Anomalous Microwave Emission (AME) is a known dust-correlated component of Galactic emission that has been detected by cosmic microwave background (CMB)

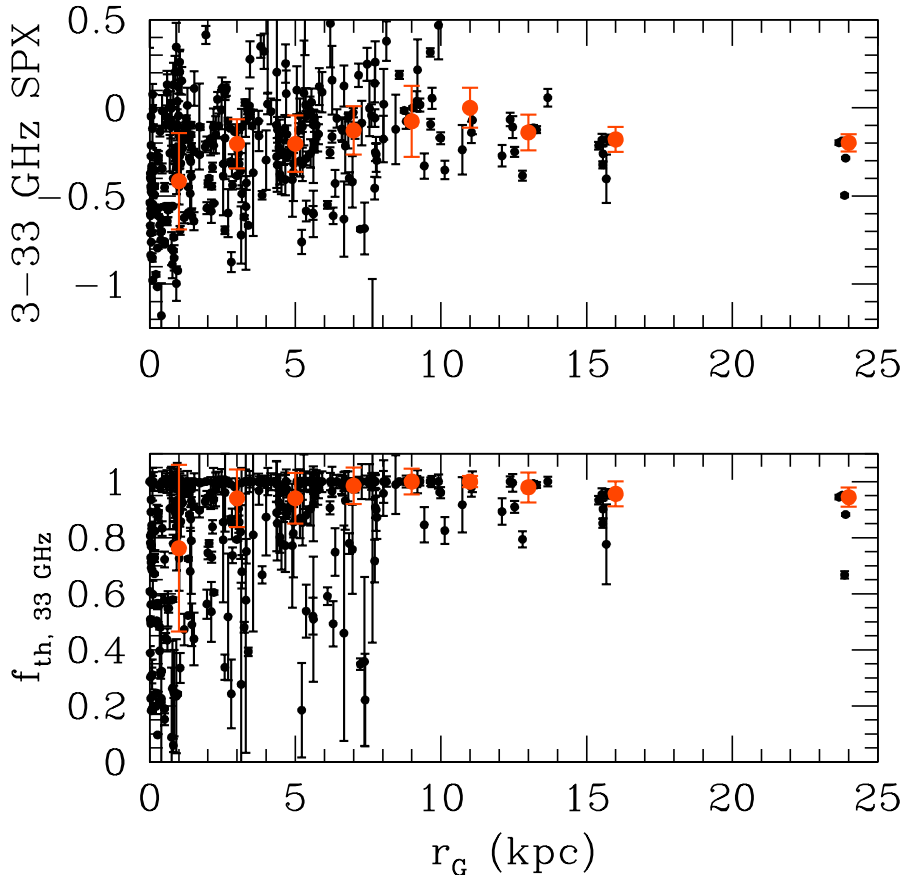


**Figure 6.** The spectral index and 33 GHz thermal fraction distributions plotted against galactocentric radius for all 325 sources identified in Figure 2. While we identify regions across the full extent of galaxy disks which are heavily dominated by thermal emission, a clear trend emerges where the scatter in both quantities increases significantly as a function of decreasing galactocentric radius (orange points). In particular, no region with a measured  $f_T < 80\%$  is found in any SFRS galaxy beyond a radius of 7 kpc. These trends are reflective of the ongoing star-formation activity occurring in the centers of nearby normal galaxies, and reinforce our ability to successfully capture the SFH of individual HII regions using the 3 – 33 GHz radio spectral slopes.

experiments and other radio/microwave instruments at frequencies 10 – 60 GHz since the mid-1990s (see [Dickinson et al. 2018](#), and articles within for recent reviews). AME is found to be spatially correlated with far-infrared thermal dust emission, but cannot be explained by synchrotron, or free-free emission mechanisms, and is far in excess of the emission contributed by thermal dust with the power-law opacity consistent with observations at sub-mm wavelengths. The most natural explanation for AME is rotational (electric dipole) emission from ultra-small dust grains (i.e., ‘spinning dust’: [Erickson 1957](#); [Draine & Lazarian 1998](#)). The emission forms part of the diffuse Galactic foregrounds that contaminate CMB data, which operate in the frequency range 30 – 300 GHz, and hence knowledge of the spatial structure and spectral shape can inform CMB component separation. However, spinning dust emission de-

pends critically on the dust grain size distribution, the type of dust, and the environmental conditions (density, temperature, interstellar radiation field, etc.). Thus, precise measurements of AME can also provide a new window into the ISM, complementing other multiwavelength tracers.

A number of searches for extragalactic AME have been undertaken with WMAP and Planck data (e.g., the Magellanic Clouds and NGC4945: [Bot et al. 2010](#); [Peel et al. 2011](#)), all of which were inconclusive. Most recently, we have identified two additional detections of AME in the SFRS sample as having anomalously high 33 GHz-to-24 $\mu$ m flux ratios (NGC 6946 E4 and NGC 4725 B: [Murphy et al. 2010, 2018b](#)). NGC 4725 B in particular appears consistent with a highly-embedded ( $A_V > 5$  mag) nascent star-forming region, in which young ( $\sim 3$  Myr) massive stars are still enshrouded by

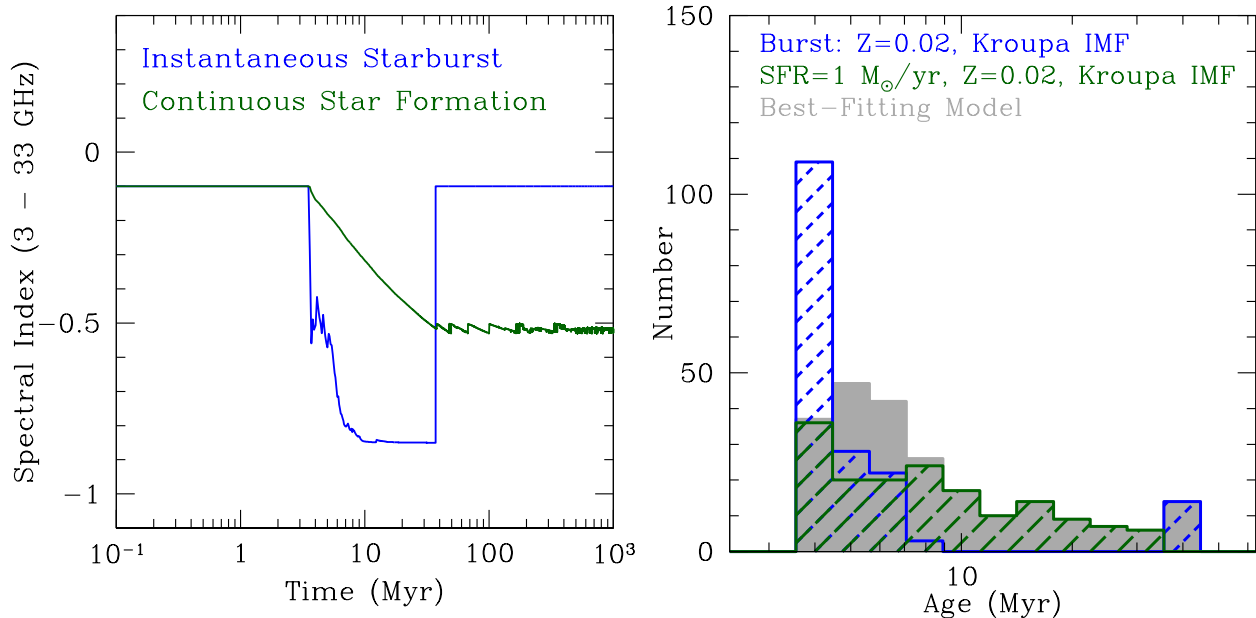


**Figure 7.** Left panel: The evolution of the 3-33 GHz spectral slope in SB99 models of both an instantaneous burst and continuous SFH, using standard Kroupa IMF, and solar metallicities. We perform a  $\chi^2$ -minimization of these models to the observed 3 – 33 GHz spectral index of each region. Right panel: The distribution of model ages for both types of SFH (blue and green) and the best-fitting model in each case (grey). It is clear that there exists two populations of regions: Those younger than  $t \sim 10$  Myr, which are best-modeled by an instantaneous burst, and those older than  $t \sim 10$  Myr, which are best-modeled by a continuous SFH.

their natal cocoons of gas and dust, lacking enough supernova to produce synchrotron emission.

While it is possible that NGC 4725 B and NGC 6946 E4 represent the most favorable conditions for AME detection, there are likely remaining regions in the SFRS that still harbor AME at a lower level relative to the other emission components (Hensley et al. 2015). Isolating the factors that govern the level of AME in these regions will lend insight into the physical mechanisms powering this emission as well as the nature of its carriers. In particular, we have observed that a common feature among both detections thus far is a shallow or even rising spectra from 3 - 33 GHz, as the contribution from AME increases and eventually dominates beyond  $\sim 20$  GHz. These regions can be identified as having elevated 33 GHz emission relative to the expected extrapolation from lower-frequency radio data using a standard two-component power law.

By measuring the 3 – 33 and 15 – 33 GHz spectral indices, we made an initial selection of 58 extragalactic AME candidates as regions that have an  $8\mu\text{m}$  counterpart, a  $S/N \geq 3$  in at least 2 radio bands, a de-projected galactocentric radius of  $r_G > 250\text{pc}$ , and a measured spectral slope that is  $\geq 3\sigma$  above the canonical  $\alpha^T = -0.1$  value expected for free-free emission. This represents a conservative upper-limit to identify regions by assuming that the non-thermal synchrotron emission is negligible at 33 GHz, and thus does not contribute to

the measured slope from 15 – 33 GHz. This assumption is well-supported here for our full spectral analysis of over 300 star-forming regions identified in the SFRS, which show that the median thermal fraction measured at 33 GHz on a few  $\sim 100$  pc scales is  $\sim 91\%$ . We then visually inspected all 58 AME candidates, only retaining 33 regions where the emission was found to be compact, similar to the previously identified extragalactic AME sources. This is done to ensure that any differences in surface brightness sensitivity between our observations would not result in diffuse emission with an artificially flattened spectrum, which is unassociated with an individual source. Our final requirement removes 4 sources (NGC 4254 Enc. 1 B, NGC 3521 Enc. 1, NGC 4736 N, and NGC 7331 D), which have very steeply rising 3-15 GHz spectral slopes, but are undetected at 33 GHz, and therefore are not confidently identified as AME candidates.

In Figure 8 we plot the 3 – 33 GHz spectrum of the 33 AME candidate regions normalized to the highest measured 3 GHz flux density. Viewed in this way we see that many of our AME candidates, similar to NGC 4725 B, have shallow or slightly negative slopes from 3 – 15 GHz, and a much steeper positive slope from 15 – 33 GHz. However, there are some regions which look more similar to NGC 6946 Enc. 4., which have steeper 3 – 15 GHz slopes and a less significant increase from 15 – 33 GHz. Importantly, these spectra cannot be explained by a

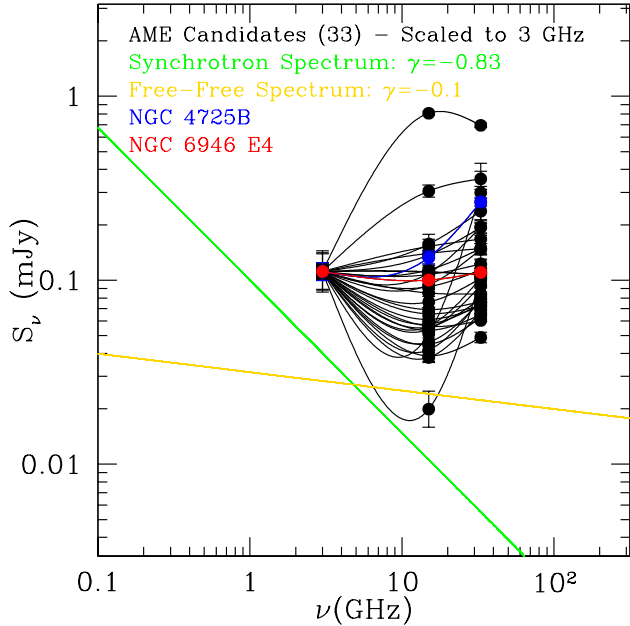


**Figure 8.** The radio spectra of all 33 AME candidates identified in the SFRS as having 3–33 GHz or 15–33 GHz spectral indices  $3\sigma$  greater than  $\alpha^T = -0.1$ . To demonstrate the diversity of our AME candidate spectra we normalize all flux density measurements to the brightest region detected at 3 GHz. We expect that, similar to NGC 6946 E4 (Red), the regions with decreasing 3–15 GHz spectral slopes contain a non-negligible amount of synchrotron emission, whereas the regions with very shallow or even rising spectra over this same frequency range (e.g. similar to NGC 4725 B: Blue) will be dominated by free-free emission.

simple combination of synchrotron (green) and free-free (yellow) emission components, suggesting that either an additional emission component peaking at  $\gtrsim 15$  GHz is required (e.g., AME), it is a (very) high-frequency GHz-peaked background galaxy, or the source is variable. A final possibility is that the free-free emission is optically-thick at 33 GHz. However, such ‘ultra-compact’ HII regions have much higher radio luminosities and SFRs ( $\sim 40 - 60$  mJy) than the regions identified here (e.g., Meier et al. 2002).

## 6. CONCLUSIONS

We have presented 3, 15, and 33 GHz imaging towards galaxy nuclei and extranuclear star-forming regions in the SFRS, and have identified 335 regions (286 SF, 10 BG, 6 SNe/R, and 33 AME) with  $S/N \geq 3$  in at least two radio bands. Through detailed measurements of their radio spectra we have confirmed that:

1. The average local background contribution to the measured 3, 15, and 33 GHz flux densities on  $\sim$

100 pc scales is  $\sim 4 - 6\%$ . This is significantly smaller than the 15–40% found for the sample of regions studied at  $25''$  ( $\sim 1$  kpc) scales with the GBT (Murphy et al. 2011).

2. On  $\sim 100$  pc scales, the median thermal fraction at 33 GHz of all regions identified as non-background galaxies is  $92 \pm 0.8\%$  with a median absolute deviation of 11%. Limiting our analysis to extranuclear ( $r_G > 250$  pc) SF regions, we measure a median thermal fraction of  $93 \pm 0.8\%$  with a median absolute deviation of 10%. Further, we find that on  $7''$  scales the median thermal fraction is  $94 \pm 0.8\%$ , and thus the thermal fraction remains  $\geq 90\%$  up to  $\sim 500$  pc scales.
3. We have confirmed through MCMC analysis that we do not introduce systematic biases when interpreting the results of the  $\chi^2$ -minimization of a two-component power-law model to fit the observed radio spectrum from 3–33 GHz, and that this model can adequately separate the thermal free-free and nonthermal synchrotron emission components over a realistic range of input values.
4. We find a systematic increase in the scatter of the measured spectral indices and thermal fractions as the de-projected galactocentric radius approaches the nucleus. This trend is reflective of the ongoing star-formation activity occurring in centers of these galaxies, and results in a larger contribution of diffuse nonthermal emission.
5. We have identified a sample of 33 sources whose rising 15–33 GHz emission may be due to anomalous microwave emission. Follow-up observations at high ( $\geq 40$  GHz) frequencies will be necessary to confirm these sources as discrete regions of extragalactic AME.

S.T.L. was supported by the NRAO Grote Reber Dissertation Fellowship. The National Radio Astronomy Observatory is a facility of the National Science Foundation operated under cooperative agreement by Associated Universities, Inc. This research has made use of the NASA/IPAC Extragalactic Database (NED) which is operated by the Jet Propulsion Laboratory, California Institute of Technology, under contract with the National Aeronautics and Space Administration.

## REFERENCES

- Aniano, G., Draine, B. T., Gordon, K. D., & Sandstrom, K. 2011, *PASP*, 123, 1218
- Bell, E. F. 2003, *ApJ*, 586, 794
- Bot, C., Ysard, N., Paradis, D., et al. 2010, *A&A*, 523, A20
- Ciardullo, R., Feldmeier, J. J., Jacoby, G. H., et al. 2002, *ApJ*, 577, 31
- Clemens, M. S., Scaife, A., Vega, O., & Bressan, A. 2010, *MNRAS*, 405, 887
- Clemens, M. S., Vega, O., Bressan, A., et al. 2008, *A&A*, 477, 95
- Condon, J. J. 1992, *ARA&A*, 30, 575
- Condon, J. J., & Yin, Q. F. 1990, *ApJ*, 357, 97
- Condon, J. J., Cotton, W. D., Fomalont, E. B., et al. 2012, *ApJ*, 758, 23
- Conway, J. E., Cornwell, T. J., & Wilkinson, P. N. 1990, *MNRAS*, 246, 490
- Cornwell, T. J. 2008, *IEEE Journal of Selected Topics in Signal Processing*, 2, 793
- Dale, D. A., Gil de Paz, A., Gordon, K. D., et al. 2007, *ApJ*, 655, 863
- Dale, D. A., Cohen, S. A., Johnson, L. C., et al. 2009, *ApJ*, 703, 517
- de Jong, T., Klein, U., Wielebinski, R., & Wunderlich, E. 1985, *A&A*, 147, L6
- de Vaucouleurs, G., de Vaucouleurs, A., Corwin, Herold G., J., et al. 1991
- Dickinson, C., Ali-Haimoud, Y., Barr, A., et al. 2018, *NewAR*, 80, 1
- Draine, B. T. 2003, *ARA&A*, 41, 241
- Draine, B. T., & Lazarian, A. 1998, *ApJ*, 508, 157
- Engelbracht, C. W., Rieke, G. H., Gordon, K. D., et al. 2008, *ApJ*, 678, 804
- Erickson, W. C. 1957, *ApJ*, 126, 480
- Foreman-Mackey, D., Hogg, D. W., Lang, D., & Goodman, J. 2013, *PASP*, 125, 306
- Freedman, W. L., Madore, B. F., Gibson, B. K., et al. 2001, *ApJ*, 553, 47
- Green, D. A. 2011, *Bulletin of the Astronomical Society of India*, 39, 289
- Guillochon, J., Parrent, J., Kelley, L. Z., & Margutti, R. 2017, *ApJ*, 835, 64
- Heesen, V., Brinks, E., Leroy, A. K., et al. 2014, *AJ*, 147, 103
- Helou, G., Soifer, B. T., & Rowan-Robinson, M. 1985, *ApJL*, 298, L7
- Hensley, B., Murphy, E., & Staguhn, J. 2015, *MNRAS*, 449, 809
- Hogg, D. W., Bovy, J., & Lang, D. 2010, arXiv e-prints, arXiv:1008.4686
- Hughes, A., Staveley-Smith, L., Kim, S., Wolleben, M., & Filipović, M. 2007, *MNRAS*, 382, 543
- Jarrett, T. H., Chester, T., Cutri, R., Schneider, S. E., & Huchra, J. P. 2003, *AJ*, 125, 525
- Kennicutt, R. C., Calzetti, D., Aniano, G., et al. 2011, *PASP*, 123, 1347
- Kennicutt, Jr., R. C., Armus, L., Bendo, G., et al. 2003, *PASP*, 115, 928
- Klein, U., Wielebinski, R., & Beck, R. 1984, *A&A*, 135, 213
- Klein, U., Wielebinski, R., & Morsi, H. W. 1988, *A&A*, 190, 41
- Koyama, K., Petre, R., Gotthelf, E. V., et al. 1995, *Nature*, 378, 255
- Lacki, B. C., & Thompson, T. A. 2010, *ApJ*, 717, 196
- Lacki, B. C., Thompson, T. A., & Quataert, E. 2010, *ApJ*, 717, 1
- Leitherer, C., Schaerer, D., Goldader, J. D., et al. 1999, *ApJS*, 123, 3
- Leroy, A. K., Evans, A. S., Momjian, E., et al. 2011, *ApJL*, 739, L25
- Leroy, A. K., Bigiel, F., de Blok, W. J. G., et al. 2012, *AJ*, 144, 3
- Linden, S. T., Song, Y., Evans, A. S., et al. 2019, *ApJ*, 881, 70
- Lonsdale Persson, C. J., & Helou, G. 1987, *ApJ*, 314, 513
- McMullin, J. P., Waters, B., Schiebel, D., Young, W., & Golap, K. 2007, in *Astronomical Society of the Pacific Conference Series*, Vol. 376, *Astronomical Data Analysis Software and Systems XVI*, ed. R. A. Shaw, F. Hill, & D. J. Bell, 127
- Meier, D. S., Turner, J. L., & Beck, S. C. 2002, *AJ*, 124, 877
- Moustakas, J., Kennicutt, Jr., R. C., Tremonti, C. A., et al. 2010, *ApJS*, 190, 233
- Murphy, E. J., Dong, D., Momjian, E., et al. 2018a, *ApJS*, 234, 24
- Murphy, E. J., Linden, S. T., Dong, D., et al. 2018b, *ApJ*, 862, 20
- Murphy, E. J., Stierwalt, S., Armus, L., Condon, J. J., & Evans, A. S. 2013, *ApJ*, 768, 2
- Murphy, E. J., Braun, R., Helou, G., et al. 2006, *ApJ*, 638, 157
- Murphy, E. J., Helou, G., Condon, J. J., et al. 2010, *ApJL*, 709, L108
- Murphy, E. J., Condon, J. J., Schinnerer, E., et al. 2011, *ApJ*, 737, 67
- Murphy, E. J., Bremseth, J., Mason, B. S., et al. 2012, *ApJ*, 761, 97
- Niklas, S., & Beck, R. 1997, *A&A*, 320, 54

- Peel, M. W., Dickinson, C., Davies, R. D., Clements, D. L., & Beswick, R. J. 2011, MNRAS, 416, L99
- Perley, R. A., & Butler, B. J. 2013, ApJS, 204, 19
- Rau, U., & Cornwell, T. J. 2011, A&A, 532, A71
- Sault, R. J., & Wieringa, M. H. 1994, A&AS, 108, 585
- Schlegel, D. J., Finkbeiner, D. P., & Davis, M. 1998, ApJ, 500, 525
- Seibert, M. 2007, The Galex Large Galaxy Atlas (glga), GALEX Proposal
- Shivvers, I., Filippenko, A. V., Silverman, J. M., et al. 2019, MNRAS, 482, 1545
- Tabatabaei, F. S., Schinnerer, E., Krause, M., et al. 2017, ApJ, 836, 185
- Weingartner, J. C., & Draine, B. T. 2001, ApJ, 548, 296
- Westcott, J., Brinks, E., Hindson, L., Beswick, R., & Heesen, V. 2018, MNRAS, 475, 5116



## APPENDIX

**Table 6.** Ancillary Source Photometry at 7'' Angular Resolution

Source ID	$f_\nu(1528 \text{ \AA})$ ( $\mu\text{Jy}$ )	$f_\nu(2271 \text{ \AA})$ ( $\mu\text{Jy}$ )	$f_{\text{H}\alpha}/10^{-13}$ ( $\text{erg s}^{-1} \text{ cm}^{-2}$ )	$f_\nu(24 \mu\text{m})$ (mJy)
	Star-Forming Regions			
NGC 0337 a	76.38 $\pm$ 11.46	163.59 $\pm$ 24.54	1.47 $\pm$ 0.29	45.73 $\pm$ 2.29
NGC 0337 b	104.70 $\pm$ 15.71	185.04 $\pm$ 27.76	1.83 $\pm$ 0.37	81.65 $\pm$ 4.08
NGC 0337 c	36.93 $\pm$ 5.54	70.52 $\pm$ 10.58	0.57 $\pm$ 0.11	8.40 $\pm$ 0.42
NGC 0337 d	47.19 $\pm$ 7.08	87.63 $\pm$ 13.15	1.18 $\pm$ 0.24	22.25 $\pm$ 1.11
NGC 0628 Enuc. 4	67.64 $\pm$ 10.15	81.23 $\pm$ 12.19	0.53 $\pm$ 0.11	9.87 $\pm$ 0.50
NGC 0628 Enuc. 2	70.55 $\pm$ 10.58	95.46 $\pm$ 14.32	0.40 $\pm$ 0.08	40.37 $\pm$ 2.02
NGC 0628 Enuc. 3	233.35 $\pm$ 35.00	282.27 $\pm$ 42.34	0.78 $\pm$ 0.16	28.94 $\pm$ 1.45
NGC 0628	16.96 $\pm$ 2.54	41.26 $\pm$ 6.19	0.06 $\pm$ 0.01	2.41 $\pm$ 0.14
NGC 0628 Enuc. 1	94.88 $\pm$ 14.23	134.80 $\pm$ 20.22	0.73 $\pm$ 0.15	75.27 $\pm$ 3.76
NGC 0855	146.72 $\pm$ 22.01	226.75 $\pm$ 34.01	...	18.70 $\pm$ 0.94
NGC 0925	182.62 $\pm$ 27.39	232.19 $\pm$ 34.83	0.34 $\pm$ 0.07	2.79 $\pm$ 0.15
NGC 1097 Enuc. 2	21.07 $\pm$ 3.16	30.92 $\pm$ 4.64	...	3.48 $\pm$ 0.18
NGC 1097	97.34 $\pm$ 14.60	242.71 $\pm$ 36.41	...	174.28 $\pm$ 8.71
NGC 1097 Enuc. 1 a	20.37 $\pm$ 3.06	32.96 $\pm$ 4.95	...	10.91 $\pm$ 0.55
NGC 1097 Enuc. 1 b	27.26 $\pm$ 4.09	42.24 $\pm$ 6.34	...	8.85 $\pm$ 0.45
NGC 1097 Enuc. 1 c	61.48 $\pm$ 9.22	77.38 $\pm$ 11.61	...	7.43 $\pm$ 0.38
NGC 1266	2.75 $\pm$ 0.48	10.77 $\pm$ 1.64	...	365.58 $\pm$ 18.28
NGC 1377	...	...	...	682.96 $\pm$ 34.15
NGC 1482	10.33 $\pm$ 1.56	31.06 $\pm$ 4.66	...	1279.02 $\pm$ 63.95
NGC 2403 Enuc. 6	354.10 $\pm$ 53.12	402.03 $\pm$ 60.30	1.19 $\pm$ 0.24	9.02 $\pm$ 0.45
NGC 2403 Enuc. 1 a	48.36 $\pm$ 7.25	67.64 $\pm$ 10.15	0.14 $\pm$ 0.03	3.70 $\pm$ 0.18
NGC 2403 Enuc. 1 b	1732.39 $\pm$ 259.86	2032.07 $\pm$ 304.81	2.70 $\pm$ 0.54	84.01 $\pm$ 4.20
NGC 2403 Enuc. 2 a	78.83 $\pm$ 11.82	101.84 $\pm$ 15.28	0.68 $\pm$ 0.14	34.77 $\pm$ 1.74
NGC 2403	42.11 $\pm$ 6.32	78.92 $\pm$ 11.84	0.15 $\pm$ 0.03	3.38 $\pm$ 0.17
NGC 2403 Enuc. 2 b	846.79 $\pm$ 127.02	1047.48 $\pm$ 157.12	2.32 $\pm$ 0.46	58.97 $\pm$ 2.95
NGC 2403 Enuc. 4	183.11 $\pm$ 27.47	218.95 $\pm$ 32.84	0.79 $\pm$ 0.16	17.24 $\pm$ 0.86
Holmberg II	373.62 $\pm$ 56.04	373.64 $\pm$ 56.05	1.42 $\pm$ 0.28	16.54 $\pm$ 0.83
NGC 2798	165.82 $\pm$ 24.87	412.77 $\pm$ 61.92	4.77 $\pm$ 0.95	1084.54 $\pm$ 54.23
NGC 2841	145.60 $\pm$ 21.84	213.22 $\pm$ 31.98	0.25 $\pm$ 0.05	12.63 $\pm$ 0.63
NGC 2976 Enuc. 1 a	15.95 $\pm$ 2.40	24.52 $\pm$ 3.68	0.55 $\pm$ 0.11	27.12 $\pm$ 1.36
NGC 2976 Enuc. 1 b	162.97 $\pm$ 24.45	216.89 $\pm$ 32.53	3.30 $\pm$ 0.66	129.05 $\pm$ 6.45
NGC 2976	63.57 $\pm$ 9.54	89.68 $\pm$ 13.45	0.54 $\pm$ 0.11	7.34 $\pm$ 0.37
NGC 2976 Enuc. 2 a	130.65 $\pm$ 19.60	154.13 $\pm$ 23.12	1.91 $\pm$ 0.38	53.39 $\pm$ 2.67
NGC 2976 Enuc. 2 b	60.44 $\pm$ 9.07	74.82 $\pm$ 11.23	1.11 $\pm$ 0.22	23.00 $\pm$ 1.15
NGC 3049	438.18 $\pm$ 65.73	736.56 $\pm$ 110.48	1.48 $\pm$ 0.30	180.25 $\pm$ 9.01
NGC 3077	...	...	3.35 $\pm$ 0.67	... †
NGC 3190	9.88 $\pm$ 1.49	57.84 $\pm$ 8.68	0.16 $\pm$ 0.03	30.72 $\pm$ 1.54
NGC 3184	121.52 $\pm$ 18.23	243.12 $\pm$ 36.48	0.25 $\pm$ 0.05	55.49 $\pm$ 2.77
NGC 3198	9.78 $\pm$ 1.47	29.67 $\pm$ 4.45	0.08 $\pm$ 0.02	176.88 $\pm$ 8.84
IC 2574 a	622.44 $\pm$ 93.37	551.40 $\pm$ 82.71	1.72 $\pm$ 0.34	4.62 $\pm$ 0.23
IC 2574 b	114.96 $\pm$ 17.24	141.24 $\pm$ 21.19	1.70 $\pm$ 0.34	19.95 $\pm$ 1.00
NGC 3265	164.32 $\pm$ 24.65	297.20 $\pm$ 44.58	...	141.65 $\pm$ 7.08
NGC 3351 a	286.98 $\pm$ 43.05	839.02 $\pm$ 125.85	2.33 $\pm$ 0.47	307.30 $\pm$ 15.36
NGC 3351 b	228.22 $\pm$ 34.23	655.21 $\pm$ 98.28	2.16 $\pm$ 0.43	389.75 $\pm$ 19.49

*Table 6 continued*

Table 6 (continued)

Source ID	$f_\nu(1528 \text{ \AA})$	$f_\nu(2271 \text{ \AA})$	$f_{\text{H}\alpha}/10^{-13}$	$f_\nu(24 \text{ }\mu\text{m})$
	( $\mu\text{Jy}$ )	( $\mu\text{Jy}$ )	( $\text{erg s}^{-1} \text{ cm}^{-2}$ )	(mJy)
NGC 3521 Enuc. 1	14.33 ± 2.15	18.52 ± 2.78	0.12 ± 0.02	6.20 ± 0.31
NGC 3521 Enuc. 3	9.02 ± 1.36	15.39 ± 2.32	0.09 ± 0.02	6.38 ± 0.32
NGC 3521	29.66 ± 4.45	135.30 ± 20.30	0.59 ± 0.12	12.56 ± 0.63
NGC 3521 Enuc. 2 a	12.34 ± 1.86	27.24 ± 4.09	0.27 ± 0.05	18.80 ± 0.94
NGC 3521 Enuc. 2 b	6.25 ± 0.95	12.44 ± 1.87	0.049 ± 0.010	2.59 ± 0.13
NGC 3621	15.55 ± 2.34	48.94 ± 7.34	...	7.92 ± 0.40
NGC 3627	16.12 ± 2.42	100.99 ± 15.15	0.93 ± 0.19	246.46 ± 12.32
NGC 3627 Enuc. 1	5.43 ± 0.83	9.08 ± 1.37	0.38 ± 0.08	170.02 ± 8.50
NGC 3627 Enuc. 2	28.07 ± 4.21	47.67 ± 7.15	0.94 ± 0.19	478.65 ± 23.93
NGC 3773	1163.59 ± 174.54	1035.24 ± 155.29	...	57.96 ± 2.90
NGC 3938 a	45.04 ± 6.76	102.39 ± 15.37	0.06 ± 0.01	5.02 ± 0.25
NGC 3938 Enuc. 2 a	76.37 ± 11.46	80.18 ± 12.04	0.28 ± 0.06	7.65 ± 0.38
NGC 3938 Enuc. 2 b	101.00 ± 15.15	109.29 ± 16.41	0.35 ± 0.07	21.20 ± 1.06
NGC 4254 Enuc. 2 a	82.48 ± 12.37	118.60 ± 17.79	0.34 ± 0.07	13.34 ± 0.67
NGC 4254 Enuc. 2 b	79.65 ± 11.95	122.20 ± 18.33	0.19 ± 0.04	11.10 ± 0.56
NGC 4254 a	43.05 ± 6.46	115.81 ± 17.37	0.45 ± 0.09	32.49 ± 1.62
NGC 4254 Enuc. 1 a	35.31 ± 5.30	53.66 ± 8.05	0.24 ± 0.05	22.07 ± 1.10
NGC 4254 b	41.12 ± 6.17	160.80 ± 24.12	0.61 ± 0.12	53.56 ± 2.68
NGC 4254 Enuc. 1 b	133.40 ± 20.01	208.80 ± 31.32	0.53 ± 0.11	18.13 ± 0.91
NGC 4254 c	38.51 ± 5.78	114.72 ± 17.21	0.40 ± 0.08	25.93 ± 1.30
NGC 4254 Enuc. 1 c	81.14 ± 12.17	145.03 ± 21.76	0.50 ± 0.10	31.93 ± 1.60
NGC 4254 d	48.25 ± 7.24	99.19 ± 14.88	0.24 ± 0.05	14.27 ± 0.71
NGC 4254 e	74.41 ± 11.16	134.91 ± 20.24	0.33 ± 0.07	25.00 ± 1.25
NGC 4254 f	53.17 ± 7.98	101.76 ± 15.26	0.24 ± 0.05	11.40 ± 0.57
NGC 4321 Enuc. 2 a	70.84 ± 10.63	101.18 ± 15.18	0.15 ± 0.03	7.99 ± 0.40
NGC 4321 Enuc. 2 b	78.57 ± 11.79	109.62 ± 16.44	0.15 ± 0.03	6.33 ± 0.32
NGC 4321 Enuc. 2	25.65 ± 3.85	35.61 ± 5.34	0.06 ± 0.01	4.76 ± 0.24
NGC 4321 a	467.33 ± 70.10	1001.88 ± 150.28	0.86 ± 0.17	88.54 ± 4.43
NGC 4321 b	208.14 ± 31.22	535.72 ± 80.36	0.90 ± 0.18	117.01 ± 5.85
NGC 4321 Enuc. 1	47.40 ± 7.11	84.43 ± 12.67	0.10 ± 0.02	4.10 ± 0.21
NGC 4536	28.74 ± 4.32	93.49 ± 14.04	1.96 ± 0.39	976.15 ± 48.81
NGC 4559 a	119.11 ± 17.87	167.28 ± 25.09	0.77 ± 0.15	9.99 ± 0.50
NGC 4559 b	199.22 ± 29.88	258.30 ± 38.75	0.61 ± 0.12	5.83 ± 0.29
NGC 4559 c	81.18 ± 12.18	126.24 ± 18.94	0.66 ± 0.13	18.40 ± 0.92
NGC 4569	330.64 ± 49.60	1095.12 ± 164.27	3.27 ± 0.65	312.76 ± 15.64
NGC 4579	89.93 ± 13.49	180.92 ± 27.14	1.94 ± 0.39	96.78 ± 4.84
NGC 4594 a	123.89 ± 18.58	238.40 ± 35.76	0.82 ± 0.16	34.38 ± 1.72
NGC 4625	83.15 ± 12.47	145.11 ± 21.77	0.16 ± 0.03	4.72 ± 0.24
NGC 4631 a	90.42 ± 13.56	105.16 ± 15.77	0.38 ± 0.08	40.73 ± 2.04
NGC 4631 b	99.88 ± 14.98	144.01 ± 21.60	0.48 ± 0.10	85.41 ± 4.27
NGC 4631 c	144.21 ± 21.63	183.56 ± 27.53	0.25 ± 0.05	167.16 ± 8.36
NGC 4631 d	61.78 ± 9.27	92.18 ± 13.83	0.41 ± 0.08	45.26 ± 2.26
NGC 4631 h	50.54 ± 7.58	68.74 ± 10.31	0.30 ± 0.06	268.79 ± 13.44
NGC 4631 Enuc. 2 a	82.13 ± 12.32	106.50 ± 15.98	0.67 ± 0.13	18.86 ± 0.94
NGC 4631 Enuc. 2 b	277.07 ± 41.56	345.20 ± 51.78	1.71 ± 0.34	41.08 ± 2.05
NGC 4725 b	1.91 ± 0.56	5.85 ± 1.00	0.013 ± 0.003	0.30 ± 0.02
NGC 4736	251.70 ± 37.75	926.35 ± 138.95	0.57 ± 0.11	302.54 ± 15.13
NGC 4736 Enuc. 1 a	330.89 ± 49.63	438.76 ± 65.81	0.88 ± 0.18	83.84 ± 4.19
NGC 4736 Enuc. 1 b	208.78 ± 31.32	265.52 ± 39.83	0.81 ± 0.16	88.34 ± 4.42
NGC 4736 Enuc. 1 c	197.88 ± 29.68	257.39 ± 38.61	0.55 ± 0.11	90.39 ± 4.52
NGC 4826	68.74 ± 10.31	227.33 ± 34.10	3.67 ± 0.73	198.25 ± 9.91
NGC 5055	44.22 ± 6.63	169.19 ± 25.38	1.29 ± 0.26	40.56 ± 2.03
NGC 5055 Enuc. 1	79.73 ± 11.96	116.15 ± 17.42	0.68 ± 0.14	22.59 ± 1.13

Table 6 continued

Table 6 (continued)

Source ID	$f_\nu(1528 \text{ \AA})$	$f_\nu(2271 \text{ \AA})$	$f_{\text{H}\alpha}/10^{-13}$	$f_\nu(24 \text{ }\mu\text{m})$
	( $\mu\text{Jy}$ )	( $\mu\text{Jy}$ )	( $\text{erg s}^{-1} \text{ cm}^{-2}$ )	(mJy)
NGC 5194 E nuc. 6 a	47.29 ± 7.09	57.62 ± 8.64	0.48 ± 0.10	25.76 ± 1.29
NGC 5194 E nuc. 2	276.65 ± 41.50	425.30 ± 63.80	1.48 ± 0.30	98.92 ± 4.95
NGC 5194 E nuc. 3	320.93 ± 48.14	548.20 ± 82.23	0.72 ± 0.14	60.68 ± 3.03
NGC 5194 E nuc. 11 a	150.83 ± 22.62	214.00 ± 32.10	0.46 ± 0.09	13.72 ± 0.69
NGC 5194 E nuc. 11 b	27.82 ± 4.17	44.70 ± 6.70	0.14 ± 0.03	9.92 ± 0.50
NGC 5194 E nuc. 11 d	17.34 ± 2.60	28.96 ± 4.34	0.12 ± 0.02	14.66 ± 0.73
NGC 5194 E nuc. 11 c	10.69 ± 1.60	17.52 ± 2.63	0.09 ± 0.02	2.85 ± 0.14
NGC 5194c	17.54 ± 2.63	46.97 ± 7.05	0.33 ± 0.07	50.31 ± 2.52
NGC 5194 b	97.75 ± 14.66	240.50 ± 36.08	0.65 ± 0.13	36.54 ± 1.83
NGC 5194 E nuc. 1 b	79.39 ± 11.91	179.50 ± 26.93	1.02 ± 0.20	73.51 ± 3.68
NGC 5194 e	135.19 ± 20.28	341.46 ± 51.22	0.72 ± 0.14	30.48 ± 1.52
NGC 5194 d	104.71 ± 15.71	316.95 ± 47.54	1.60 ± 0.32	95.37 ± 4.77
NGC 5194 E nuc. 10 a	15.55 ± 2.33	31.76 ± 4.76	0.19 ± 0.04	19.80 ± 0.99
NGC 5194 E nuc. 4 b	107.63 ± 16.15	171.40 ± 25.71	0.017 ± 0.004	33.66 ± 1.68
NGC 5194 E nuc. 4c	47.73 ± 7.16	75.01 ± 11.25	0.017 ± 0.004	12.98 ± 0.65
NGC 5194 a	239.15 ± 35.87	521.05 ± 78.16	0.63 ± 0.13	104.98 ± 5.25
NGC 5194 E nuc. 10 b	37.37 ± 5.61	70.53 ± 10.58	0.37 ± 0.07	38.48 ± 1.92
NGC 5194 E nuc. 4 d	117.81 ± 17.67	208.64 ± 31.30	0.017 ± 0.004	22.84 ± 1.14
NGC 5194 E nuc. 5 a	244.35 ± 36.65	386.49 ± 57.97	0.017 ± 0.004	32.37 ± 1.62
NGC 5194 E nuc. 9	71.73 ± 10.76	126.37 ± 18.96	0.37 ± 0.07	51.39 ± 2.57
NGC 5194 E nuc. 7 a	63.36 ± 9.50	93.36 ± 14.00	0.42 ± 0.08	9.06 ± 0.45
NGC 5194 E nuc. 8	172.68 ± 25.90	256.71 ± 38.51	0.66 ± 0.13	109.50 ± 5.48
NGC 5194 E nuc. 7 b	142.52 ± 21.38	217.91 ± 32.69	1.10 ± 0.22	50.44 ± 2.52
NGC 5194 E nuc. 7 c	77.98 ± 11.70	110.21 ± 16.53	0.37 ± 0.07	14.50 ± 0.73
NGC 5398	371.57 ± 55.74	454.84 ± 68.23	...	94.86 ± 4.74
NGC 5457 E nuc. 6 a	801.24 ± 120.19	854.11 ± 128.12	1.69 ± 0.34	61.86 ± 3.09
NGC 5457 E nuc. 6 b	414.22 ± 62.13	511.89 ± 76.78	1.37 ± 0.27	56.33 ± 2.82
NGC 5457 E nuc. 6 c	240.17 ± 36.03	312.87 ± 46.93	1.22 ± 0.24	63.55 ± 3.18
NGC 5457 E nuc. 5 a	1012.84 ± 151.93	1143.52 ± 171.53	2.53 ± 0.51	74.87 ± 3.74
NGC 5457 E nuc. 1	55.52 ± 8.33	99.52 ± 14.93	0.21 ± 0.04	13.01 ± 0.65
NGC 5457	286.03 ± 42.90	537.52 ± 80.63	0.46 ± 0.09	52.97 ± 2.65
NGC 5457 E nuc. 3 a	94.93 ± 14.24	112.13 ± 16.82	0.49 ± 0.10	15.02 ± 0.75
NGC 5457 E nuc. 3 b	203.99 ± 30.60	238.33 ± 35.75	0.98 ± 0.20	51.61 ± 2.58
NGC 5457 E nuc. 3 c	751.75 ± 112.76	898.85 ± 134.83	4.92 ± 0.98	597.00 ± 29.85
NGC 5457 E nuc. 3 d	36.79 ± 5.52	43.18 ± 6.48	0.30 ± 0.06	38.97 ± 1.95
NGC 5457 E nuc. 4 a	357.24 ± 53.59	375.74 ± 56.36	0.55 ± 0.11	7.03 ± 0.35
NGC 5457 E nuc. 4 b	430.15 ± 64.52	441.69 ± 66.25	0.58 ± 0.12	11.24 ± 0.56
NGC 5457 E nuc. 4 c	422.89 ± 63.43	413.00 ± 61.95	1.16 ± 0.23	39.65 ± 1.98
NGC 5457 E nuc. 4 d	401.84 ± 60.28	432.77 ± 64.92	1.17 ± 0.23	26.85 ± 1.34
NGC 5474	63.65 ± 9.55	97.97 ± 14.70	0.10 ± 0.02	1.23 ± 0.06
NGC 5713 E nuc. 2 a	157.17 ± 23.58	254.86 ± 38.23	0.39 ± 0.08	57.55 ± 2.88
NGC 5713 E nuc. 2 b	36.34 ± 5.45	72.06 ± 10.81	0.06 ± 0.01	32.09 ± 1.60
NGC 5713	91.36 ± 13.70	208.13 ± 31.22	0.06 ± 0.01	54.73 ± 2.74
NGC 5713 E nuc. 1	123.22 ± 18.48	322.24 ± 48.34	0.09 ± 0.02	364.30 ± 18.21
NGC 5866	12.80 ± 1.93	48.21 ± 7.24	...	19.91 ± 1.00
NGC 6946 E nuc. 4 b	5.65 ± 0.99	9.19 ± 1.41	...	1.06 ± 0.05
NGC 6946 E nuc. 4 c	5.45 ± 0.97	11.02 ± 1.68	...	121.25 ± 6.06
NGC 6946 E nuc. 8	6.02 ± 1.04	9.83 ± 1.51	1.34 ± 0.27	78.79 ± 3.94
NGC 6946 E nuc. 5 a	8.29 ± 1.35	11.09 ± 1.69	0.62 ± 0.12	4.21 ± 0.21
NGC 6946 E nuc. 3 a	7.23 ± 1.20	9.65 ± 1.48	1.14 ± 0.23	5.22 ± 0.26
NGC 6946 a	20.27 ± 3.08	37.11 ± 5.58	1.58 ± 0.32	70.92 ± 3.55
NGC 6946 c	6.61 ± 1.12	13.80 ± 2.09	0.97 ± 0.19	43.93 ± 2.20
NGC 6946 E nuc. 6 a	14.49 ± 2.23	22.62 ± 3.41	2.86 ± 0.57	103.34 ± 5.17

Table 6 continued

**Table 6** (*continued*)

Source ID	$f_\nu(1528 \text{ \AA})$	$f_\nu(2271 \text{ \AA})$	$f_{\text{H}\alpha}/10^{-13}$	$f_\nu(24 \text{ }\mu\text{m})$
	( $\mu\text{Jy}$ )	( $\mu\text{Jy}$ )	( $\text{erg s}^{-1} \text{ cm}^{-2}$ )	(mJy)
NGC 6946 Enuc. 6 b	$8.41 \pm 1.36$	$9.23 \pm 1.42$	$1.02 \pm 0.20$	$42.42 \pm 2.12$
NGC 6946 Enuc. 7	$9.88 \pm 1.57$	$13.28 \pm 2.02$	$1.13 \pm 0.23$	$71.13 \pm 3.56$
NGC 6946 Enuc. 2 b	$134.48 \pm 20.18$	$173.55 \pm 26.03$	$8.20 \pm 1.64$	$67.97 \pm 3.40$
NGC 7331	$8.70 \pm 1.31$	$53.98 \pm 8.10$	$< 0.20$	$16.82 \pm 0.84$
NGC 7793 Enuc. 1	$384.10 \pm 57.61$	$381.23 \pm 57.18$	$0.64 \pm 0.13$	$5.09 \pm 0.25$
NGC 7793 Enuc. 3	$291.93 \pm 43.79$	$357.16 \pm 53.57$	$0.68 \pm 0.14$	$25.96 \pm 1.30$
NGC 7793 a	$201.40 \pm 30.21$	$286.53 \pm 42.98$	$0.58 \pm 0.12$	$10.60 \pm 0.53$
NGC 7793 b	$313.42 \pm 47.01$	$462.00 \pm 69.30$	$0.69 \pm 0.14$	$15.49 \pm 0.77$
NGC 7793 Enuc. 2	$37.06 \pm 5.56$	$45.85 \pm 6.88$	$0.22 \pm 0.04$	$5.59 \pm 0.28$
Likely Associated with Supernovae				
NGC 6946 Enuc. 5 b	$24.28 \pm 3.68$	$31.79 \pm 4.78$	$2.18 \pm 0.44$	$10.55 \pm 0.53$
Likely AME Candidates				
NGC 2403 Enuc. 5	$1061.51 \pm 159.23$	$1026.40 \pm 153.96$	$2.31 \pm 0.46$	$52.86 \pm 2.64$
NGC 2403 Enuc. 3	$1405.70 \pm 210.85$	$1561.28 \pm 234.19$	$4.83 \pm 0.97$	$284.47 \pm 14.22$
NGC 3938 b	$29.22 \pm 4.39$	$68.29 \pm 10.26$	$0.07 \pm 0.01$	$3.38 \pm 0.17$
NGC 4631 Enuc. 1	$305.75 \pm 45.86$	$392.26 \pm 58.84$	$0.79 \pm 0.16$	$7.55 \pm 0.38$
NGC 4631 e	$106.11 \pm 15.92$	$154.92 \pm 23.24$	$0.45 \pm 0.09$	$92.84 \pm 4.64$
NGC 4631 f	$80.71 \pm 12.11$	$114.54 \pm 17.18$	$0.38 \pm 0.08$	$74.10 \pm 3.70$
NGC 4631 g	$65.91 \pm 9.89$	$88.30 \pm 13.25$	$0.34 \pm 0.07$	$143.47 \pm 7.17$
NGC 4725 a	$39.11 \pm 5.89$	$82.23 \pm 12.34$	$< 0.01$	$21.29 \pm 1.06$
NGC 5194 Enuc. 1 a	$17.13 \pm 2.57$	$34.57 \pm 5.19$	$0.55 \pm 0.11$	$81.10 \pm 4.06$
NGC 5194 Enuc. 11 e	$14.96 \pm 2.24$	$27.54 \pm 4.13$	$0.25 \pm 0.05$	$23.20 \pm 1.16$
NGC 5194 Enuc. 1c	$40.12 \pm 6.02$	$95.83 \pm 14.37$	$0.68 \pm 0.14$	$32.22 \pm 1.61$
NGC 5194 Enuc. 4 a	$30.59 \pm 4.59$	$41.93 \pm 6.29$	$0.018 \pm 0.004$	$10.45 \pm 0.52$
NGC 5457 Enuc. 2	$237.86 \pm 35.68$	$314.69 \pm 47.20$	$0.68 \pm 0.14$	$24.21 \pm 1.21$
NGC 5457 Enuc. 7	$< 0.26$	$< 0.46$	$3.43 \pm 0.69$	$53.60 \pm 2.68$
NGC 6946 Enuc. 4 a	$33.30 \pm 5.02$	$47.68 \pm 7.16$	$\dots$	$17.07 \pm 0.85$
NGC 6946 Enuc. 3 b	$42.01 \pm 6.32$	$51.32 \pm 7.70$	$2.24 \pm 0.45$	$21.79 \pm 1.09$
NGC 6946 b	$4.34 \pm 0.83$	$11.18 \pm 1.71$	$4.60 \pm 0.92$	$2075.43 \pm 103.77$
NGC 6946 Enuc. 9	$23.67 \pm 3.59$	$36.83 \pm 5.53$	$3.46 \pm 0.69$	$115.07 \pm 5.75$
NGC 6946 Enuc. 1	$29.23 \pm 4.41$	$38.37 \pm 5.76$	$2.83 \pm 0.57$	$46.55 \pm 2.33$
NGC 6946 Enuc. 2 a	$31.82 \pm 4.80$	$41.20 \pm 6.19$	$2.37 \pm 0.47$	$17.27 \pm 0.86$

NOTE—<sup>†</sup> Photometry unreliable and not reported due to saturation by the nucleus in the 24  $\mu\text{m}$  image.

**Table 7.** Local Background Measurements

Source ID	$\text{Back}_{3 \text{ GHz}}$	$\text{Back}_{15 \text{ GHz}}$	$\text{Back}_{33 \text{ GHz}}$	$f_{\text{Back}}^{3 \text{ GHz}}$	$f_{\text{Back}}^{15 \text{ GHz}}$	$f_{\text{Back}}^{33 \text{ GHz}}$
	(mJy)	(mJy)	(mJy)	( $\dagger$ )	( $\dagger$ )	( $\dagger$ )
Star-Forming Regions						
NGC 0337 D	0.207	0.099	0.019	0.174	0.130	0.062
NGC 0337 A	0.046	0.070	0.024	0.046	0.100	0.085
NGC 0337 B	0.133	0.059	-0.022	0.027	0.022	0.012

*Table 7 continued*

Table 7 (continued)

Source ID	Back <sub>3 GHz</sub>	Back <sub>15 GHz</sub>	Back <sub>33 GHz</sub>	$f_{Back}^{3 GHz}$	$f_{Back}^{15 GHz}$	$f_{Back}^{33 GHz}$
	(mJy)	(mJy)	(mJy)	( $\dagger$ )	( $\dagger$ )	( $\dagger$ )
NGC 0337 C	0.026	0.019	0.005	0.087	0.064	0.024
NGC 0337 G	0.030	0.013	-0.005	0.082	0.068	0.032
NGC 0337 E	0.026	0.027	0.010	0.096	0.099	0.034
NGC 0337 F	0.021	0.038	0.023	0.075	0.195	0.104
NGC 0628 Enuc. 4	-0.004	0.013	0.013	0.015	0.049	0.057
NGC 0628 Enuc. 2	0.017	-0.012	0.026	0.033	0.033	0.092
NGC 0628 Enuc. 3 C	0.009	0.010	0.018	0.033	0.050	0.080
NGC 0628 Enuc. 3 A <sup>†</sup>	-0.007	0.019	-0.012	0.013	0.052	0.024
NGC 0628 Enuc. 3 B	0.023	0.018	0.014	0.080	0.091	0.066
NGC 0628 Enuc. 1 B	...	0.063	...	...	0.156	...
NGC 0628 Enuc. 1 A	0.007	0.029	-0.031	0.026	0.114	0.118
NGC 0855 C	0.082	0.071	0.018	0.045	0.067	0.024
NGC 0855 A <sup>†</sup>	0.057	0.037	-0.042	0.025	0.024	0.049
NGC 0855 B	0.022	0.026	0.022	0.060	0.110	0.120
NGC 0925 D	-0.004	0.005	...	0.014	0.022	...
NGC 0925 A	0.020	...	...	0.211	...	...
NGC 0925 B	-0.001	-0.003	...	0.004	0.019	...
NGC 1097 Enuc. 2	0.005	...	0.000	0.004	...	0.002
NGC 1097 D	1.142	0.248	0.223	0.096	0.083	0.100
NGC 1097 B	2.604	0.681	0.481	0.367	0.203	0.159
NGC 1097 A <sup>†</sup>	5.145	0.574	0.810	0.049	0.020	0.038
NGC 1097 E	1.014	0.248	0.180	0.103	0.084	0.095
NGC 1097 C	1.450	0.285	0.235	0.119	0.087	0.100
NGC 1097 Enuc. 1	...	...	0.023	...	...	0.073
NGC 1266 C	0.089	0.039	0.051	0.003	0.004	0.009
NGC 1266 A <sup>†</sup>	0.079	0.006	0.037	0.002	0.001	0.009
NGC 1266 B	0.121	0.031	0.014	0.006	0.007	0.006
NGC 1377	0.003	-0.005	0.004	0.014	0.073	0.069
IC 342 B	3.176	1.428	1.135	0.081	0.078	0.081
IC 342 A <sup>†</sup>	2.376	0.743	0.477	0.026	0.020	0.018
IC 342 C	2.542	0.970	0.790	0.109	0.093	0.098
IC 342 D	0.077	0.027	...	0.086	0.199	...
NGC 1482 C	1.810	0.339	0.237	0.039	0.026	0.026
NGC 1482 A <sup>†</sup>	1.692	0.078	0.255	0.014	0.003	0.023
NGC 1482 B	1.855	0.606	0.270	0.043	0.048	0.031
NGC 2146 A	0.855	0.020	0.101	0.139	0.045	0.044
NGC 2146 B	1.934	0.046	0.377	0.106	0.040	0.065
NGC 2146 C	4.865	0.136	0.971	0.132	0.081	0.097
NGC 2146 D	16.740	-0.052	1.332	0.067	0.002	0.022
NGC 2146 E	2.349	0.122	0.290	0.173	0.210	0.081
NGC 2403 Enuc. 5 C	0.066	0.080	0.049	0.072	0.107	0.066
NGC 2403 Enuc. 5 A <sup>†</sup>	0.014	0.114	0.045	0.007	0.055	0.025
NGC 2403 Enuc. 5 E	0.004	0.012	...	0.018	0.052	...
NGC 2403 Enuc. 5 B	0.004	0.006	0.006	0.026	0.033	0.059
NGC 2403 Enuc. 6 A	-0.023	0.026	0.008	0.026	0.030	0.011
NGC 2403 Enuc. 6 B	0.015	...	0.000	0.130	...	0.002
NGC 2403 Enuc. 1 E	0.014	0.010	...	0.058	0.035	...
NGC 2403 Enuc. 1 A	-0.001	0.013	-0.001	0.001	0.033	0.003
NGC 2403 C	0.002	0.012	...	0.017	0.091	...
NGC 2403 Enuc. 1 B	0.031	0.066	0.040	0.020	0.048	0.035
NGC 2403 Enuc. 1 C	0.036	0.005	0.003	0.076	0.048	0.035
NGC 2403 Enuc. 1 D	0.022	0.023	0.009	0.108	0.170	0.079
NGC 2403 Enuc. 2 B	-0.008	0.018	-0.002	0.020	0.055	0.009

Table 7 continued

Table 7 (continued)

Source ID	Back <sub>3</sub> GHz	Back <sub>15</sub> GHz	Back <sub>33</sub> GHz	$f_{Back}^{3\text{ GHz}}$	$f_{Back}^{15\text{ GHz}}$	$f_{Back}^{33\text{ GHz}}$
	(mJy)	(mJy)	(mJy)	( $\dagger$ )	( $\dagger$ )	( $\dagger$ )
NGC 2403 Enuc. 2 D	0.039	0.030	0.029	0.061	0.054	0.053
NGC 2403 Enuc. 2 A <sup>†</sup>	0.024	0.024	0.061	0.011	0.015	0.041
NGC 2403 Enuc. 2 C	0.050	0.025	0.022	0.084	0.055	0.055
NGC 2403 B	0.027	...	...	0.138	...	...
NGC 2403 E	0.013	...	...	0.096	...	...
NGC 2403 Enuc. 3 B	0.177	0.165	0.229	0.046	0.052	0.079
NGC 2403 Enuc. 4 B	...	0.018	0.003	...	0.158	0.039
NGC 2403 Enuc. 4 C	...	0.013	0.008	...	0.122	0.098
NGC 2403 Enuc. 4 A	0.016	0.066	0.034	0.016	0.066	0.037
Holmberg II B	0.006	0.011	0.019	0.041	0.080	0.115
Holmberg II A	0.017	0.016	0.031	0.050	0.050	0.091
NGC 2798 B	0.180	0.041	0.011	0.102	0.067	0.057
NGC 2798 A	0.624	0.184	0.058	0.056	0.073	0.062
NGC 2841 A	-0.003	...	...	0.005	...	...
NGC 2976 Enuc. 1 A	0.043	0.044	0.032	0.038	0.057	0.043
NGC 2976 Enuc. 1 D	0.143	0.101	0.073	0.064	0.056	0.047
NGC 2976 Enuc. 1 C	0.019	0.019	0.019	0.039	0.052	0.059
NGC 2976 Enuc. 1 B <sup>†</sup>	0.106	0.145	0.063	0.032	0.058	0.031
NGC 2976 B	0.014	0.004	-0.001	0.086	0.025	0.005
NGC 2976 A	...	-0.004	...	...	0.027	...
NGC 2976 Enuc. 2 A	0.069	0.068	0.025	0.041	0.046	0.020
NGC 2976 Enuc. 2 C	0.047	0.045	0.015	0.084	0.099	0.038
NGC 2976 C	0.012	...	...	0.048	...	...
NGC 3049 A	0.007	0.021	0.018	0.005	0.039	0.040
NGC 3049 B	0.005	0.014	0.014	0.015	0.066	0.090
NGC 3049 C	0.009	...	...	0.041	...	...
NGC 3077 A	0.523	0.387	0.170	0.046	0.054	0.027
NGC 3190 A	0.024	0.008	0.005	0.043	0.013	0.004
NGC 3184 B	0.013	0.012	...	0.040	0.062	...
NGC 3184 A	0.027	-0.006	-0.004	0.042	0.018	0.012
NGC 3198 B	0.014	0.001	...	0.067	0.005	...
NGC 3198 A	0.020	0.013	-0.023	0.041	0.044	0.120
NGC 3198 C	-0.019	0.015	...	0.112	0.085	...
IC 2574 D	0.032	0.016	0.010	0.033	0.053	0.021
IC 2574 C	0.160	0.112	0.060	0.179	0.178	0.077
IC 2574 A	0.009	0.004	0.011	0.016	0.008	0.023
IC 2574 B	-0.005	0.005	...	0.056	0.049	...
NGC 3265 A	0.145	0.044	0.028	0.053	0.066	0.066
NGC 3351 C	-0.016	-0.022	-0.010	0.007	0.021	0.008
NGC 3351 A	0.497	0.179	0.036	0.069	0.065	0.018
NGC 3351 B	0.409	0.101	0.109	0.046	0.028	0.048
NGC 3521 Enuc. 1	-0.022	0.023	...	0.162	0.080	...
NGC 3521 Enuc. 3 A	...	0.027	...	...	0.085	...
NGC 3521 Enuc. 2 A	0.021	0.016	-0.019	0.032	0.047	0.068
NGC 3521 Enuc. 3 C	0.021	...	...	0.021	...	...
NGC 3521 Enuc. 2 B	0.011	0.012	...	0.037	0.034	...
NGC 3621 C	0.025	0.032	...	0.065	0.099	...
NGC 3621 A	0.060	0.026	...	0.057	0.095	...
NGC 3621 H	0.012	...	...	0.103	...	...
NGC 3621 G <sup>†</sup>	0.109	0.079	...	0.051	0.051	...
NGC 3621 B	0.035	0.048	...	0.037	0.086	...
NGC 3621 F	0.002	...	...	0.013	...	...
NGC 3621 E	-0.001	-0.010	...	0.002	0.054	...

Table 7 continued



Table 7 (continued)

Source ID	Back <sub>3 GHz</sub>	Back <sub>15 GHz</sub>	Back <sub>33 GHz</sub>	$f_{Back}^{3 GHz}$	$f_{Back}^{15 GHz}$	$f_{Back}^{33 GHz}$
	(mJy)	(mJy)	(mJy)	( $\dagger$ )	( $\dagger$ )	( $\dagger$ )
NGC 3627 Enuc. 1 G	0.037	...	...	0.072	...	...
NGC 3627 Enuc. 1 F	0.015	...	...	0.064	...	...
NGC 3627 Enuc. 1 E	-0.002	...	0.003	0.006	...	0.007
NGC 3627 B	0.382	0.392	-0.004	0.096	0.162	0.003
NGC 3627 A	0.008	0.037	0.021	0.004	0.034	0.030
NGC 3627 Enuc. 2 D	0.140	0.073	0.060	0.034	0.029	0.032
NGC 3627 Enuc. 1 A	0.074	0.118	0.035	0.031	0.081	0.028
NGC 3627 Enuc. 2 A <sup>†</sup>	0.161	0.208	0.029	0.022	0.049	0.008
NGC 3627 Enuc. 2 E	0.197	0.120	0.077	0.048	0.057	0.046
NGC 3627 Enuc. 2 C	-0.008	0.039	0.003	0.019	0.092	0.012
NGC 3627 Enuc. 2 B	0.027	0.059	...	0.035	0.117	...
NGC 3773	0.078	0.049	0.017	0.031	0.036	0.015
NGC 3938 B	0.028	...	...	0.102	...	...
NGC 3938 Enuc. 2 B	0.002	-0.003	0.011	0.009	0.027	0.060
NGC 3938 Enuc. 2 A	-0.007	0.000	-0.003	0.021	0.000	0.013
NGC 4254 Enuc. 2 D	...	0.008	0.019	...	0.081	0.112
NGC 4254 Enuc. 2 C	...	...	0.007	...	...	0.089
NGC 4254 Enuc. 1 E	0.020	0.013	...	0.068	0.114	...
NGC 4254 Enuc. 2 E	-0.003	...	...	0.019	...	...
NGC 4254	0.024	0.095	0.014	0.059	0.185	0.038
NGC 4254 Enuc. 1 D	0.056	0.011	0.014	0.071	0.046	0.040
NGC 4254 Enuc. 1 B	0.033	-0.004	0.023	0.152	0.028	0.056
NGC 4254 Enuc. 1 C	0.002	...	-0.008	0.008	...	0.063
NGC 4321 Enuc. 2	0.014	...	-0.010	0.082	...	0.084
NGC 4321 C	0.424	0.192	0.101	0.165	0.176	0.173
NGC 4321 F	0.215	0.099	0.067	0.231	0.218	0.214
NGC 4321 H	0.115	0.055	0.037	0.176	0.177	0.136
NGC 4321 A <sup>†</sup>	0.326	0.381	-0.122	0.014	0.042	0.024
NGC 4321 B	0.379	0.153	0.089	0.153	0.193	0.197
NGC 4321 G	0.330	0.115	0.076	0.186	0.184	0.198
NGC 4321 D	0.387	0.173	0.129	0.119	0.135	0.156
NGC 4321 E	0.750	0.277	0.158	0.190	0.199	0.182
NGC 4321 Enuc. 1 B	-0.012	0.008	...	0.043	0.045	...
NGC 4536 C	2.914	0.834	0.455	0.086	0.066	0.057
NGC 4536 A <sup>†</sup>	1.452	0.485	0.149	0.016	0.017	0.009
NGC 4536 B	2.138	0.635	0.335	0.079	0.064	0.051
NGC 4559 E	-0.017	0.013	...	0.116	0.106	...
NGC 4559 C	-0.013	0.028	0.005	0.065	0.158	0.026
NGC 4559 D	...	0.026	...	...	0.228	...
NGC 4559 B	0.012	0.010	0.002	0.130	0.064	0.018
NGC 4559 A	0.002	0.008	0.002	0.014	0.073	0.013
NGC 4569 A	0.253	0.180	0.057	0.088	0.125	0.065
NGC 4579	-0.139	0.254	0.152	0.068	0.092	0.255
NGC 4594	-0.021	0.011	0.021	0.025	0.023	0.026
NGC 4631 Enuc. 1	-0.000	0.064	0.049	0.000	0.097	0.080
NGC 4625 A	...	0.035	...	...	0.323	...
NGC 4631 A	0.044	0.178	0.034	0.006	0.072	0.023
NGC 4631 H	0.128	0.195	0.071	0.130	0.149	0.084
NGC 4631 B	0.456	0.220	0.208	0.083	0.066	0.068
NGC 4631 G	0.043	0.050	0.030	0.047	0.068	0.049
NGC 4631 Enuc. 2 B	0.014	0.042	-0.000	0.009	0.030	0.000
NGC 4631 Enuc. 2 C	...	0.019	...	...	0.088	...
NGC 4725 C	-0.007	0.000	...	0.032	0.006	...

Table 7 continued

Table 7 (continued)

Source ID	Back <sub>3</sub> GHz	Back <sub>15</sub> GHz	Back <sub>33</sub> GHz	$f_{Back}^{3\text{ GHz}}$	$f_{Back}^{15\text{ GHz}}$	$f_{Back}^{33\text{ GHz}}$
	(mJy)	(mJy)	(mJy)	( $\dagger$ )	( $\dagger$ )	( $\dagger$ )
NGC 4725 A	0.003	0.002	0.001	0.038	0.014	0.002
NGC 4736 K	0.004	0.015	...	0.007	0.020	...
NGC 4736 J	0.104	0.001	...	0.103	0.002	...
NGC 4736 I	0.097	0.034	...	0.077	0.052	...
NGC 4736 G	0.044	...	...	0.163	...	...
NGC 4736 L	0.047	...	...	0.084	...	...
NGC 4736 H	0.088	0.080	0.026	0.069	0.074	0.074
NGC 4736 M	-0.016	...	...	0.103	...	...
NGC 4736 F	0.134	0.108	...	0.099	0.121	...
NGC 4736 N	-0.004	0.133	...	0.017	0.124	...
NGC 4736 A	0.193	-0.016	0.021	0.031	0.007	0.017
NGC 4736 O	0.015	0.086	0.024	0.084	0.194	0.062
NGC 4736 E	...	0.141	...	...	0.182	...
NGC 4736 P	0.133	0.036	-0.008	0.126	0.120	0.013
NGC 4736 D	0.015	0.112	0.009	0.025	0.107	0.020
NGC 4736 Enuc. 1 D	0.015	0.015	0.030	0.096	0.044	0.109
NGC 4736 Enuc. 1 A	0.049	0.099	0.093	0.032	0.093	0.106
NGC 4736 Enuc. 1 B	0.148	0.038	0.065	0.053	0.024	0.063
NGC 4736 Enuc. 1 C	-0.002	0.062	0.027	0.001	0.054	0.043
NGC 4736 Enuc. 1 E	0.013	...	0.015	0.148	...	0.110
NGC 4826 C	0.049	0.086	0.033	0.068	0.177	0.152
NGC 4826 B	0.134	0.109	0.039	0.185	0.205	0.155
NGC 4826 A	0.779	0.470	0.174	0.064	0.103	0.062
NGC 4826 F <sup>†</sup>	0.236	0.899	0.044	0.021	0.093	0.012
NGC 4826 E	0.048	0.087	0.019	0.110	0.189	0.136
NGC 4826 D	0.077	0.075	0.030	0.136	0.229	0.096
NGC 5055 C	0.005	...	...	0.033	...	...
NGC 5055 D	0.023	0.040	...	0.106	0.207	...
NGC 5055 A	0.204	0.150	0.066	0.103	0.149	0.197
NGC 5055 B	-0.011	0.002	...	0.010	0.006	...
NGC 5055 Enuc. 1	0.002	0.024	0.020	0.005	0.055	0.050
NGC 5194 Enuc. 6	0.034	0.043	0.044	0.050	0.082	0.078
NGC 5194 Enuc. 3 B	...	0.026	0.022	...	0.074	0.165
NGC 5194 Enuc. 3 A	0.050	0.035	0.040	0.062	0.064	0.069
NGC 5194 Enuc. 11 G	-0.031	...	0.009	0.105	...	0.030
NGC 5194 Enuc. 11 A	0.053	...	0.008	0.114	...	0.036
NGC 5194 Enuc. 11 B	...	0.035	0.010	...	0.220	0.053
NGC 5194 Enuc. 11 C	...	0.004	0.009	...	0.042	0.064
NGC 5194 Enuc. 11 D	0.074	0.029	0.000	0.087	0.109	0.004
NGC 5194 H	0.055	-0.011	-0.017	0.019	0.009	0.060
NGC 5194 L	0.333	0.092	0.031	0.200	0.140	0.179
NGC 5194 M	0.089	0.050	0.012	0.130	0.199	0.090
NGC 5194 Enuc. 11 E	0.018	0.034	0.009	0.086	0.149	0.056
NGC 5194 A	0.240	0.079	0.008	0.170	0.144	0.030
NGC 5194 Enuc. 11 F	0.025	0.015	0.005	0.100	0.101	0.036
NGC 5194 K	0.095	0.108	0.011	0.111	0.165	0.048
NGC 5194 B	0.028	0.018	0.008	0.014	0.029	0.022
NGC 5194 G	0.220	0.095	0.010	0.194	0.198	0.100
NGC 5194 J	0.077	0.036	0.015	0.130	0.261	0.200
NGC 5194 E	0.559	0.306	0.094	0.045	0.070	0.056
NGC 5194 O	0.011	0.111	...	0.028	0.238	...
NGC 5194 I	0.474	0.124	0.039	0.088	0.087	0.055
NGC 5194 C <sup>†</sup>	0.491	0.203	0.050	0.046	0.072	0.041

Table 7 continued

Table 7 (continued)

Source ID	Back <sub>3 GHz</sub>	Back <sub>15 GHz</sub>	Back <sub>33 GHz</sub>	$f_{Back}^{3 GHz}$	$f_{Back}^{15 GHz}$	$f_{Back}^{33 GHz}$
	(mJy)	(mJy)	(mJy)	( $\dagger$ )	( $\dagger$ )	( $\dagger$ )
NGC 5194 Enuc. 1 A	0.025	0.001	0.007	0.076	0.010	0.027
NGC 5194 Enuc. 4 D	...	...	0.007	...	...	0.057
NGC 5194 N	0.237	0.069	...	0.179	0.258	...
NGC 5194 F	0.024	0.041	0.014	0.032	0.079	0.044
NGC 5194 Enuc. 4 C	0.021	0.004	0.004	0.129	0.036	0.033
NGC 5194 P	0.112	0.014	0.002	0.157	0.048	0.010
NGC 5194 Enuc. 4 E	...	...	0.002	...	...	0.034
NGC 5194 Enuc. 10	0.065	0.041	0.037	0.092	0.117	0.105
NGC 5194 Enuc. 4 B	0.005	...	-0.002	0.046	...	0.026
NGC 5194 Enuc. 5 B	0.021	0.005	0.000	0.079	0.027	0.001
NGC 5194 Enuc. 4 F	0.018	0.004	0.000	0.083	0.027	0.003
NGC 5194 Enuc. 4 G	0.029	0.026	-0.000	0.052	0.090	0.004
NGC 5194 Enuc. 5 A	0.024	0.022	0.014	0.038	0.063	0.038
NGC 5194 Enuc. 9	0.002	-0.020	0.010	0.004	0.055	0.026
NGC 5194 Enuc. 8 C	0.005	0.032	...	0.014	0.118	...
NGC 5194 Enuc. 8 B	0.052	0.048	0.005	0.078	0.075	0.024
NGC 5194 Enuc. 7 E	...	0.028	0.002	...	0.150	0.008
NGC 5194 Enuc. 8 A	0.070	0.044	-0.012	0.126	0.082	0.030
NGC 5194 Enuc. 7 A	0.103	0.022	0.019	0.086	0.055	0.057
NGC 5194 Enuc. 7 C	0.048	0.009	-0.003	0.117	0.049	0.018
NGC 5194 Enuc. 7 B	0.022	-0.013	...	0.067	0.081	...
NGC 5194 Enuc. 7 F	0.011	0.052	...	0.002	0.029	...
NGC 5194 Enuc. 8 D	0.002	-0.018	...	0.006	0.092	...
NGC 5398	0.000	0.024	0.002	0.000	0.014	0.001
NGC 5457 Enuc. 6 A	0.092	0.099	0.018	0.088	0.106	0.033
NGC 5457 Enuc. 6 E	0.071	0.077	0.024	0.106	0.174	0.052
NGC 5457 Enuc. 6 B	0.183	0.118	0.060	0.078	0.075	0.079
NGC 5457 Enuc. 6 C	0.060	0.066	0.013	0.060	0.090	0.023
NGC 5457 Enuc. 6 D	0.023	0.031	0.005	0.040	0.084	0.016
NGC 5457 Enuc. 6 F	0.009	0.009	...	0.042	0.084	...
NGC 5457 Enuc. 2 B	0.001	-0.001	...	0.007	0.012	...
NGC 5457 Enuc. 2 C	-0.007	0.004	...	0.046	0.077	...
NGC 5457 Enuc. 5 B	0.099	0.118	0.033	0.067	0.099	0.029
NGC 5457 Enuc. 5 A <sup>†</sup>	0.101	0.115	0.034	0.048	0.053	0.027
NGC 5457 Enuc. 5 C	0.103	0.062	0.045	0.118	0.100	0.065
NGC 5457 Enuc. 1	0.009	...	0.005	0.083	...	0.058
NGC 5457	0.015	0.021	0.013	0.017	0.086	0.035
NGC 5457 Enuc. 3 E	-0.008	0.003	...	0.034	0.016	...
NGC 5457 Enuc. 3 D	0.013	0.032	...	0.022	0.090	...
NGC 5457 Enuc. 3 A	0.029	0.065	0.043	0.032	0.075	0.065
NGC 5457 Enuc. 3 B	0.257	0.299	0.087	0.022	0.032	0.012
NGC 5457 Enuc. 3 C	0.030	0.018	-0.001	0.031	0.033	0.003
NGC 5457 Enuc. 4 A	0.043	0.026	-0.001	0.104	0.101	0.006
NGC 5457 Enuc. 4 B	0.049	0.045	0.010	0.145	0.160	0.038
NGC 5457 Enuc. 4 C	0.081	0.078	0.041	0.098	0.140	0.090
NGC 5457 Enuc. 4 D	0.081	0.047	0.026	0.080	0.081	0.073
NGC 5457 Enuc. 7 D <sup>†</sup>	0.238	0.130	0.074	0.040	0.030	0.019
NGC 5457 Enuc. 7 B	0.115	0.151	0.081	0.054	0.200	0.111
NGC 5713 A	0.095	0.101	0.035	0.052	0.106	0.058
NGC 5713 F	0.035	0.063	0.025	0.094	0.194	0.127
NGC 5713 B	0.234	0.128	0.054	0.062	0.075	0.041
NGC 5713 Enuc. 2	0.100	0.081	-0.013	0.081	0.105	0.046
NGC 5713 Enuc. 2 A	0.185	0.141	0.024	0.096	0.131	0.038

Table 7 continued

Table 7 (continued)

Source ID	Back <sub>3</sub> GHz	Back <sub>15</sub> GHz	Back <sub>33</sub> GHz	$f_{Back}^{3\text{ GHz}}$	$f_{Back}^{15\text{ GHz}}$	$f_{Back}^{33\text{ GHz}}$
	(mJy)	(mJy)	(mJy)	( $\dagger$ )	( $\dagger$ )	( $\dagger$ )
NGC 5713 C	0.420	0.186	0.103	0.078	0.093	0.069
NGC 5713 G <sup>†</sup>	1.348	1.190	0.271	0.120	0.176	0.126
NGC 5713 D	0.334	0.182	0.096	0.044	0.056	0.040
NGC 5713 Enuc. 1 A	...	0.031	...	...	0.164	...
NGC 5713 E	0.209	0.142	0.016	0.151	0.165	0.028
NGC 5866	0.088	0.105	0.035	0.013	0.021	0.016
NGC 6946 Enuc. 4 A	0.047	0.035	0.045	0.122	0.103	0.116
NGC 6946 Enuc. 4 B	0.004	0.011	0.023	0.020	0.052	0.112
NGC 6946 Enuc. 4 H	-0.002	-0.003	0.000	0.023	0.028	0.002
NGC 6946 Enuc. 8 A	0.223	0.041	0.042	0.099	0.056	0.051
NGC 6946 Enuc. 5 A	...	...	0.007	...	...	0.064
NGC 6946 Enuc. 8 B	...	0.015	...	...	0.067	...
NGC 6946 Enuc. 5 B	0.009	0.027	0.010	0.028	0.071	0.026
NGC 6946 Enuc. 3 A	-0.014	0.014	0.010	0.135	0.069	0.043
NGC 6946 Enuc. 3 B	-0.011	0.029	0.014	0.089	0.143	0.069
NGC 6946 A	0.751	0.529	0.154	0.036	0.062	0.035
NGC 6946 Enuc. 3 C	0.015	0.049	0.028	0.031	0.103	0.065
NGC 6946 B	0.007	0.027	-0.007	0.015	0.069	0.025
NGC 6946 C	0.101	0.060	0.034	0.136	0.096	0.107
NGC 6946 Enuc. 6 J	0.017	0.000	0.014	0.148	0.005	0.138
NGC 6946 Enuc. 6 I	0.025	0.008	0.022	0.113	0.073	0.210
NGC 6946 Enuc. 6 H	0.019	0.004	0.014	0.101	0.034	0.089
NGC 6946 Enuc. 6 F	0.013	0.012	0.015	0.056	0.188	0.127
NGC 6946 Enuc. 6 E	...	0.008	0.008	...	0.050	0.049
NGC 6946 Enuc. 6 B	0.011	0.011	0.001	0.032	0.038	0.007
NGC 6946 Enuc. 6 C	0.006	0.006	...	0.056	0.100	...
NGC 6946 Enuc. 9 E	-0.004	0.006	...	0.031	0.077	...
NGC 6946 Enuc. 9 D	0.031	0.023	...	0.161	0.104	...
NGC 6946 Enuc. 9 A	0.060	0.090	0.033	0.070	0.122	0.053
NGC 6946 Enuc. 6 L	0.051	0.006	0.010	0.072	0.026	0.026
NGC 6946 Enuc. 9 C	-0.007	0.020	0.011	0.057	0.100	0.102
NGC 6946 Enuc. 9 B	0.009	0.024	0.015	0.057	0.143	0.117
NGC 6946 Enuc. 7 A	-0.007	0.045	0.013	0.035	0.060	0.027
NGC 6946 Enuc. 7 B	-0.008	0.017	0.009	0.059	0.079	0.057
NGC 6946 Enuc. 1 A	-0.003	0.029	0.031	0.004	0.045	0.047
NGC 6946 Enuc. 2 C	0.003	0.004	...	0.018	0.025	...
NGC 7331 G	0.120	...	...	0.172	...	...
NGC 7331 F	0.073	0.115	...	0.106	0.268	...
NGC 7331 H	0.069	-0.029	...	0.052	0.025	...
NGC 7331 I	0.076	0.143	...	0.062	0.097	...
NGC 7331 A	-0.020	0.045	...	0.123	0.123	...
NGC 7331 E	0.061	...	-0.057	0.067	...	0.117
NGC 7331 B	0.055	0.111	...	0.108	0.138	...
NGC 7331 D	0.014	0.076	...	0.096	0.170	...
NGC 7793 Enuc. 1 E	-0.001	-0.004	...	0.008	0.059	...
NGC 7793 Enuc. 3	-0.006	0.002	...	0.030	0.009	...
NGC 7793 Enuc. 1 A	0.006	0.004	...	0.059	0.051	...
NGC 7793 C	-0.004	0.004	-0.001	0.020	0.025	0.007
NGC 7793 A	-0.008	0.013	-0.003	0.035	0.067	0.016
NGC 7793 Enuc. 1 B	...	0.008	...	...	0.079	...
NGC 7793 Enuc. 1 C	-0.005	0.001	...	0.026	0.005	...
NGC 7793 Enuc. 2	...	...	-0.006	...	...	0.042

Table 7 continued

Table 7 (continued)

Source ID	Back <sub>3 GHz</sub>	Back <sub>15 GHz</sub>	Back <sub>33 GHz</sub>	$f_{Back}^{3 GHz}$	$f_{Back}^{15 GHz}$	$f_{Back}^{33 GHz}$
	(mJy)	(mJy)	(mJy)	( $\dagger$ )	( $\dagger$ )	( $\dagger$ )
Likely Background Galaxies						
NGC 0925 C	-0.001	-0.004	0.003	0.001	0.006	0.011
IC 342 E	0.113	0.039	...	0.143	0.139	...
Holmberg II C	0.006	0.011	0.019	0.041	0.080	0.115
NGC 2841 B	-0.003	...	...	0.026	...	...
NGC 2976 Enuc. 1 E	-0.005	...	...	0.031	...	...
NGC 3077 B	-0.004	0.009	...	0.066	0.078	...
NGC 3190 B	0.089	0.027	0.017	0.042	0.040	0.034
NGC 3265 B	0.001	-0.001	...	0.001	0.017	...
NGC 3351 D	-0.011	0.014	...	0.035	0.139	...
NGC 3627 Enuc. 1 B	-0.000	...	...	0.003	...	...
NGC 4569 B	-0.017	...	...	0.034	...	...
NGC 4625 B	0.001	0.004	0.001	0.001	0.016	0.004
NGC 6946 Enuc. 4 F	0.145	0.105	0.032	0.025	0.061	0.035
NGC 6946 Enuc. 4 G	-0.044	-0.002	0.011	0.018	0.002	0.022
Likely Associated with Supernovae						
NGC 2403 Enuc. 3 D	...	-0.038	...	...	0.022	...
NGC 4736 B	-0.016	...	...	0.100	...	...
NGC 4736 C	-0.027	...	...	0.169	...	...
NGC 5194 D	0.034	0.065	0.045	0.028	0.103	0.055
NGC 5194 Enuc. 7 D	0.028	-0.003	...	0.018	0.017	...
NGC 6946 F	0.016	0.012	...	0.079	0.108	...
NGC 6946 Enuc. 6 D	0.004	0.013	-0.003	0.013	0.036	0.015
NGC 6946 Enuc. 2 B	0.006	0.087	0.029	0.005	0.061	0.015
NGC 7331 C	0.040	0.379	0.055	0.051	0.205	0.076
NGC 7793 B	-0.002	...	...	0.013	...	...
Likely AME Candidates						
NGC 2403 Enuc. 5 D	0.045	0.073	0.036	0.071	0.115	0.059
NGC 2403 Enuc. 2 E	0.038	0.057	0.022	0.032	0.059	0.018
NGC 2403 Enuc. 3 A	0.015	0.030	0.033	0.038	0.075	0.063
NGC 2403 Enuc. 3 C	0.112	0.070	0.093	0.045	0.037	0.049
NGC 3627 Enuc. 1 D	0.014	0.048	0.014	0.036	0.086	0.023
NGC 3627 Enuc. 1 C	0.005	0.085	-0.004	0.011	0.134	0.004
NGC 4254 Enuc. 2 A	0.005	0.008	0.011	0.041	0.052	0.049
NGC 4254 Enuc. 1 A	0.013	0.007	0.020	0.037	0.053	0.088
NGC 4631 C	0.115	0.020	0.081	0.066	0.023	0.065
NGC 4631 D	0.065	0.013	0.078	0.042	0.025	0.083
NGC 4631 E	0.075	0.038	0.065	0.080	0.083	0.083
NGC 4631 F	0.418	0.259	0.212	0.061	0.079	0.053
NGC 4631 Enuc. 2 A	0.033	0.006	0.005	0.055	0.027	0.013
NGC 4725 B	-0.003	0.001	0.003	0.024	0.005	0.008
NGC 5194 Enuc. 2	0.019	0.011	0.018	0.015	0.024	0.032
NGC 5194 Enuc. 1 C	0.053	0.030	0.033	0.098	0.064	0.045
NGC 5194 Enuc. 1 B	0.034	0.025	0.023	0.069	0.051	0.043
NGC 5194 Enuc. 4 A	0.040	-0.004	0.018	0.056	0.012	0.044
NGC 5457 Enuc. 2 A	0.020	0.007	0.006	0.050	0.026	0.017
NGC 5457 Enuc. 7 A	0.084	0.071	0.048	0.079	0.127	0.068
NGC 5457 Enuc. 7 C	0.263	0.243	0.162	0.074	0.135	0.084

Table 7 continued

**Table 7** (*continued*)

Source ID	Back <sub>3 GHz</sub>	Back <sub>15 GHz</sub>	Back <sub>33 GHz</sub>	$f_{Back}^{3\text{ GHz}}$	$f_{Back}^{15\text{ GHz}}$	$f_{Back}^{33\text{ GHz}}$
	(mJy)	(mJy)	(mJy)	( $\dagger$ )	( $\dagger$ )	( $\dagger$ )
NGC 6946 E nuc. 4 C	0.026	0.037	0.042	0.017	0.026	0.027
NGC 6946 E nuc. 4 D	-0.001	0.013	0.004	0.011	0.016	0.005
NGC 6946 E nuc. 4 E	0.014	0.035	0.023	0.011	0.026	0.018
NGC 6946 E	0.060	0.062	0.055	0.083	0.086	0.043
NGC 6946 D	0.018	0.064	0.005	0.045	0.126	0.010
NGC 6946 E nuc. 6 M	-0.005	-0.012	0.006	0.009	0.133	0.014
NGC 6946 E nuc. 6 G	0.050	0.019	0.044	0.064	0.038	0.080
NGC 6946 E nuc. 6 K	0.063	0.025	0.051	0.090	0.064	0.112
NGC 6946 E nuc. 6 A <sup>†</sup>	0.080	0.036	0.097	0.043	0.033	0.081
NGC 6946 E nuc. 1 B	0.078	0.006	0.009	0.108	0.016	0.013
NGC 6946 E nuc. 2 A	-0.008	0.028	0.004	0.074	0.092	0.012
NGC 7793 E nuc. 1 D	-0.010	0.001	...	0.044	0.006	...

NOTE—<sup>†</sup> The aperture used for this star-forming region contained multiple smaller individual regions.

NOTE—<sup>‡</sup> The fractional contribution of the absolute value of the local background measurement to the aperture flux density.

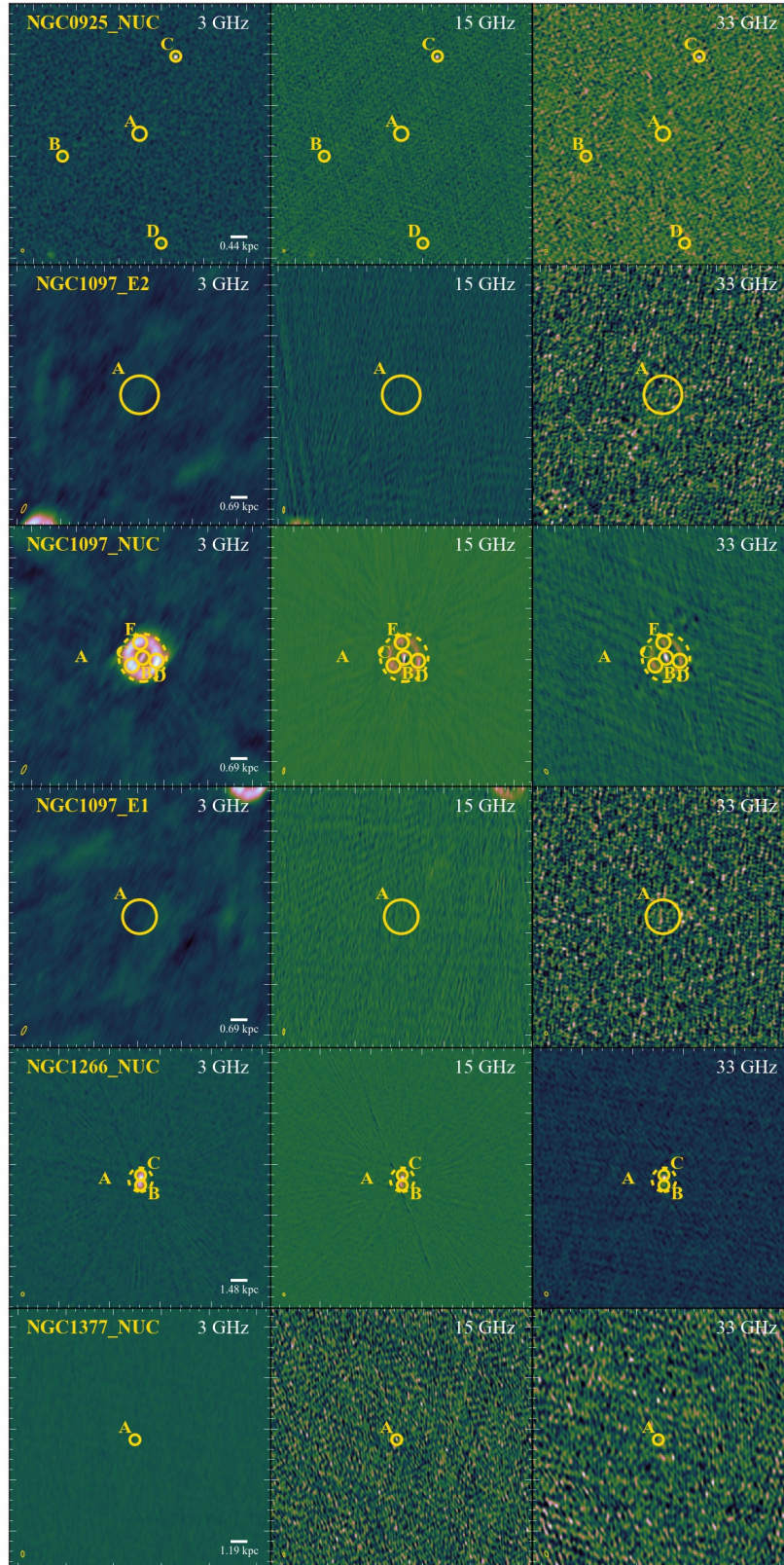


**Figure 9.** See description in Figure 1.



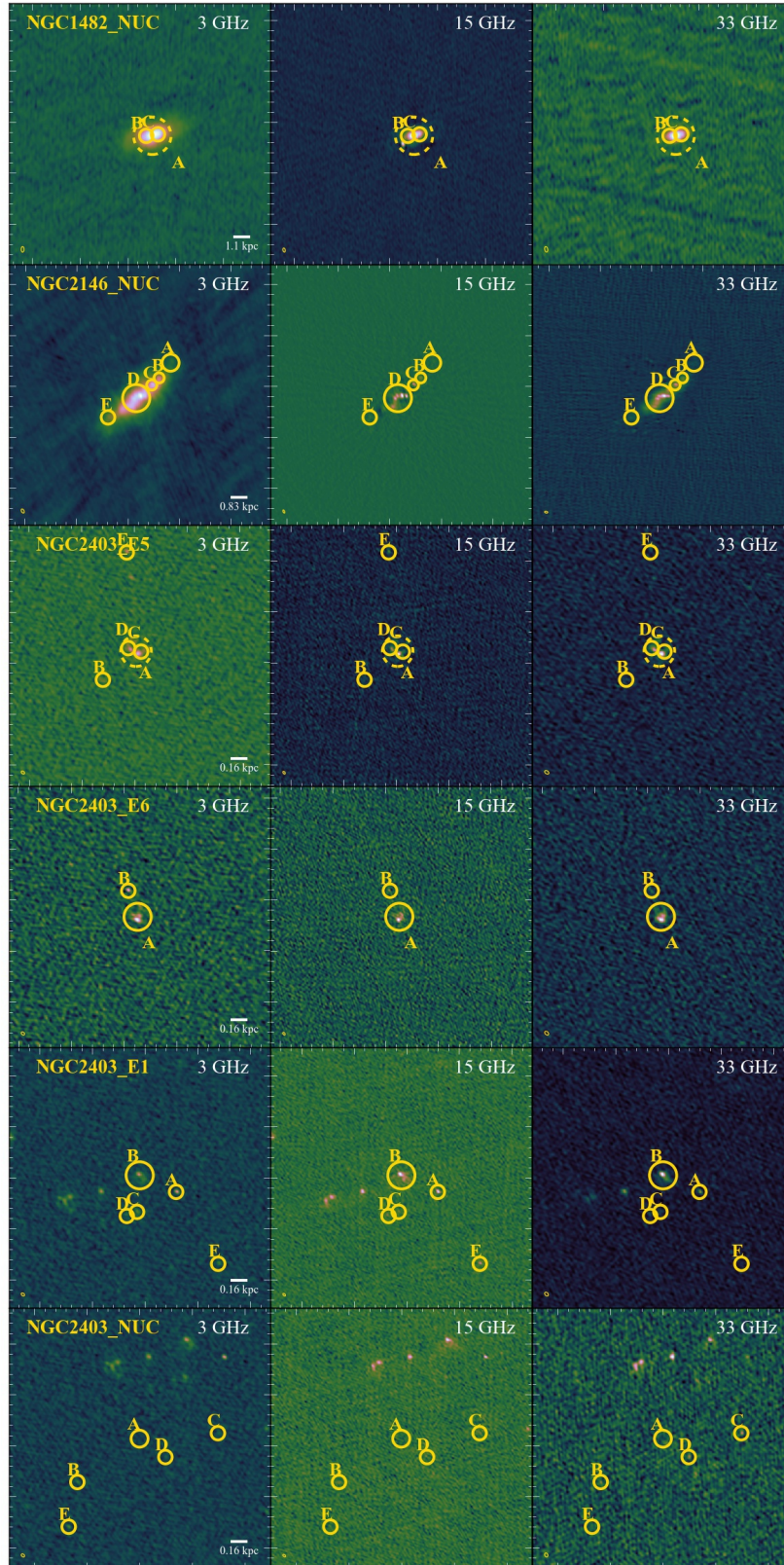


**Figure 10.** See description in Figure 1.



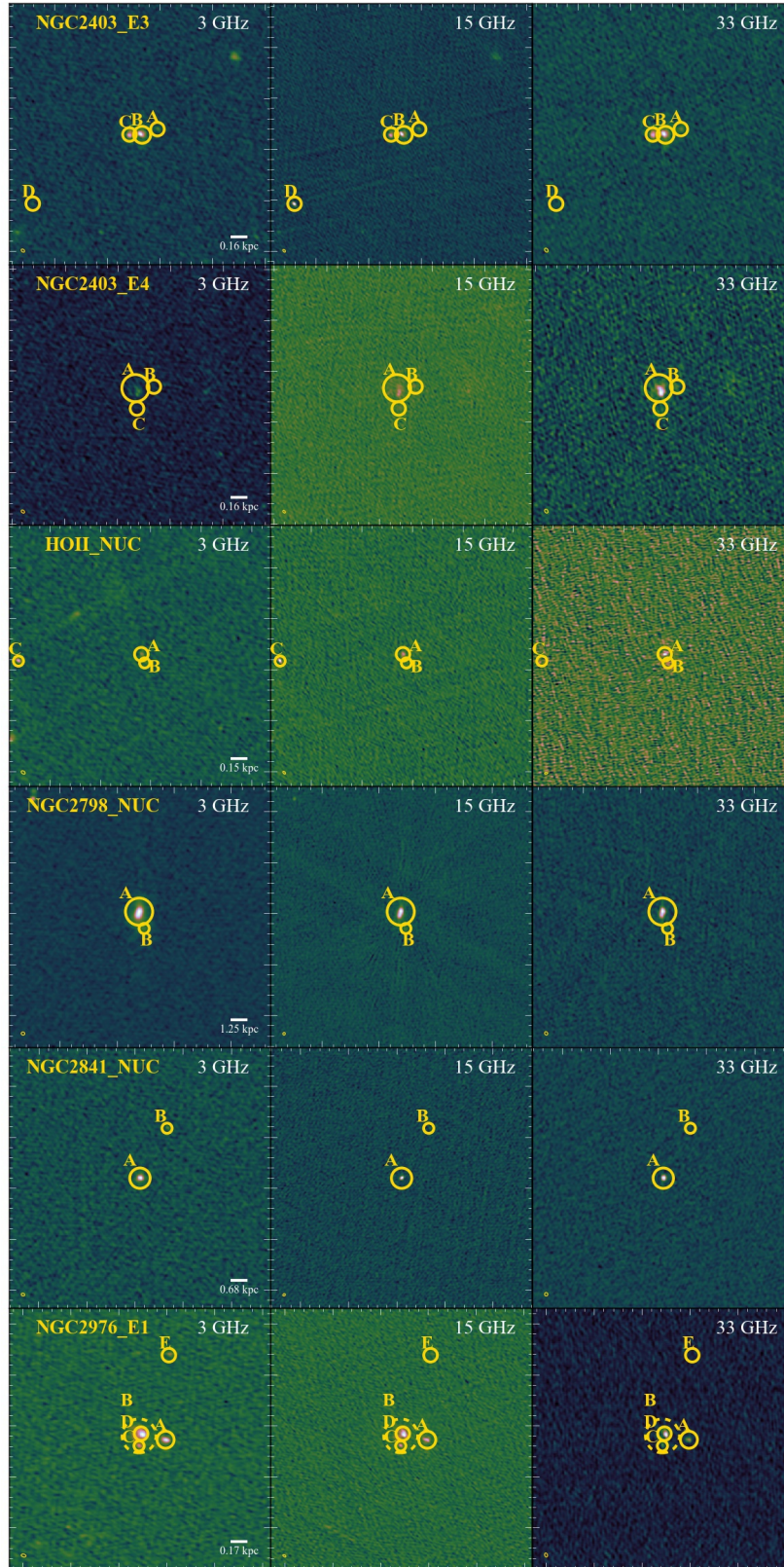


**Figure 11.** See description in Figure 1.



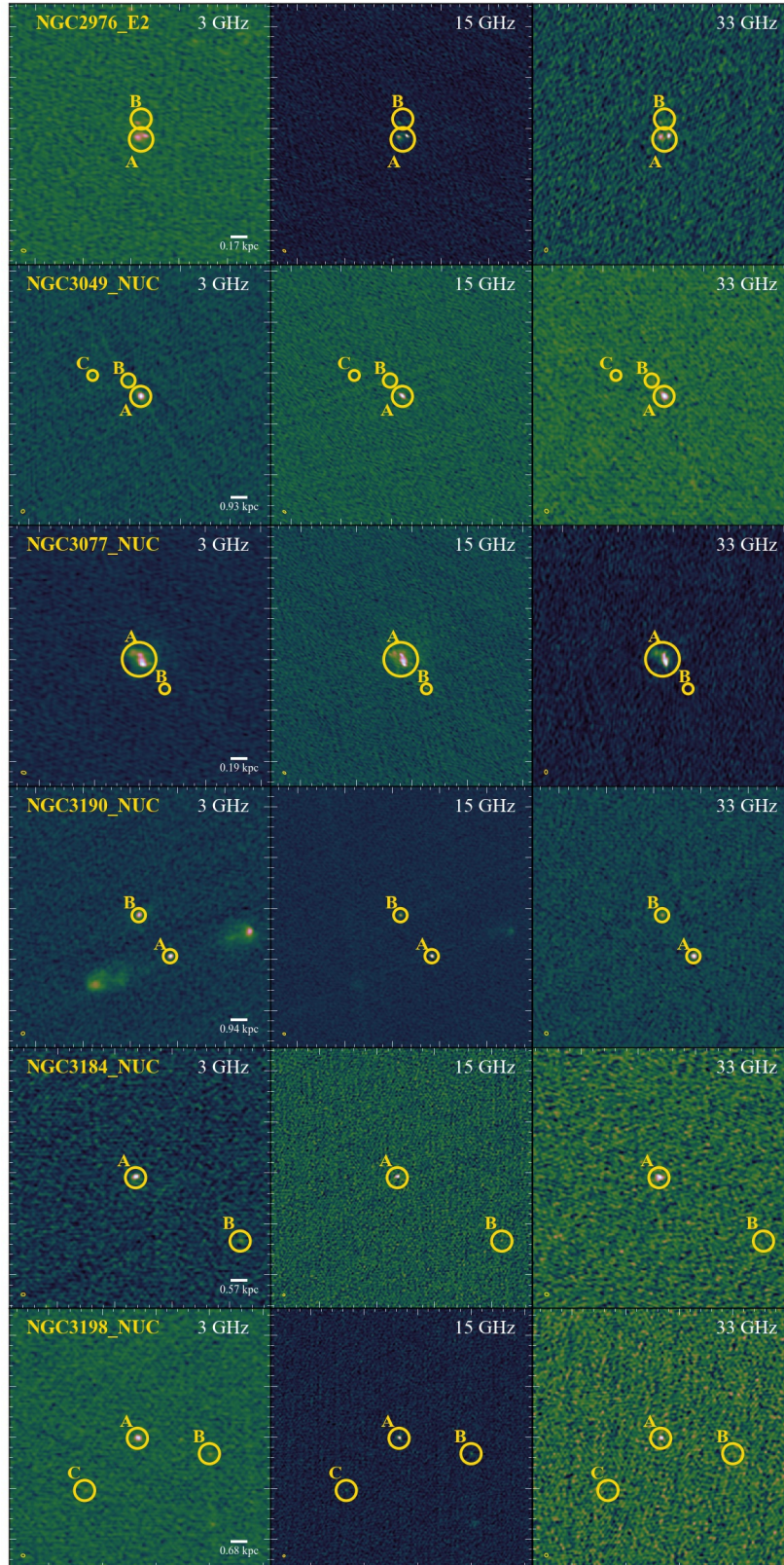


Figure 12. See description in Figure 1.



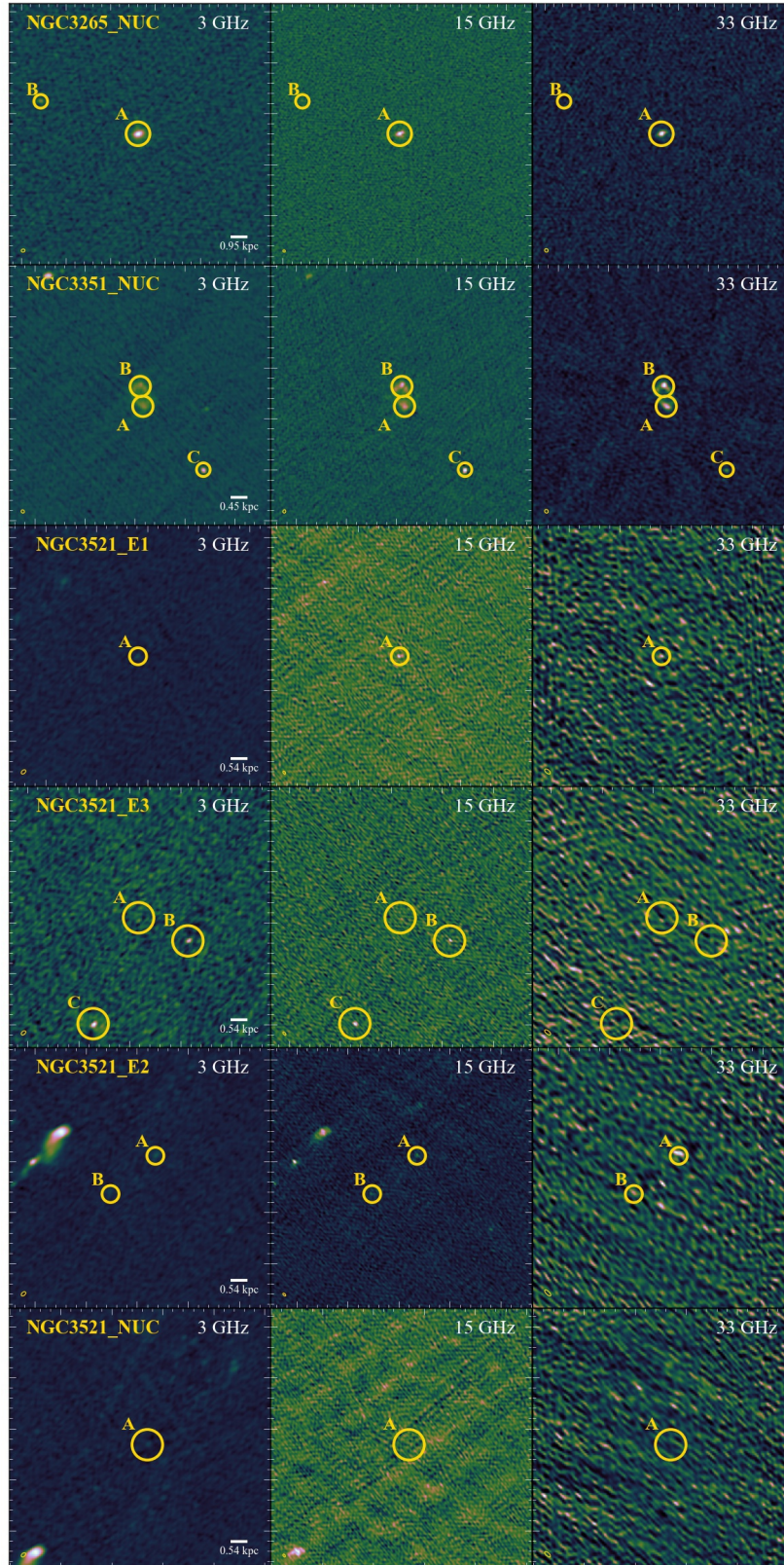


Figure 13. See description in Figure 1.



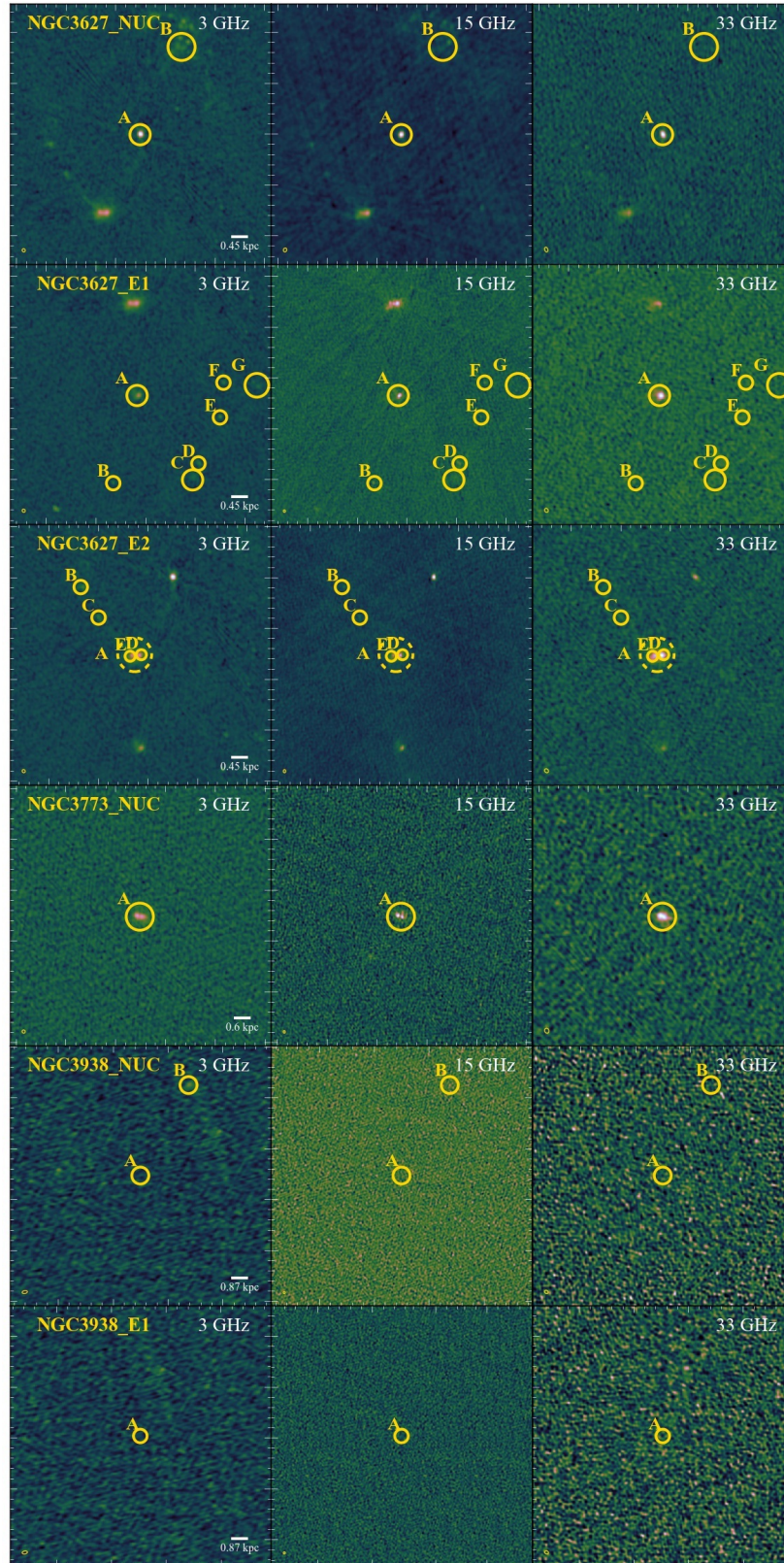


Figure 14. See description in Figure 1.



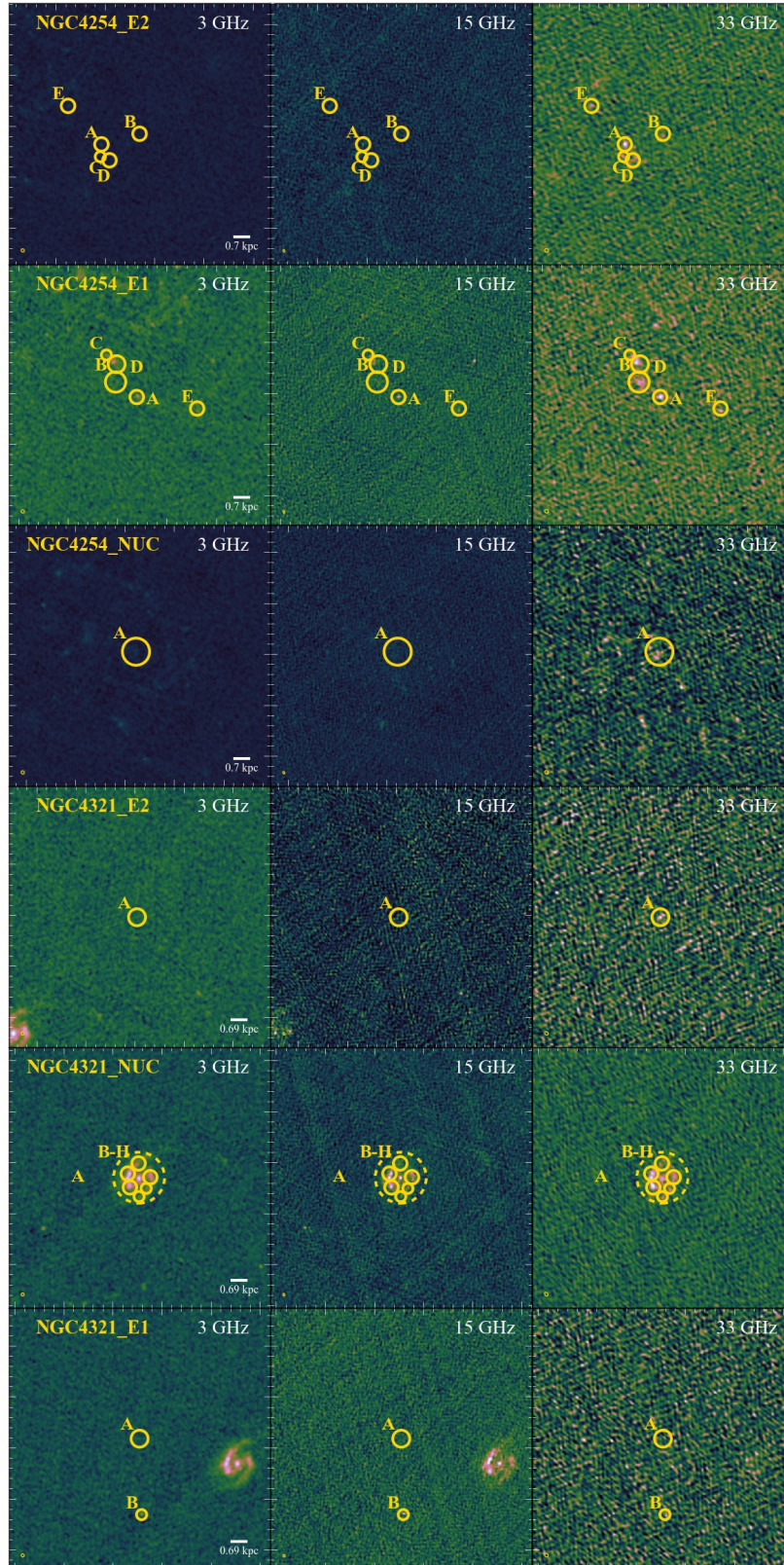


Figure 15. See description in Figure 1.



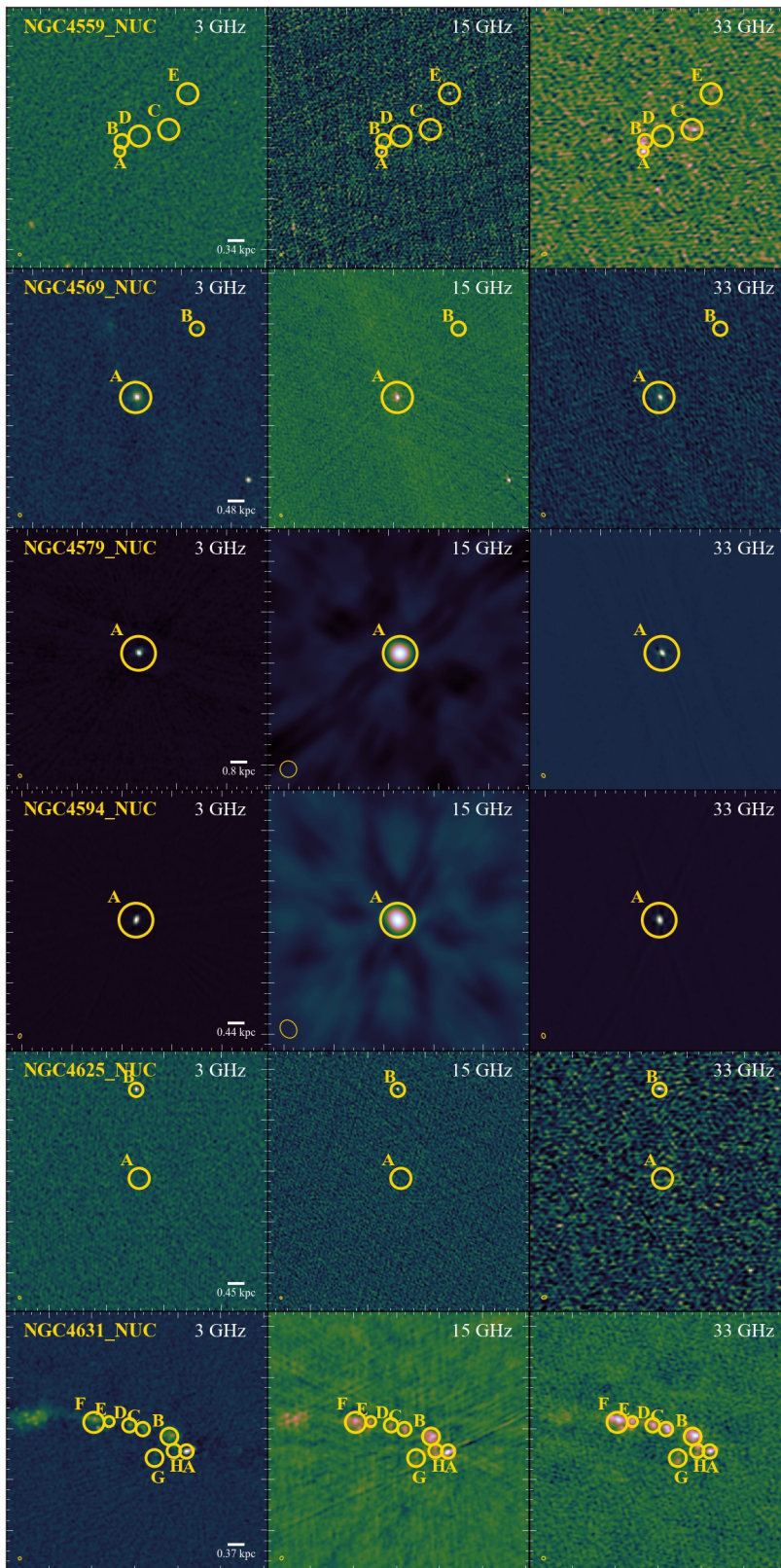


Figure 16. See description in Figure 1.



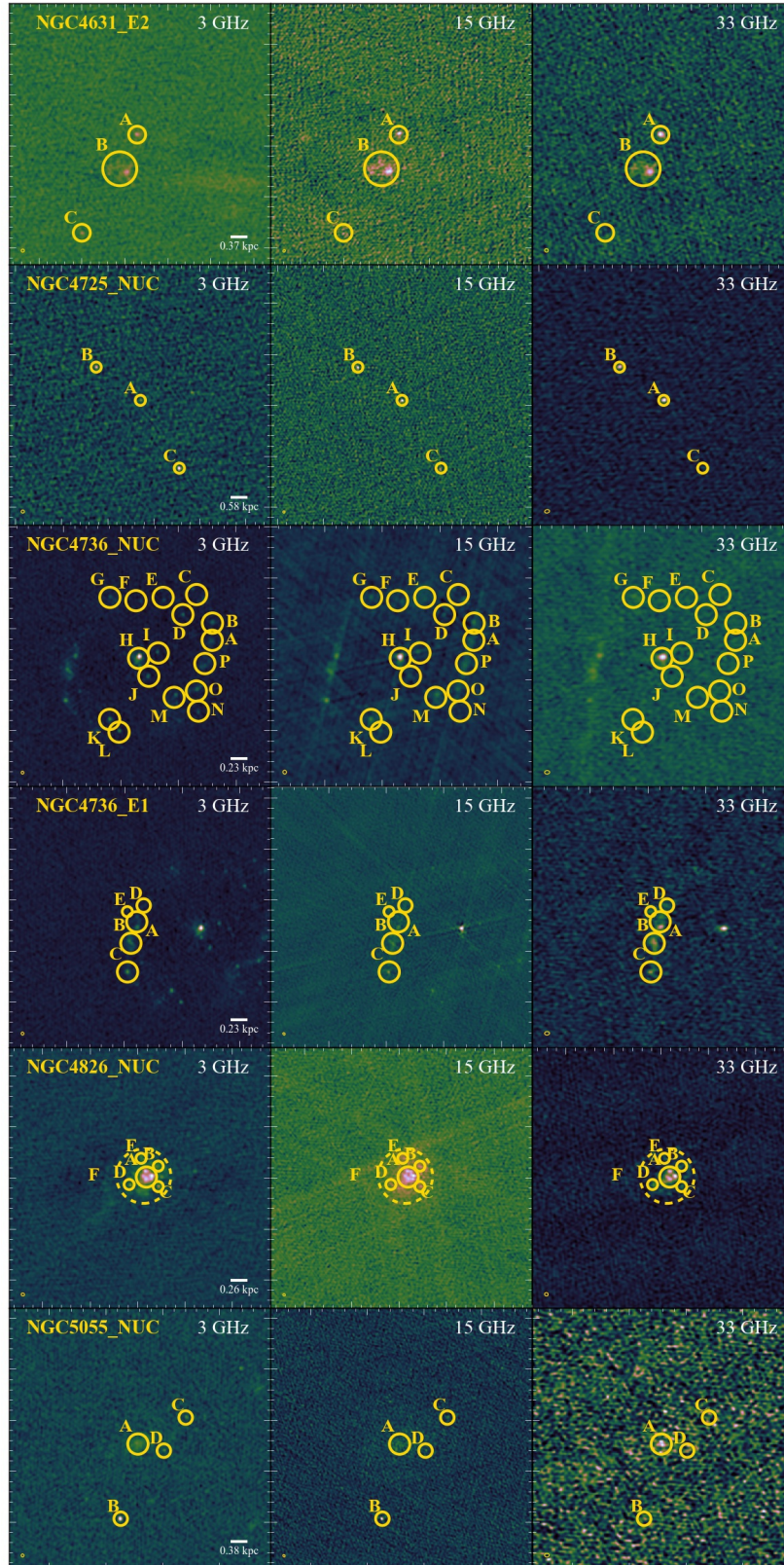


Figure 17. See description in Figure 1.



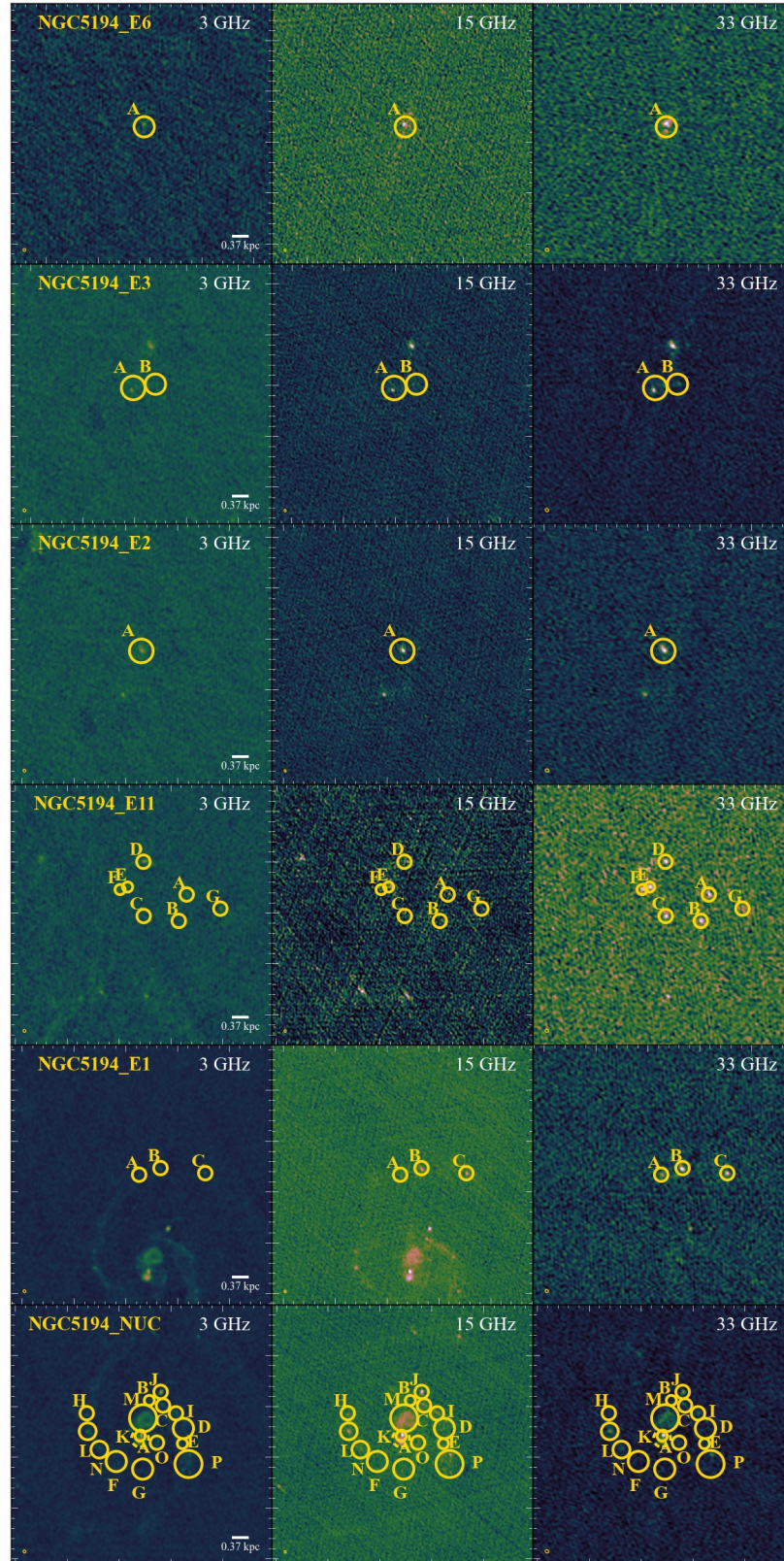


Figure 18. See description in Figure 1.



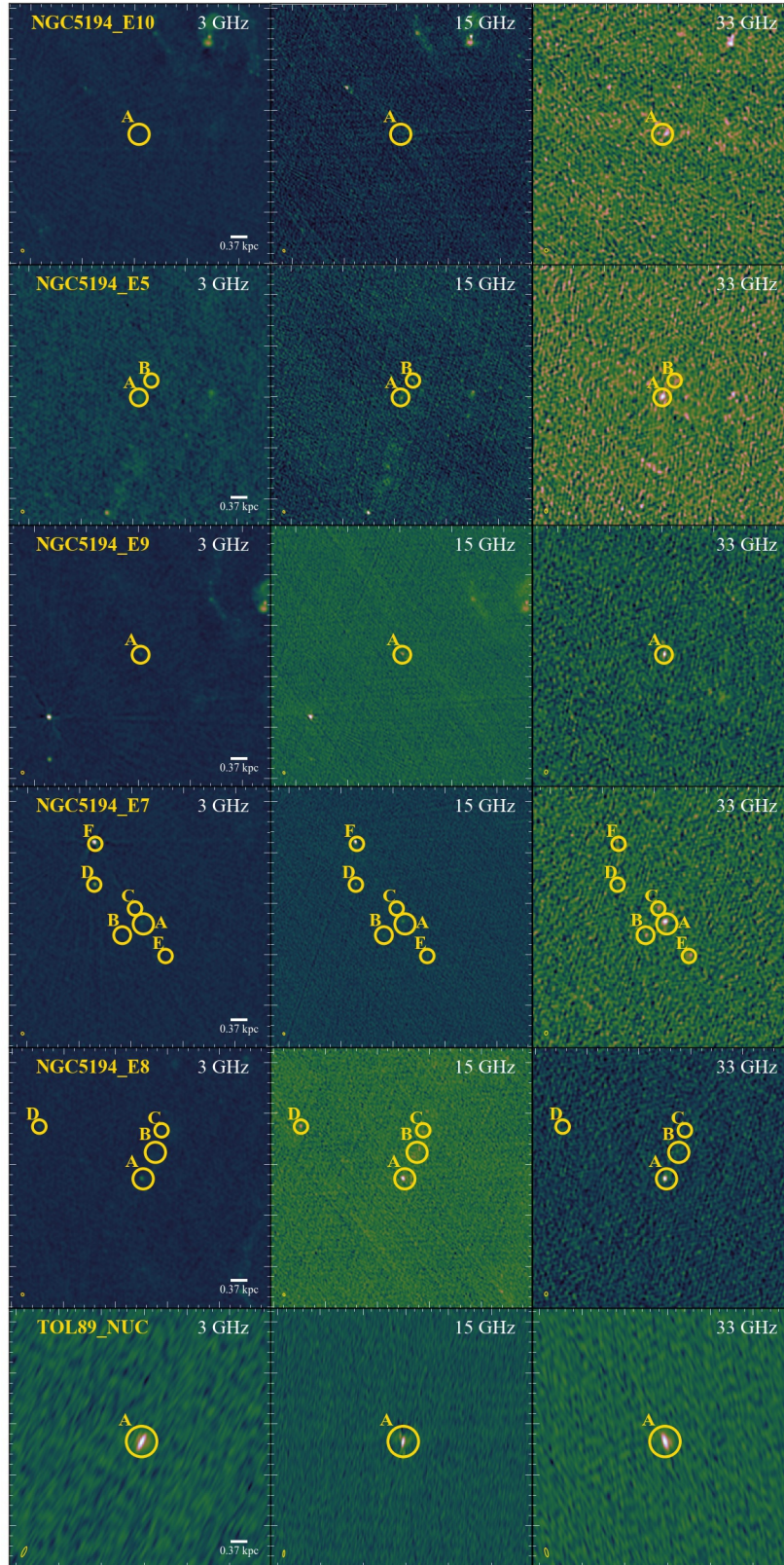


Figure 19. See description in Figure 1.



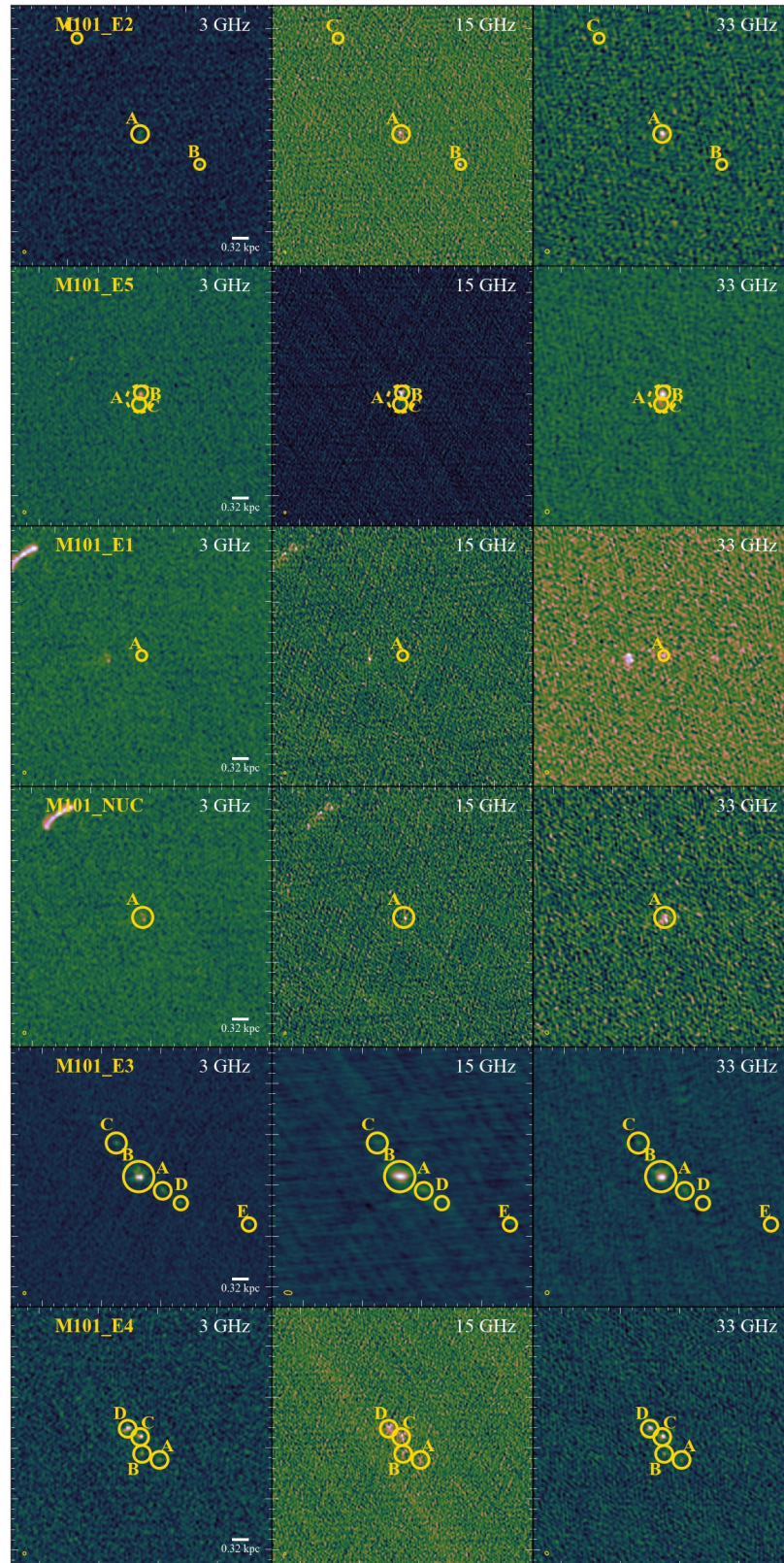


Figure 20. See description in Figure 1.



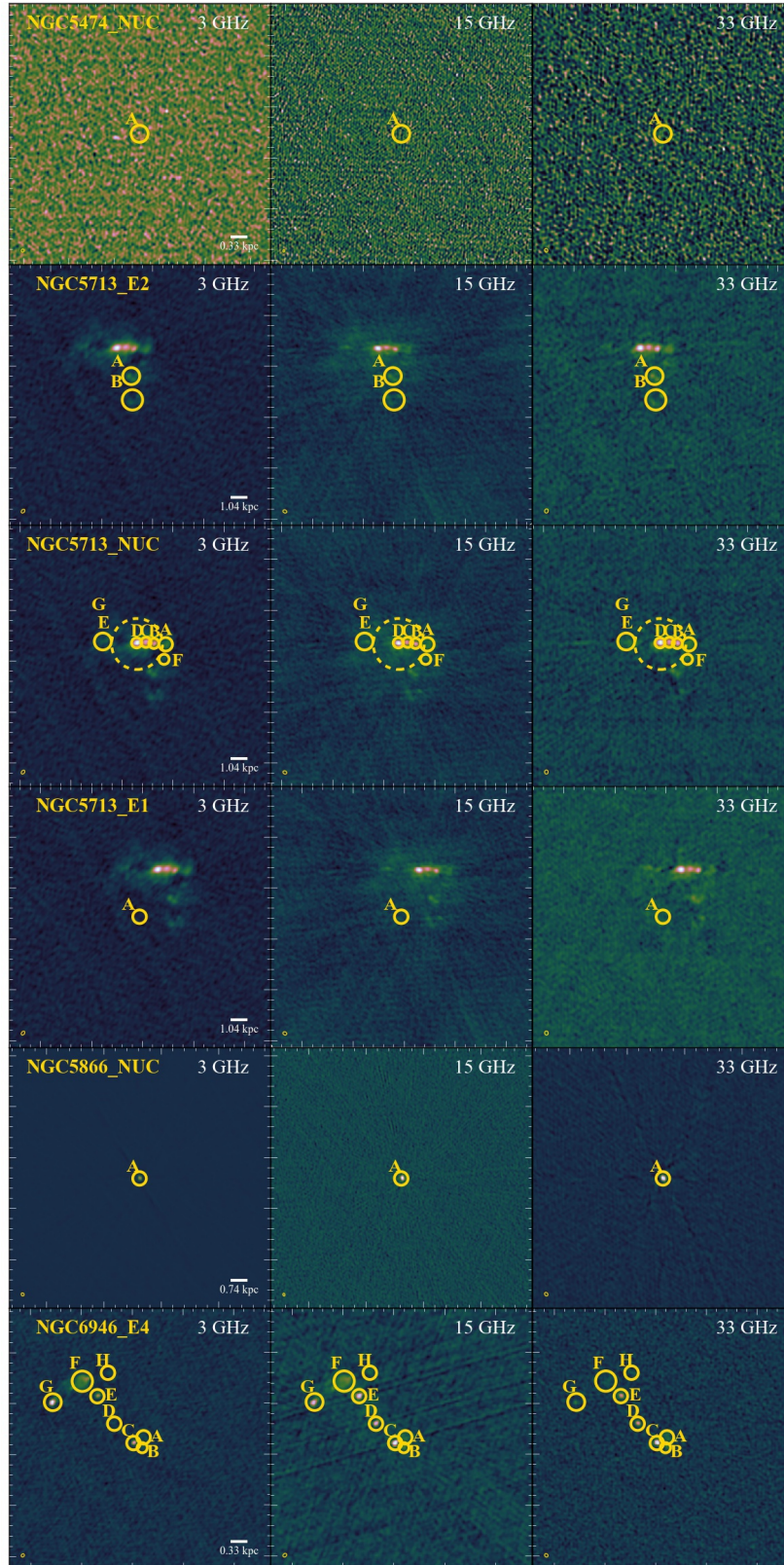
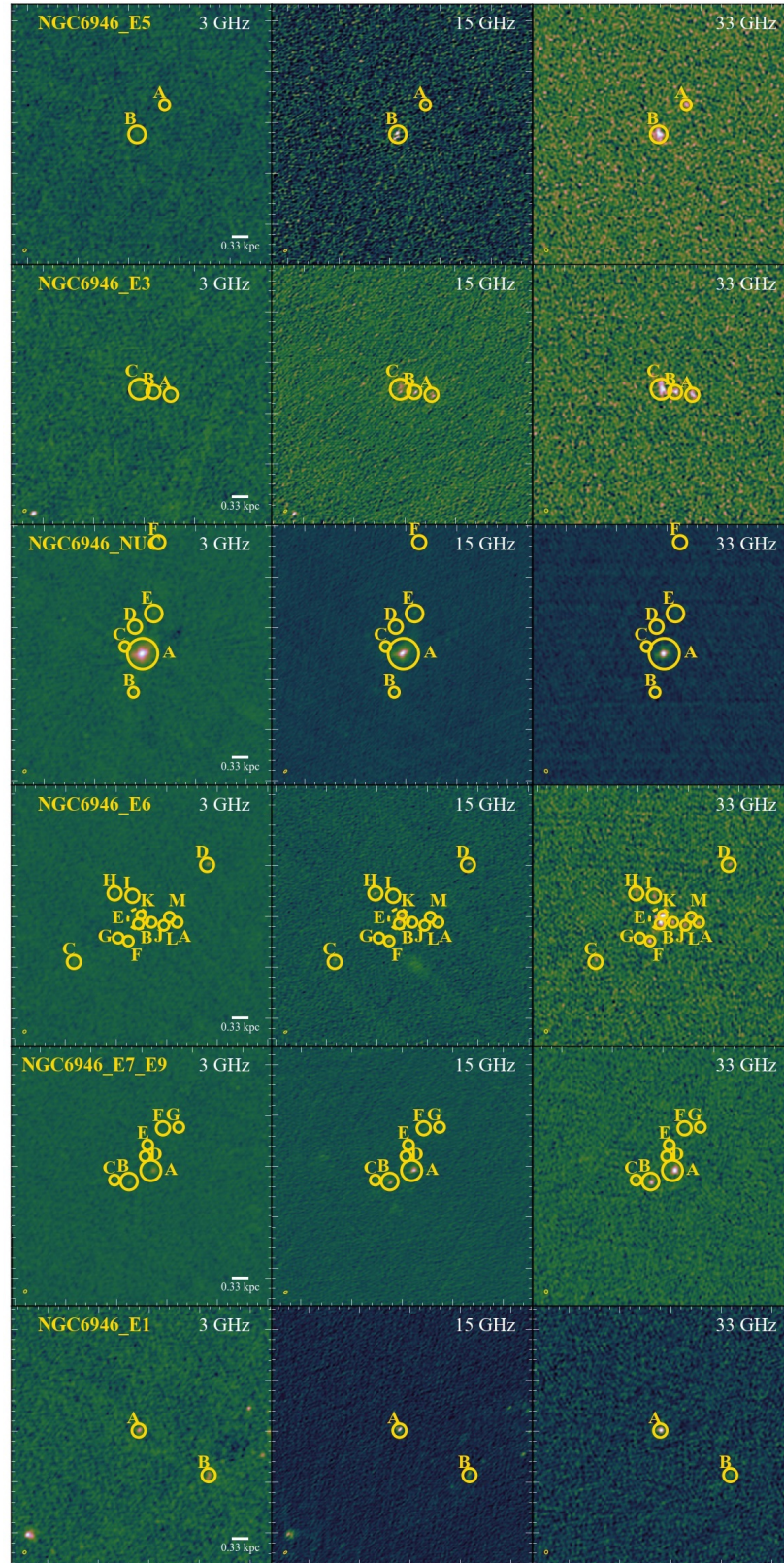


Figure 21. See description in Figure 1.





**Figure 22.** See description in Figure 1.



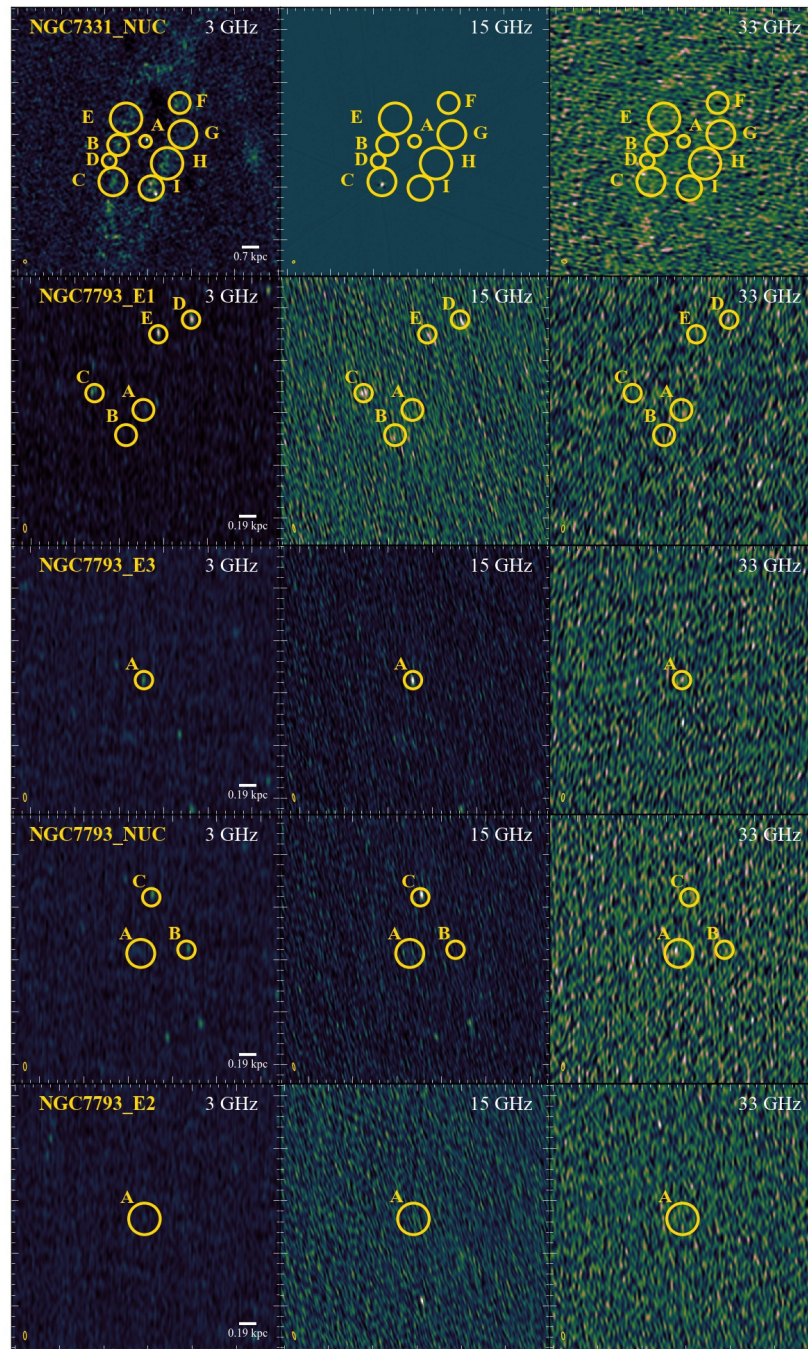


**Figure 23.** See description in Figure 1.